AN INVESTIGATION OF THE STRUCTURE OF OXIDE GLASSES USING EXAFS

by

J. M. TAYLOR, B.Sc.

A thesis submitted to the University of Warwick
for admission to the degree of
Doctor of Philosophy

February, 1984

To My Mom and Dad

ABSTRACT

The atomic species sensitivity of EXAFS lends itself to the investigation of the local atomic structure of certain cations within multi-component disordered systems. To this end, X-ray absorption measurements were performed on two systems of glasses, containing ZrO_2 and TiO_2 as major constituents. Both of these oxides are known to confer technologically important properties, however, their exact structural role is far from well understood.

For the case of ZrO_2, the R_2O-CaO-ZrO_2-SiO_2 (R = Li, Na, K) system was chosen and structural changes were monitored as a function of alkali type and content and by the method of preparation. For annealed specimens, the results show a considerably ordered arrangement of, on average, six oxygens at 2.09 $\pm$ 0.05 Å, indicating that the Zr site can be classified as network forming. The comparison of annealed and quenched specimens show that structural changes are observable as a result of heat treatment below T_g.

Previous investigations of TiO_2-containing glasses have shown that the coordination of Ti^{4+} ions varies as a function of composition. Such effects should be observable by the EXAFS technique and a series of Na_2O-TiO_2-SiO_2 glasses were measured. Furthermore, the Ti K-edge is characterized by transitions to bound states of the excited atom (XANES) which reflect the symmetry of the surrounding atoms. Results using both of these phenomena support the overall trend of increasing low coordination states (< 6) with increasing TiO_2 concentration, although discrepancies with other works are observed at low TiO_2 content, where tetrahedral coordination is still observed, which may be due to the method of glass preparation. At the compositional ratio SiO_2:TiO_2 ~ 1-2 a maximum in this coordination, thought to be due to isostructural substitution of Si^{4+} ions, is observed as a function of Na_2O content. Further addition of TiO_2 results in phase separation.

CONTENTS

LIST OF FIGURES

LIST OF TABLES

ACKNOWLEDGEMENTS

My thanks are extended to the many people who have aided and encouraged me in all aspects throughout the duration of this thesis: to those I forget to mention by name, I apologise, but who nevertheless have contributed as much. In particular, I would like to express my regard for Professor P. W. McMillan for his supervision and encouragement which enabled this thesis to be written. Both he and Professor P. N. Butcher are also thanked, in their capacities as Chairman of the Department of Physics, for allowing me to use the facilities therein. My thanks go as well to all the technical and research members of the glass-ceramics group, both past and present, for their help. Of special note were the helpful, or otherwise, discussions I had with Nigel Pratten, Diane Holland and Ray Todhunter.

Many of the measurements presented in this thesis would not have been performed had it not been for the kind help of Tony Cox and Diane Gonzalez (SSRL) and Roman Kozlowski and Robert Pettifer of the Department of Physics; their patience and hard work is greatly appreciated. I would also like to mention Robert's generosity in letting me use his computer software, his guidance through the lean years and his helpful criticisms in preparing Chapters 3 and 4.

I am endebted to the staff of Pilkington Brothers plc. (the collaborating body in the CASE studentship) for their support and generosity throughout the study. Special thanks go to Harold Charnock, Jane Greengrass and Ron Gaskell. I also thank the SERC for awarding the initial grant.

A special thanks to Nada Cvero, who has displayed patience and diligence in typing this thesis under, at times, difficult conditions.

Finally, but most importantly, I thank my family for their love and support. To Andy, Ray, Simon and (not least of all) Sue goes my love, best wishes and fond regard.

Chapter 1

INTRODUCTION

1.1. DEFINITION OF A GLASS

The ability of a material to form a glass depends on its composition. The majority of inorganic compounds and elements melt to form liquids having a relatively low viscosity (~ 10^{-2} Poise). Irrespective of the rate of cooling, these liquids crystallize at a temperature T_f (see Fig. 1.1.) to form a solid possessing a periodic array of structural units that combine to give a crystal its long-range order. This is represented in Fig. 1.2(a). However, there are some materials which, on cooling to temperatures below their freezing point, past the region of supercooling, will not crystallize, but rather remain in metastable state having a viscosity ~ 10^{13} Poise. Crudely, the rate of crystallization can be related to the inverse of the viscosity. Such materials are called glasses; the American Society for Testing Materials defines a glass as "... an inorganic product of fusion which has been cooled to a rigid condition without crystallizing". This describes what could be called the classical formation from the melt. However, other techniques are commonly used in order to obtain glasses and will be mentioned where appropriate.

Of all the glass forming systems, of partiular technological importance are the oxide systems SiO_2, GeO_2, B_2O_3, P_2O_5, As_2O_3 and Sb_2O_3 readily form glasses from the melt. Silica is the most widely researched of these and most of the discussion hereinafter will be concerned with slicate glasses.

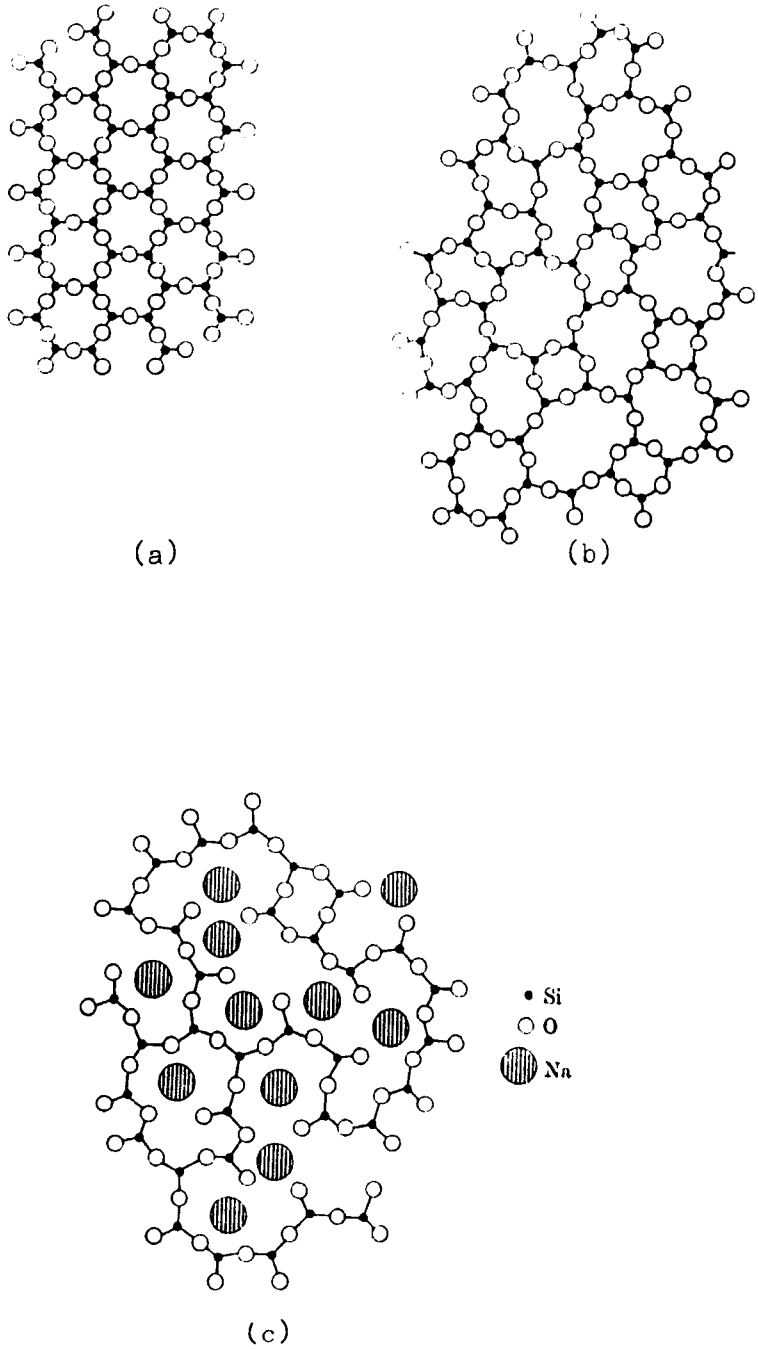

Figure 1.2 Two-dimensional representation of (a) SiO_2, (b) vitreous SiO_2 and (c) Na_2O-SiO_2 glass as envisaged by Zachariasen and Warren.

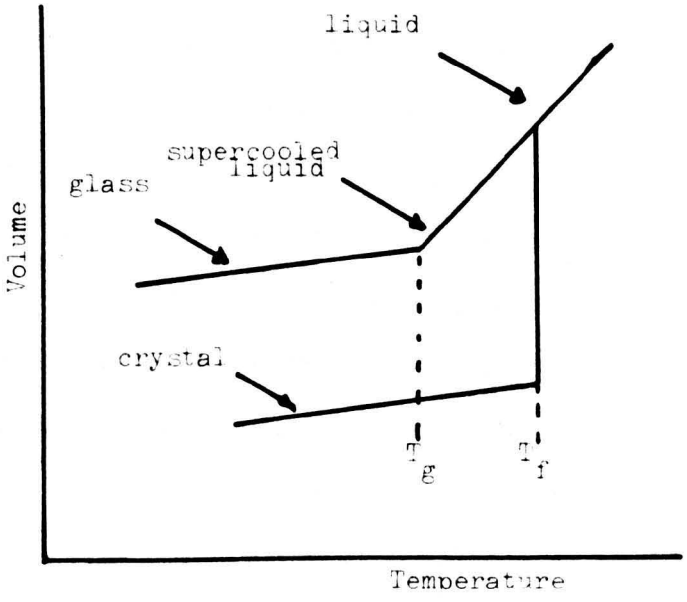

Figure 1.1 Relationship between glassy, liquid and crystalline states(Jones, 1956).

1.2. THE ZACHARIASEN OR RANDOM NETWORK MODEL

It would be expected that the atomic structure of a glass would be similar to that of its parent liquid; in as much that it is characterised by broad X-ray diffraction patterns as opposed to the sharp lines associated with a crystal. This is in fact the case and implies that a glass lacks any long-range order. However, as the primary short range order forces are similar for all condensed phases of matter, it could be assumed that for a crystal and a glass of given composition the bond angles, bond lengths and coordination of the nearest neighbours would be analogous.

1.2.1. Vitreous Silica

Zachariasen (1932) had noted the probable amorphous nature of glass as suggested by X-ray diffraction and following earlier work by Goldschmidt (1926), who laid down certain rules for glass formation on the basis of cation:anion radii *per pro* ionic crystals he argued further

that the increase in internal energy of a glass compared to that of a crystal of given composition must be small so as not to cause devitrification, implying that the polyhedral building blocks underlying the structure of crystals will be the same, although the strength of the metal-ligand bonds will vary, producing asymmetries. Moreover, the polyhedra must be joined to each other in a similar fashion to further reduce the internal energy. Thus, the tetrahedral [SiO_4] units - see Fig. 1.2(a). - that comprise the three thermodynamically stable phases of SiO_2 (quartz, cristobalite and tridymite) will be the same in vitreous silica, the only difference being the relative orientation of these tetrahedra as shown in Fig. 1.2(b). Distortions of the order of 10% are sufficient to produce an overall randomness in the network resulting in an "infinitely large unit cell".

This theory was first proposed for one component glasses such as vitreous silica. The next section proceeds to discuss the extension of this theory to more complicated systems.

1.2.2. Binary Silicates

By the addition of suitable ionic oxides, it is possible to disrupt the continuous silica network and still produce a glass. For instance, the introduction of Na_2O allows a surplus of O^{2-} ions at melt time (due to the low electron affinity of Na^+) which react with the [SiO_4] units. This has the effect of creating so-called "non-bridging oxygens" through the reaction

$$\rightarrow\!\!\!\!\diagup\!\!\!\!\diagdown Si - O - Si \diagup\!\!\!\!\diagdown\!\!\!\!\leftarrow + Na_2O \rightarrow 2 \rightarrow\!\!\!\!\diagup\!\!\!\!\diagdown Si - O^- + 2Na^+$$

forming oxygens that are bonded to only one silicon as shown in Fig. 1.2(c). The net effect of this structural breakdown is to reduce the

viscosity, strength and melting temperature of the glass. For example, the addition of 2.5 mole % to SiO_2 at 1700°C causes the viscosity to drop from 2×10^7 to 2×10^3 Poise.

Zachariasen (later supported by Warren, 1937) proposed that the large Na^+ ions occupy the interstices between $[SiO_4]^{n-}$ tetrahedra, (Fig. 1.2c.), preserving the electrical neutrality in the vicinity of the non-bridging oxygens. Li_2O and K_2O behave in a similar way to Na_2O, although their respective size and bond strength mean that they confer contrasting physical properties such as different thermal expansion coefficients.

Table I lists the cations which act similarly to the alkali oxides; the so-called "network modifiers" (Group III), together with network formers (Group I) and "intermediates" (Group II). This grouping of ions was based on the criterion of bond strength between cation and anions (oxygen), first proposed by Stanworth (1948) and updated by Pauling (1960).

Formers Group I	Intermediates Group II	Modifiers Group III
B	Ti	Sc
Si	Zr	La
Ge	Pb	Mg
V	Al	Li
As	Th	Ba
Sb	Be	Ca
		Na
		K
		Rb
		Cs

TABLE I

Classification of metal oxide in the structure of glasses based on the criterion of bond strength. After Pauling (1960)

The term intermediate is often used to describe ions, the oxides of which will not by themselves melt to form glasses but when combined with a glass former do possess such a propensity. However, for this work the term will be used to describe those ions which are thought to be able to enter the glass structure as a network former or as a modifier. Their role is not exactly known, and it is the hope of this work that their exact structure may be elucidated.

Thus, as can be seen, it is possible to form very complex multi-component glasses by combining network formers, modifiers and intermediates.

1.3. OTHER STRUCTURAL THEORIES

1.3.1. The Modern Crystallite Theory

It has been suggested that the theory of Warren and Zachariasen on the atomic arrangement of glasses has been regarded by technologists more as an article of faith rather than a law of nature. However, right from its conception the interpretation has been criticized and even today has not been fully resolved.

The first criticism of Warren's interpretation came from Valenkov and Porai-Koshits (1936). As in all structural theories they proposed that the network forming anions occupy sites that are similar, as far as first shell coordination is concerned, to that of a crystal of given composition. However, they pointed out that Warren had failed to appreciate the significance of the thermal history of glasses. In investigations of the Na_2O-SiO_2 system, up to the metasilicate composition, several glasses were produced that had undergone varying heat treatments and they found that the X-ray diffraction data could be approximated by a superposition of data from vitreous silica and sodium

silicate (Na_2SiO_3), weighted by a factor that depended on the fraction of Na_2O present. This interpretation suggests that binary silicates possess a two-phase character, the region between these phases consisting of a highly disordered unknown phase. Such a theory, called the modern crystallite theory differs from previous crystallite theories, as expounded by Randall, et al. (1930), in which the individual phases were postulated to be delineated by sharp boundaries and as such should exhibit small-angle X-ray scattering (SAXS).

Since this early diffraction work, more reliable interpretational techniques have been employed. These have invariably involved the Fourier transform of the data to produce a radial distribution function (RDF) (see Section 1.4.1.). Such a method produces a superposition of pair correlation functions corresponding say, for a binary system (Na_2O-SiO_2), to Si-O, Si-Si, O-O, Na-O, Na-Na and Na-Si scattering. Porai-Koshits (1953) and Lukesh (1942) used such a technique to measure the alkaline and the alkaline-earth silicate systems, and the borosilicate system. The technique called the difference method, rests on the approximation that the interactions between Si-Si, Si-O and O-O will be the same in vitreous silica as for that of a binary silicate. Thus the RDF for the former may be subtracted from the unknown function resulting in informaion on the atomic disposition around the modifying ions.

The results supported the earlier work that the morphology of a glass is heterogeneous and varied from point-to-point throughout the volume. Such a theory has a phenomological backing as well, as it accomodates the possibility that these heterogeneities may act as nucleation sites in the early stages of crystal growth to produce a glass-ceramic. Furthermore, it explains also why SiO_2-Na_2O mixtures containing small amounts of Na_2O (less than 1.5 mole per cent) do not melt to form a glass. Smyth (1972) argued that there are areas in the melt that possess sodium ions

bound only to one oxygen. As there are insufficient non-bridging oxygens available, the internal energy is high and produces a characteristic immiscibility dome at the high-silica side of the free energy curve. As the soda content is increased more and more non-bridging oxygens are produced and the free energy is lowered.

Recent work by Goodman (1983) has tended to support the modern crystallite theory. He attributes the glass formation process as a strained-mixed-cluster model, the clusters being ~ 3nm in size and of a phase determined by the crystalline polymorphs that exist either side of the eutectic composition.

1.3.2. Discrete Anion Model

One major shortcoming of the random network and crystallite theories is their failure to explain the large increases in the thermal expansion and changes in the energy of activation for flow at alkali contents of 10-20 mole per cent in binary silicate glasses. Such a change is observed in liquid binary silicates and it is the contention of this theory that the atomic arrangement in silicates above their liquidus temperatures persists or is "frozen-in" as the liquid is supercooled, through T_g, to form a glass. Spectroscopic investigations (see next section) have led to the postulate that multicomponent glasses possess a more complicated structure than was first envisaged. Rather than having a [3-D] continuous random network, discrete complex ions, such as rings or chains, similar to those found in crystalline silicates, have been shown to lead to a better description of thermal conductivity (Mackenzie, 1956), viscosity (Bockris et al. 1955) and surface tension (King, 1953). Table II lists the anionic species present as a function of alkali oxide content according to Endell and Hellbrugge (1942) for a liquid binary silicate. Such a model has been suggested for glasses by Huggins et al. (1943). Bockris et al. (1955)

have suggested that the complex ions present at certain percentages of alkali oxide are produced by the polymerization of $[SiO_4]^{4-}$ tetrahedra, the latter being the discrete structural units present at the orthosilicate composition. With the addition of SiO_2, more complex anions are produced until at 10 mole % these now become unstable with respect to a 3D random network and the material reverts to a Zachariasen/Warren type glass.

Metal Oxide mole %	Si:O ratio	Anionic Units
66	0.25	Single $[SiO_4]^{4-}$ tetrahedra
60	0.286	Short chain of two $[SiO_4]^{4-}$
60-50	0.286-0.333	Large chains and rings
50	0.333	Infinitely long chains
50-33	0.333-0.40	Long chains and sheets
33	0.4	Infinite [2D] sheets
33-0	0.4-0.5	Sheets and [3D] SiO_2 network
0	0.5	[3D] network

TABLE II
Structure of liquid silicates according to Endell and Hellbrugge (1942)

1.4. STRUCTURAL INVESTIGATIONS

The following sections are included here to illustrate the difficulties that are inherent in the structural investigations of amorphous materials. Although not intended to be a complete survey, the major contributions to the understanding of glass structure are stated and where relevent comparisons between these techniques and X-ray absorption spectroscopy analysis will be underlined and developed in Chapter 3.

1.4.1. Diffraction Studies

For crystals, coherent scattering is strong due to the periodicity of the lattice. In glasses, this translational symmetry is lost, angular information is averaged out and scattering is usually couched in terms of the radial density $\rho_{ij}(r)$ of atoms of type i at a distance r from an atom of type j, averaged over all i atoms in the material. For a material comprising two atomic species A and B, 3 pair-correlation functions g(r), corresponding to A-A, A-B and B-B have to be considered. For n atomic species, n(n+1)/2 independent functions are required. Such a condition imposes serious experimental constraints on the diffraction studies of glasses. As many independent experiments as pair correlation functions need to be performed in order to fully describe the material. In practice this is rarely obtained and can only be remedied by the introduction of certain approximations.

The scattering intensity for an isotropic medium $I^{coh}(Q)$, $Q = 4\pi\sin\theta/\lambda$ is

$$I(Q) = \sum_i C_i^2 + \sum_{i \neq j} C_i C_j \int_0^\infty 4\pi r^2 \rho_{ij}(r) \frac{\sin Qr}{Qr} dr \qquad (1.1.)$$

where ρ_{ij} is the average pair distribution function.

The atom radial distribution function $4\pi r^2 \rho_{ij}(r)$ is normalized

such that

$$\sum_j \int_0^\infty 4\pi r^2 \rho_{ij}(r)dr = N_T \qquad (1.2.)$$

the total number of j atoms in the sample.

Following Warren (1969), it is now beneficial to define the interference function Qi(Q). Eqn. 1.1. may now be written as

$$Qi(Q) = \sum_i C_i \sum_j 4\pi \int_0^\infty r[\rho_{ij}(r) - \rho_a]\sin(Qr)F_{ij}(Q)dr \qquad (1.3.)$$

where C_i is the concentration factor and $F_{ij}(Q)$ is the normalized product of the individual scattering factors. ρ_a is the average density of the material in the limit $r \to \infty$. Eqn. 1.3. is of the general form of a Fourier (FT) transform with the pair correlation function defined as

$$d_{ij} = 4\pi r[\rho_{ij}(r) - \rho_a] \qquad (1.4.)$$

That is

$$d_{ij}(r) = \frac{1}{2\pi} \int_0^\infty Qi(Q)\sin(Qr)F_{ij}(Q)dQ \qquad (1.5.)$$

or the Fourier transform of the interference function (obtained from experiment) can be expressed as a convolution of the form

$$FT[Qi(Q)] = \sum_i C_i \sum_j \int_0^{Q_m} d_{ij}(r)P_{ij}(r - r')dr'$$

$$= \sum_i C_i \sum_j \int_0^{Q_m} \frac{\rho_{ij}(r)}{r} P_{ij}(r - r')dr' \qquad (1.6.)$$

where P_{ij} is a peak function (Leadbetter and Wright, 1972) containing

the normalized atomic scattering factors multiplied by a window function. For neutrons P_{ij} is independent of Q. The value Q_m reflects the range of available momentum transfer obtainable for the experiment which is ~ 30 $\mathring{A}^{-1}$ for synchrotron radiation. The termination of the Fourier transform produces "termination ripples" (Bragg and West, 1930) and ultimately determines the resolution of the RDF.

Independent interference functions may be obtained directly by the choice of suitable experiments. For single oxide glasses these may be obtained by the combined use of X-ray and neutron scattering. For example Henninger et al. (1967) for vit. SiO_2 and Leadbetter and Wright (1972) for vit. GeO_2.

The use of heavy ion substitution (Ba, Tb and Pb) offers a promising way of establishing the role of modifying ions. The RDFs for these glasses are dominated by the strong X-ray scattering of these ions. Results by Brosset (1958) on soda-lime-silica glasses tend to substantiate the two phase model for silicate glasses. However, it must be stressed that the use of isostructural substitution methods presupposes that these ions behave in a similar role.

For the case of neutron diffraction, very little work on multicomponent systems has as yet been performed. A short study by Suzuki and Keno (1981) has proved that the technique is worthy of more merit. Loshmanov et al. (1974) used the isotropic sensitivity of Ti scattering to study Na_2O-TiO_2-SiO_2 glasses and will be discussed in more detail in Chapter 5.

1.4.2. Nuclear Magnetic Resonance (NMR)

NMR spectroscopy is an extremely useful technique for the study of glass structure. The quadropole and chemical shift interactions are sensitive to the local environment of the excited nucleus. For low atomic

number elements having a spin $I \geq 1$, the dominant interaction is the quadropole. This has meant that the majority of work on glasses has been performed on borates using ^{11}B and ^{10}B nuclei. Therefore, by way of contrast, in this section the structure of borate glasses will be presented.

The first structural investigations on vit. B_2O_3 was carried out by Warren and Biscoe (1938a). They concluded that it was comprised of $[BO_3]$ triangles linked so as to form a random network. Although, other theories have been offered, their original appraisal is generally accepted.

For the case of binary borates R_2O-B_2O_3 (R = Li, Na, K) the structure is more complex. As the alkali content is increased up to the value of 16 mole % Na_2O, the expansion coefficient decreases. From then on it is observed to increase. Such a behaviour is uncharacteristic of a Zachariasen/Warren type glass where the addition of extra oxygens should weaken the structure. Warren and Biscoe (1938b) attributed this behaviour to the creation of $[BO_4]$ tetrahedra, which will increase the rigidity, up to 16 mole % and from then on, non-bridging oxygens are formed and the glass reverts to its classical behaviour.

However, NMR results have tended to suggest rather that $[BO_4]$ production increases steadily as a function of alkali content according to the equation

$$N_4 \text{ (no. of } BO_4 \text{ tetrahedra)} = \frac{x}{1 - x} \qquad (x = \% R_2O)$$

a relationship expected if it is assumed that each added oxygen converts two boron atoms from triangular to tetrahedral coordination. This phenomenon was experimentally observed by Silver and Bray (1958) by the steady increase of the $[BO_4]$ line at the expense of the highly

quadropole active, broad [BO_3] resonance.

More recently, Jellison and Bray (1978) have shown that the glassy NMR spectra can be related to structural units (complex anions) within the glass similar to those found in crystalline borates, (e.g. boroxol, tetraborate, diborate, metaborate, etc.). Here, computer simulations model the data by weighting each individual phase in a fitting algorithm. Such a theory agrees with earlier results of Krogh-Moe (1965).

The application of the NMR technique to silicate glasses is considerably less favourable due to both the absence of any quadropole moment and also the low relative abundance. However, one promising new technique has been developed which makes it possible to examine these ions. The technique called "magic-angle" spinning (MAS) requires the rotation of a sample (~ 4 kHz) at an angle such that the dipolar interaction is 'quenched'. This interaction is usually so broad that it masks out any weaker processes. Results on Na_2O-SiO_2 glasses (Dupree et al. 1984) show that it is possible to detect chemical shifts of the Si resonance due to changes in coordination properties and to discriminate between Si tetrahedra possessing one, two or three non-bridging oxygens. Moreover, measurements on the Na resonance show that the immediate environment of these ions within the glass is distinct from that found in crystalline compounds and it is proposed that the Na^+ ions occupy random sites. Such a model conflicts with previous work on the two-phase make up of glasses.

1.4.3. EXAFS Studies

Extended X-ray absorption fine structure (EXAFS) is the name given to the oscillations observed on the high energy side of an absorption edge and extend typically from 50 to several hundred eV. They arise from an interference effect between the outgoing photoelectron wave and waves

scattered back from the neighbouring atoms. As an interference effect the periodicity of these oscillations is related to the distance between emitter and scatterer. The amplitude gives a measure of the type, number and disposition of these scatterers. The phenomenon is radially sensitive and as such provides an excellent method for examining the local atomic structure of disordered systems for which translational symmetry is lacking. Moreover, the technique is beneficial for the investigation of multi-component materials as each absorption edge may be sampled individually.

By far the most extensively studied of all oxide glasses is the germanate system in view of the fact that its K-edge (11103 eV) is readily accessible. Sayers et al. (1972) and Wong and Lytle (1980) have compared the structure of vitreous GeO_2 with the two crystalline forms of germania: the hexagonal structure, where the Ge atoms are tetrahedrally coordinated by oxygen; and tetragonal GeO_2 for which the coordination is octahedral. Results have concluded that vitreous GeO_2 is related to the hexagonal form and as such acts in a similar way to SiO_2 as a glass former. It was found that the degree of order in the first shell is greater than that found in the corresponding crystal and can be attributed to a relaxation of the immediate atomic environment at the expense of any translational symmetry. Any of the latter is lost due to the variation in Ge-O-Ge bond angle and can be readily seen by the lack of any second shell contribution to the EXAFS.

Cox and McMillan (1981) have measured the EXAFS spectra for a series of lithia-germanate glasses and again found that the signal was solely due to the oxygen arrangement around the Ge^{4+} ion. However, the coordination number of the Ge^{4+} ion is a function of the alkali oxide content. It was found that the ratio of octahedral sites to tetrahedral sites increased as oxygens were donated by Li^{+} ions.

Sandstrom et al. (1980, 1983) have studied the binary silicate system $xSiO_2(1-x)TiO_2$, prepared by a flame hydrolysis method and found the system to be very complex indeed. For a very small TiO_2 concentration (< 1 wt. %), EXAFS measurements were obtained by a fluorescence technique and show the Ti^{4+} ions to occupy an octahedral (TiO_2-like) site within the SiO_2 glass, suggesting that Ti^{4+} ions occupy an interstitial site between $[SiO_4]^{n-}$ tetrahedra. As the TiO_2 content is increased up to a maximum (x = 0.07), the Ti^{4+} ions take on a different role and exhibit a tetrahedral coordination for which the ions substitute isostructurally for Si^{4+} but still maintaining a small amount (~ 5 wt. %) in octahedral symmetry. On further addition of TiO_2 the ratio of sixfold to fourfold coordination increases appreciably and eventually (~ 15 wt %) the structure is "rutile like". Such a duality of roles establishes the intermediate nature of Ti^{4+} ions as suggested by bond strength criteria.

One particular study of sodium silicate glasses carried out by Pettifer (1979) shows how useful information may be extracted from EXAFS data with a modicum of analysis. It was thought that Zn^{4+} ions may behave in a similar way to Ti and possess a dual character. However by direct comparisons of the first peaks in the EXAFS spectra of the glasses with $ZnSiO_4$, for which the Zn^{4+} ions are tetrahedrally coordinated, it was possible to categorize the Zn role firmly as a network former for this particular system.

For Si, the K-edge X-ray absorption spectra becomes difficult to measure (the Si K-edge ~ 1800 eV). Greaves et al. (1980) have measured the fine structure for sodium disilicate, vit. SiO_2 and soda-lime-silica glass, prepared by blowing thin films directly from the melt. Bond length and bond angle (Si-O-Si) results are in agreement with earlier diffraction data. Greaves et al. (1981) and Gaskell et al. (1982) have also measured

the K-edges of modifier oxides: Na^+ and Ca^{2+} respectively. Results indicate that these ions behave in a different way than was first postulated by the Zachariasen/Warren model; that is they do not simply fit into random holes within the SiO_2 network but occupy rather a more well defined site similar to that found in crystalline counterparts. These conclusions lend support to those models presented in Section 1.3.2.

One of the severe limitations of the orthodox transmission EXAFS technique which was highlighted in the previous studies on the Si and Na K-edges, where absorption is very large, is that the thickness of sample imposes, in some cases, impractical limits. One technique which alleviates this problem is to measure the specular reflectivity of the sample, making it possible to reach edges as soft as oxygen (~ 400 eV). Fox and Gurman (1980) have calculated this scattering for various media and demonstrated the feasibility of the technique and furthermore have shown it to be surface sensitive.

Taylor and McMillan (1983) have investigated the role of ZrO_2 as a nucleating agent in the development of cordierite glass-ceramics. Results show that before the onset of crystallization an incipient ordering takes place, indicated by an increasing second-shell contribution.

1.5. CHOICE OF GLASSES

The technological uses of oxide glasses are many fold. Their employment in both industrial and domestic environments has increased in recent years and for this reason, research into the physical properties by empirical investigation has accelerated at the expense of fundamental structural work into 'how' certain oxide glasses confer these properties.

Zirconia is one such oxide and is of importance technologically from two points of view. Firstly, ZrO_2 is an effective nucleating agent in

some glass-ceramic compositions. Secondly, it is a major constituent of glasses having a high resistance to alkali attack and is used in the fibre reinforcement of cement. It is for this latter reason, that the project was first conceived in collaboration with Pilkington Brothers plc.

The exact structural role played by Zr is far from understood. Its bonding characteristics with oxygen are such that its classification as a network fomer or as network modifier is ill-defined. Using Pilkington Brothers "Cem-Fil" composition as a guide line (sample ZrA in Table IV) a system of glasses was prepared.

In the preceeding section a recent study on the role of Ti ions has been discussed. Titanium dioxide is an important additive in glasses in view of the fact that by varying the TiO_2 concentration in SiO_2-TiO_2-containing glasses it is possible to produce a material with a very low thermal expansion. Sandstrom et al. (1980) were quick to point out that the complex nature of Ti may be a function of glass preparation. On the basis of this work it was decided to extend this study and investigate the ternary silicate Na_2O-TiO_2-SiO_2 system.

1.6. PLAN OF THESIS

Chapter 2 discusses the experimental techniques employed in this work. This is divided into two sections: (1) Glass and sample preparation; (2) EXAFS instrumentation and measurement. The latter includes a brief survey of the salient features of synchrotron radiation.

Chapter 3 involves a theoretical outline of the basic physics of EXAFS leading to the fundamental equation. There then follows a discussion on the interpretation of the data and the relative merits of the differing techniques.

Chapter 4 reports the X-ray absorption measurements for a series of

ZrO_2 containing glasses. Two techniques are used for the interpretation of these data on the basis of which, a structural model for the role of Zr is presented and is used for the interpretation of infrared data.

Chapter 5 reports on the X-ray absorption measurements for a series of TiO_2-containing glasses. EXAFS and near edge results are used to discuss the coordination of Ti^{4+} ions with reference to previous structural models.

Chapter 6 concludes the work by a general discussion of the applicability of EXAFS for glasses and underlines the main findings of the structural investigations, on the basis of which the prospects for extending these studies are discussed.

Chapter 2

EXPERIMENTAL TECHNIQUES

2.1. INTRODUCTION

For a given composition, the physical properties of a glass are influenced by its thermal history. Therefore, in any discussion on the structure of glasses it is particularly important to bear in mind this aspect of glass science.

Glass preparation can be regarded as a three stage process: firstly the decomposition of batch materials below the liquidus temperature; the firing of the melt to remove inclusions, etc.; and finally, the homogenization of the glass.

Glass compositions will not be presented in this chapter but deferred to the relevant results and discussion sections.

2.2. GLASS PREPARATION

2.2.1. Melting and Annealing

The following procedure was used to produce glasses and although not a complete description, many of the techniques are used in commercial glass manufacture.

1. Batch materials (e.g. Limoges quartz, sodium carbonate and calcium carbonate) were mixed thoroughly prior to any thermal treatment. Fine particle size and thorough mixing speed up the initial reactions within the melt.

2. When necessary, decarbonation and sintering were carried out. At 850°C sodium carbonate melts with the violent release of CO_2. This effect accelerates the mixing process and speeds up the reaction

$$Na_2CO_3 + SiO_2 \rightarrow Na_2O\text{-}SiO_2 + CO_2$$

3. Depending on composition, glasses were melted at approximately 100°C above the liquidus temperature for 3 hours to ensure full refining. At this stage there are two standard methods for securing a homogeneous glass: (i) the liquid may be stirred *in situ* ; or (ii) as was employed in this work, melts were cast, crushed and then remelted in an iteration process. Preliminary casting was performed on to a mild steel plate and the glass was then 'grizzled' (quenched) with distilled water. For glasses that were fairly stable final casting was performed onto a warmed plate to avoid cracking. However, for some glasses faster cooling rates were required to avoid devitrification and in preference to mild steel, a cooled copper plate was used as the casting medium. As a preliminary check on the glassy nature of the material, X-ray diffraction spectra were measured. Fig. 2.1. shows the characteristic amorphous broad peak expected of disordered materials.

4. After the final cast the glass, where appropriate, was placed in an electric furnace for annealing. This allows any internal stress within the quenched glass to be relieved by a viscous flow process and can be directly observed by examining the absence of birefringence under polarized light. The annealing temperatures were determined by differential scanning calorimetry (DSC) as shown in Fig. 2.2., taking a value T_{Ann}, as the extrapolated onset of T_g.

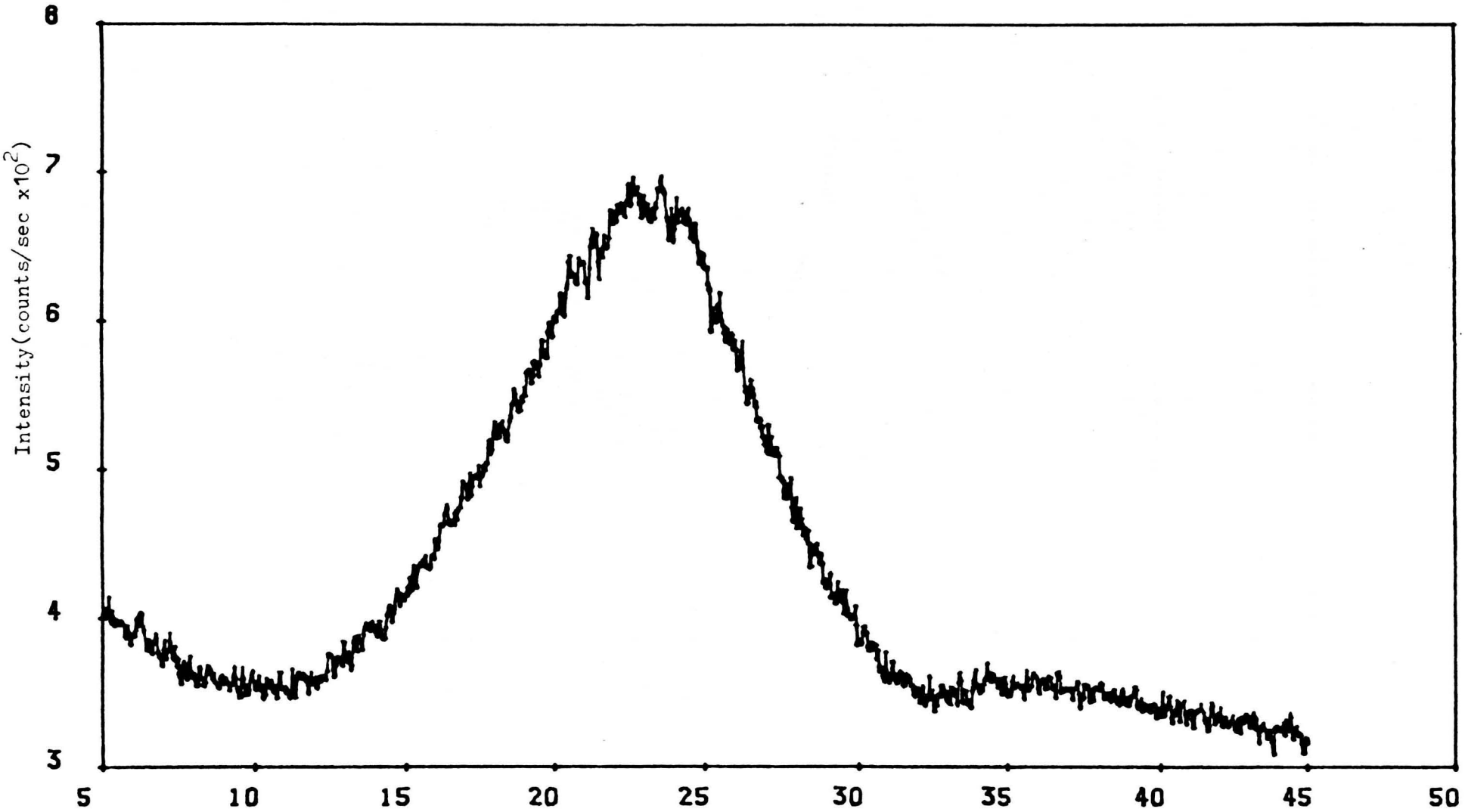

Figure 2.1. X-ray diffraction pattern of sample ZrA showing the characteristic amorphous peak.

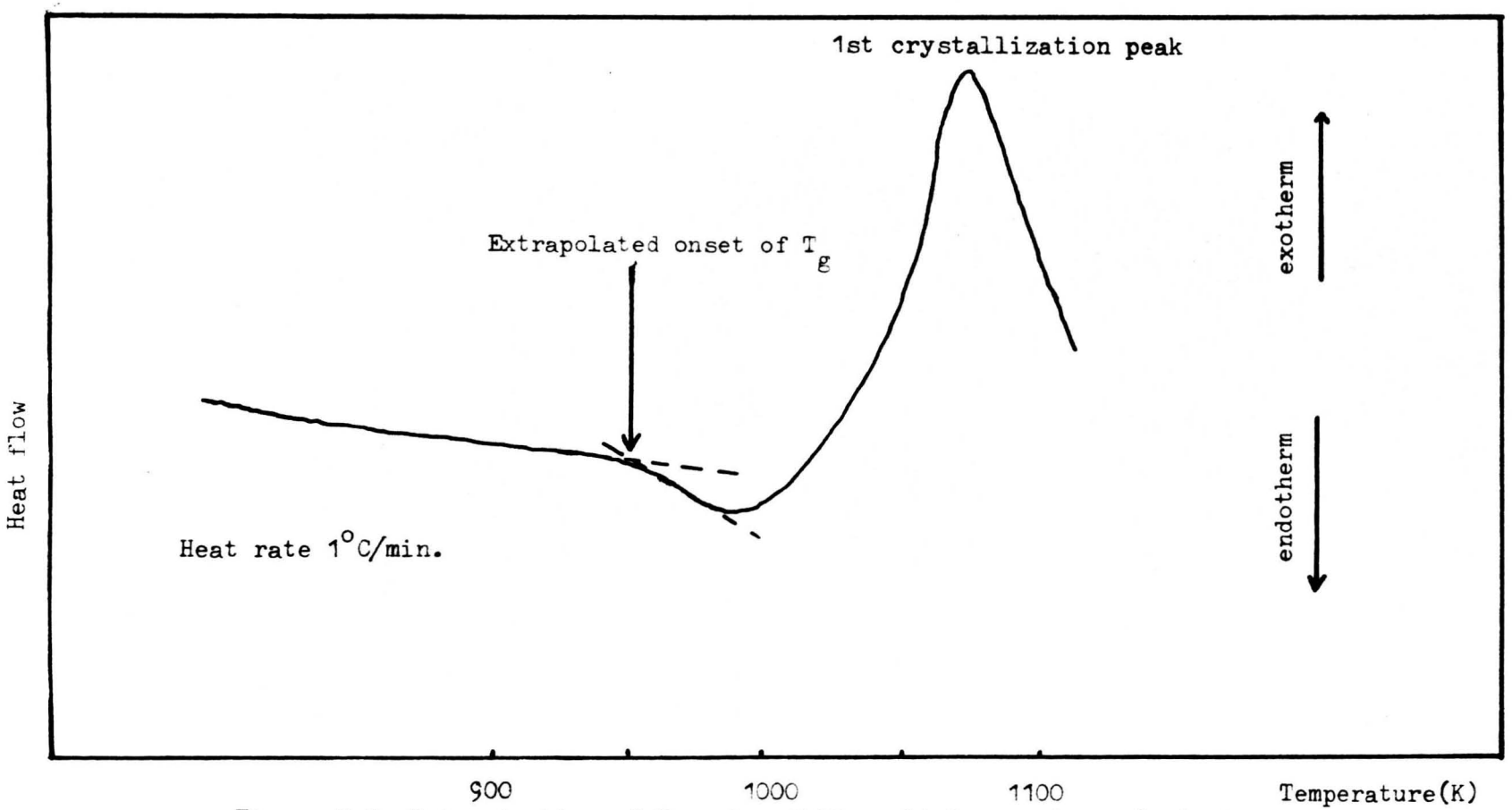

Figure 2.2. Determination of T_g using differential scanning calorimetry.

Annealing was carried out for 2 hours at the appropriate temperature and the glass was then allowed to cool down slowly to ambient temperature.

For many of the glasses hydration was not a problem. However, as a precautionary measure, samples were stored in evacuated desiccators until required for experiment.

One particular EXAFS study involved the comparison of two glasses from the same batch having different thermal histories. This required a rapdily quenched material obtained by drawing glass fibres from a single-tipped bushing furnace onto a rotating, mild steel drum.

2.1.2. Homogeneity

It is possible that phase separation may be so fine that it is unresolved by large angle X-ray scattering. In order to check this high resolution microscopy was attempted using a JEM 200 instrument.

Specimens were prepared by placing very thin slices of the glass (obtained by grinding or blowing bubbles directly from the melt) and placing them in a 5 keV argon, ion beam thinner until perforation.

Fig. 2.3a. and Fig. 2.3b. presents two micrographs obtained from this study. The mottled structure present is due to the carbon coating placed on the surface of the specimen to prevent charge build-up when under the electron beam. Fig. 2.3c. and Fig. 2.3d. are electron diffraction patterns complementary to the areas in a and b. The complete absence of structure and strong coherent diffraction suggests that the glasses are continuously amorphous and no phase separation has occurred. For some compositions, the stability of the sample in the presence of the beam was poor. In seconds, cavitation could be observed making analysis difficult.

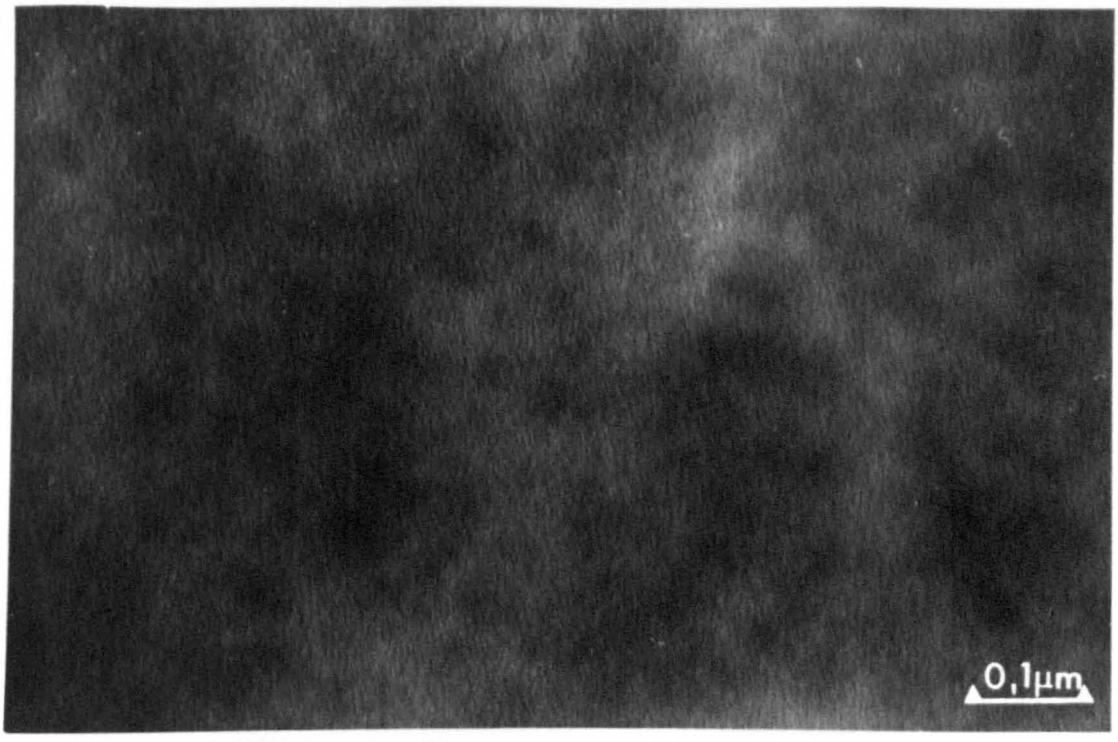

a)

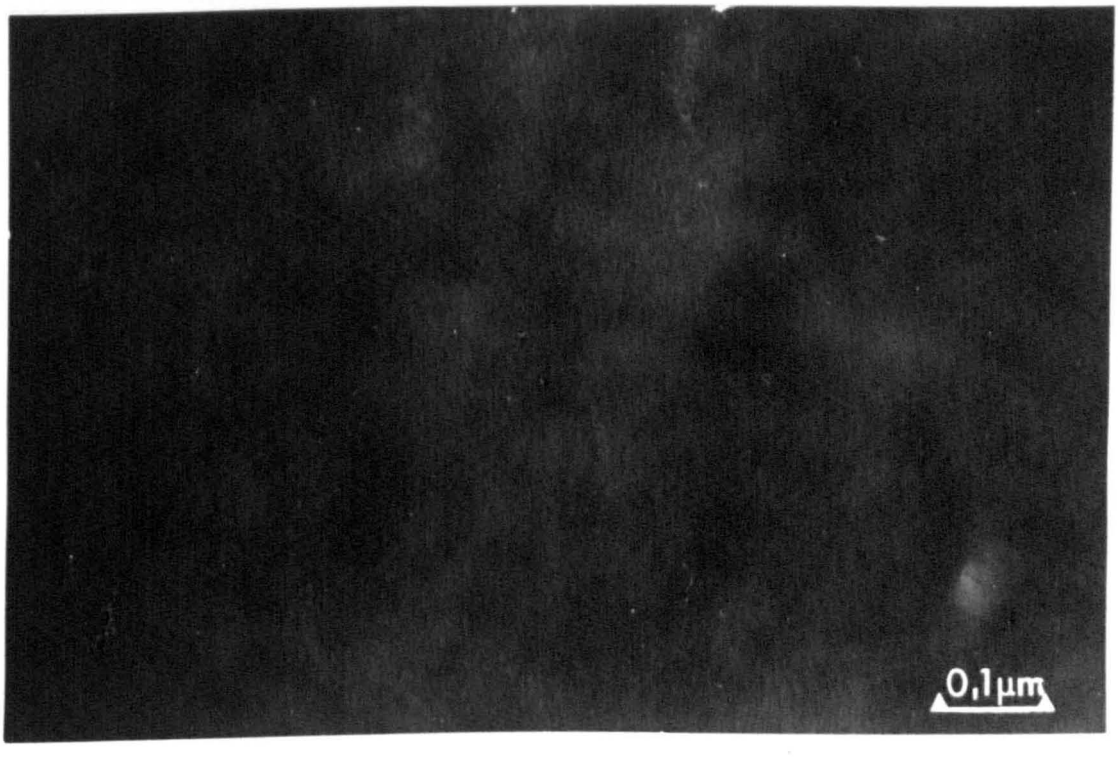

b)

Fig.2.3. Electron micrographs for samples:
a) ZrA and b) ZrE (see table IV)

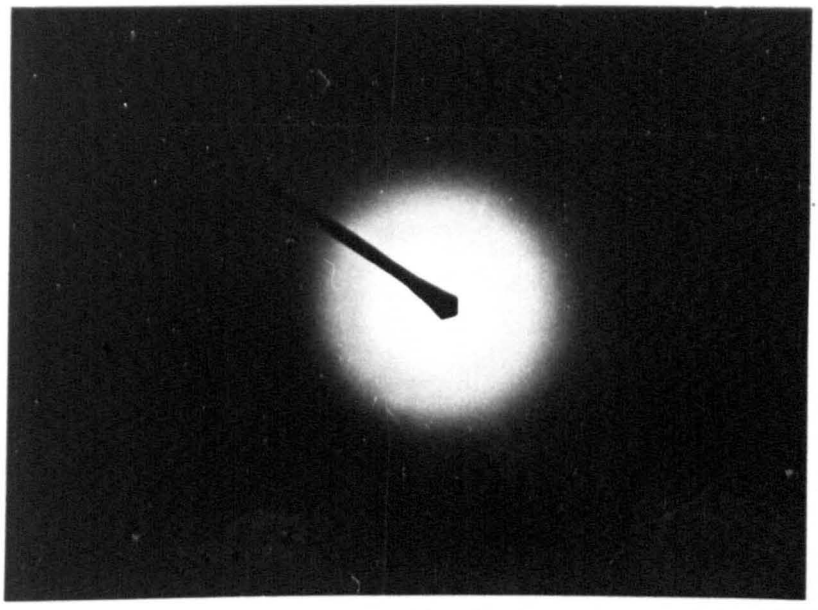

c)

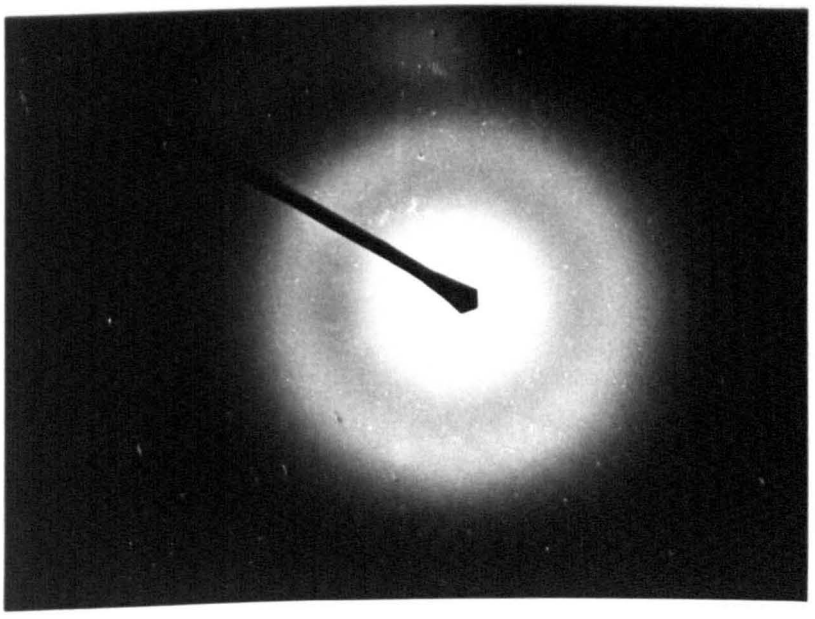

d)

Fig.2.3. Electron diffraction patterns taken from the same area as a) and b).

2.1.3. Crystal Preparation

For most of the data analysis comparison with model compounds is essential. Where possible, readily available 'Analar' grade laboratory chemicals were chosen. However, for some of the analysis more complex compounds were required. For the most part, these were chosen for their ease of growth and were obtained by solid state reaction and then checked for crystallinity using an X-ray powder camera.

2.1.4. EXAFS Specimen Preparation

Following Kincaid (1976), EXAFS specimens were prepared according to the specifications that the absorption thickness product (μt) should be ~ 1.2 at the edge in order to minimize the effects of inhomogeneities and harmonic contamination.

In any absorption process, the intensity of X-rays is logarithmically decreased according to the equation

$$I = I_0 \exp(-\mu t) \qquad (2.1.)$$

where I_0 and I are respectively, the intensities before and after absorption through a medium of absorption coefficient μ and thickness t. Experimentally $\ln(I_0/I)$ is measured as a function of photon energy.

The linear absorption coefficient can be calculated using the fact that, to a good approximation, the total mass absorption coefficient μ/ρ, for a material is related to the individual mass absorption coefficients of the elements comprising the material by the following additive equation

$$\mu/\rho = \sum_i g_i (\mu/\rho)_i \qquad (2.2.)$$

where $_i$ is the mass fraction contributed by the element i with mass

absorption coefficient $(\mu/\rho)_i$.

Once t has been determined, thin, parallel slices of glass were mounted onto brass blocks and polished on diamond paste wheels to a 1 μm finish.

The above procedure was found to work well for specimen thicknesses greater than 100 μm. Below this, specimens tended to crack and became unmanageable. To circumvent this problem, thin films of powdered samples were prepared by a technique used by Pettifer (1977). Slurries of the required material were prepared by mixing finely ground powder held in a suspension of amyl acetate and "durofix" glue, and cast onto "sellotape" and allowed to set. For each sample several films were cast and checked for homogeneity and pin-holes.

Alternatively, one further technique was used for the TiO_2-Na_2O-SiO_2 system which proved rewarding on two counts: glass bubbles were blown straight from the melt. This was a very quick way of obtaining thin films (~ 20 μm) and also permitted very fast rates of cooling.

2.3. SYNCHROTRON RADIATION

2.3.1. Introduction and History

Early electron accelerators were developed to study the plethora of particles produced when matter interacts at high energies, giving an insight into the forces that ultimately control nature.

Within the past twenty years however, cyclic accelerators have been used as a means of obtaining large X-ray fluxes This radiation is produced when the electron orbit is perturbed by an electro-magnetic interaction that maintains the closed orbit of the electron. This perturbation increases the electron acceleration and classically such

increases give rise to the emission of radiation, so-called synchrotron radiation.

Much of the early spectroscopic work was performed in a parasitic role, using already existing accelerators, and although this is in fact still true, increasingly more amounts of beam-time are being given to X-ray users. Moreover, within the past ten years dedicated synchrotron sources have been built in order to facilitate a whole range of atomic, molecular and solid-state physics experiments, together with an increasing amount of biological research (see Forty, 1979)

2.3.2. The Theory

The instantaneous power radiated by a charged particle undergoing acceleration can be written in Lorentz invariant form as:

$$P = \frac{2}{3}\frac{e^2}{m^2c^3}\left(\frac{dp}{d\tau}\frac{dp}{d\tau}\right) \quad , \qquad (2.3.)$$

where p is a 4-component momentum vector and $d\tau$ is the element of proper time. In the non relativistic limit, eqn. 2.1. reduces to the classical expression

$$P = \frac{2}{3}\frac{e^2}{c^3}a^2 \quad , \qquad (2.4.)$$

a being the particle acceleration. Lienard (1898) recognized that for a charged particle in circular motion, the rate of change of energy is small compared with the rate of change of momentum and under this approximation eqn. 2.3. reduces to

$$P = \frac{2}{3}\frac{e^2}{m^2c^3}\gamma^4\omega^2p^2 \qquad (2.5.)$$

since,

$$\left(\frac{d\gamma p}{d\tau}\right)^2 = \gamma^4 \left(\frac{dp}{d\tau}\right)^2 = \gamma^4 \omega^2 p^2$$

where $\omega = \frac{v}{R}$, R being the radius of the orbit.

Rewriting, we have

$$P = \frac{2}{3} \frac{e^2 c \beta^4}{R^2} \left(\frac{E}{mc^2}\right)^4 \qquad (2.6.)$$

That is, the power radiated is proportional to the fourth power in energy and inversely proportional to the square of the radius.

Schwinger (1949), in a theory of synchrotron characteristics from a classical standpoint, calculated the angular and spectral dependence of the instantaneous power. The most important equation to come from this theory is that

$$\lambda_c = \frac{2.35[R(m)]}{[E(BeV)]^3} \qquad (2.7.)$$

where λ_c is the maximum in the wavelength distribution function (Fig. 2.4a.). Eqn. 2.7. shows that the machine parameters (energy and radius) dictate the wavelength continuum obtained from a synchrotron. Schwinger also showed that the dipole radiation pattern expected from an accelerating charge is warped forward into a direction tangential to the electron's orbit (Fig. 2.4c.). One further characteristic of the radiation is the high degree of polarization as a function of azimuth angle ψ (Fig. 2.4b.), indicating that at $\psi = 0$, the radiation is completely polarized with its electric vector parallel to the plane of the electron orbit.

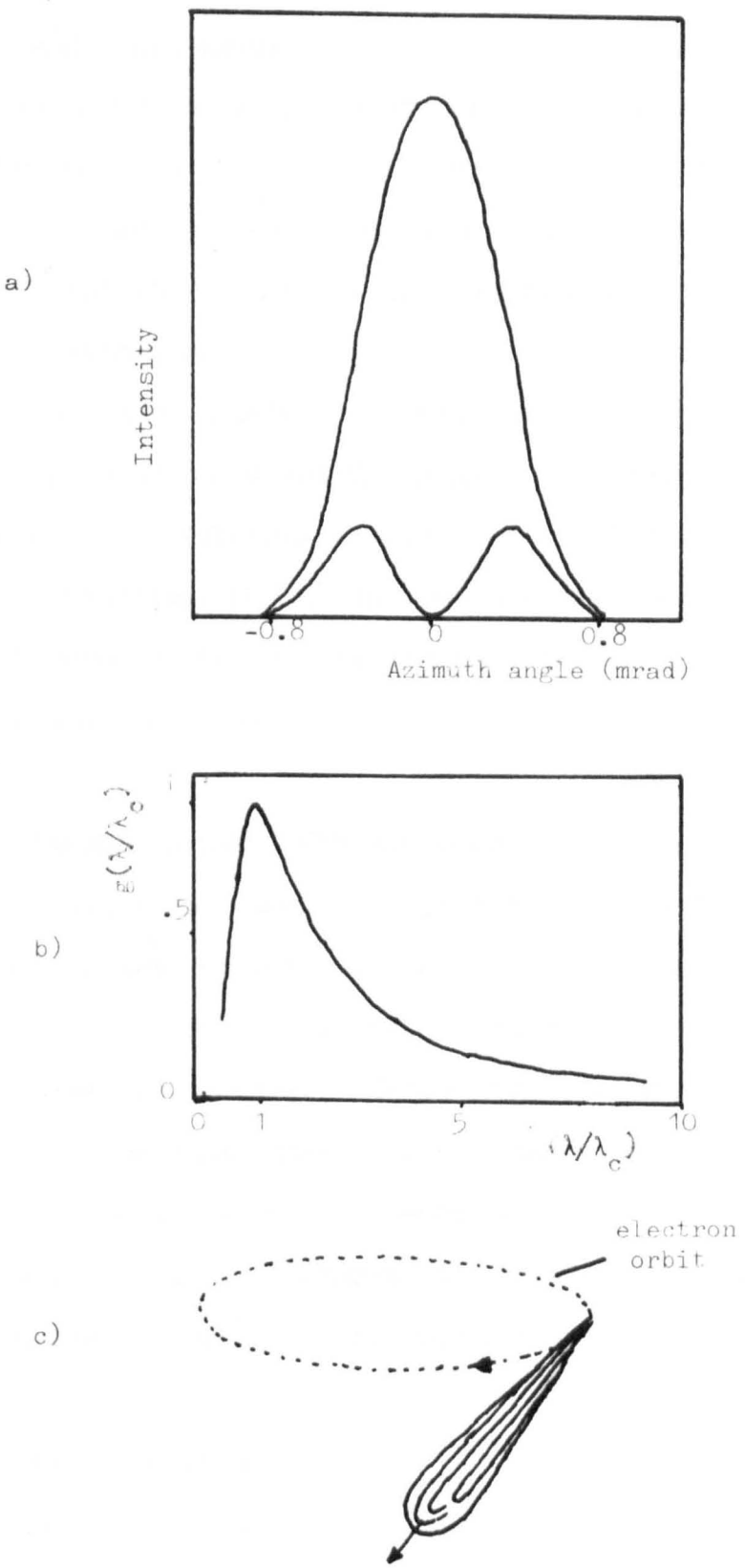

Fig.2.4. Characteristics of Synchrotron Radiation.(a) Angular and polarization distribution;(b) The universal power distribution g;(c) High energy dipole pattern.

2.3.3. Practical Aspects

Synchrotron radiation offers several substantial benefits over a conventional X-ray source: a continuum of X-ray wavelengths, enabling discrete energies to be sampled; a high photon flux; and highly polarized radiation enabling experiments to be performed on materials which exhibit dichroism dependence.

In absorption studies, all these effects have resulted in quite a dramatic increase in scientific output. For example, in 1976 the only EXAFS work being performed on glasses in the U.K., employed a laboratory X-ray set (Pettifer, 1977). This neccessitated many measurements on each material compared to the one spectrum (collected in approximately 30 minutes) taken on a synchrotron.

2.3.4. The Synchrotron Radiation Source

All absorption measurements presented herein were originally to be performed on the Synchrotron Radiation Source (SRS) at the Daresbury Laboratory. Unfortunately, several problems were encountered in using this equipment and, coupled with the unavailability of the Wiggler magnet, some of the absorption studies were taken elsewhere, namely Hamburg and Stanford. However, in the following sections, the experimental apparatus and techniques will be discussed with reference to the SRS, although the EXAFS instrumentation is usually standard.

2.3.5. Instrumentation

A schematic representation of the apparatus used is shown in Fig. 2.5. The system and computer software for data acquisition and control were designed at the Daresbury Laboratory.

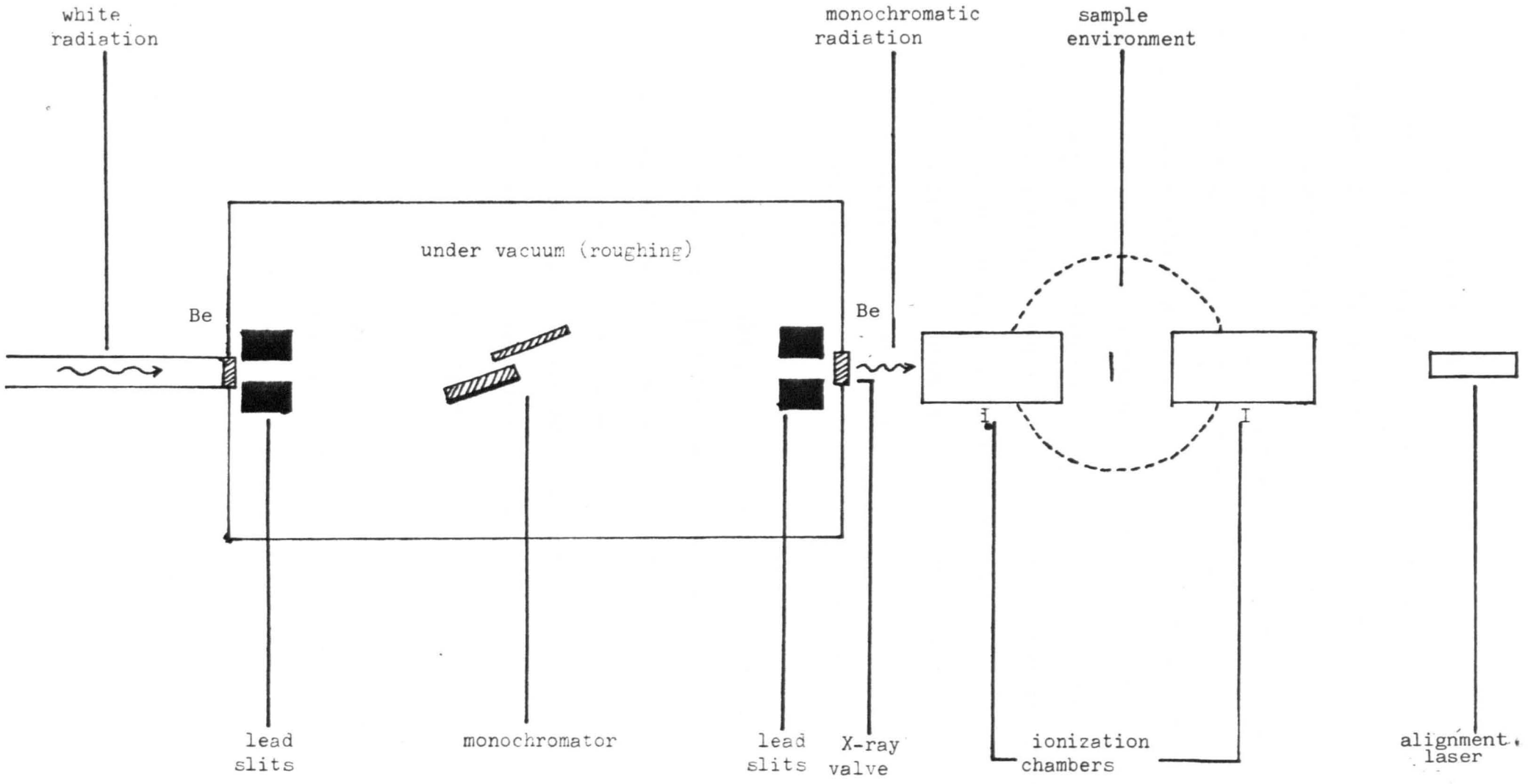

Fig. 2.5. Schematic Representation of EXAFS Equipment at the SRS.

1. Two types of monochromator were used for EXAFS measurements. Early results were taken using a channel-cut crystal; a two crystal arrangement manufactured from the same piece of material. Depending on the energy spectrum of the incoming radiation the diffracted beam will contain λ and the higher order harmonics $\lambda/2$, $\lambda/3$ ... etc. The presence of higher order harmonics significantly affects absorption measurements. Of the two channel cut crystals available, viz. Si 220 and Si 111, the latter was preferred as its second order harmonic is forbidden and therefore measurements taken at 3 $\mathring{A}$ were not contaminated by 1 $\mathring{A}$ radiation; a wavelength that is near to λ_c for the SRS. For higher energies (L-edges of Hf) it would be more beneficial to use a Si 220 crystal. If higher harmonics are a problem, the pressure in the ionization chambers could be reduced so as to absorb less of the second harmonic. This sacrifices some of the fundamental intensity, but at these energies such a loss is tolerable.

By late 1982, the Si 220 double crystal monochromator (Bonse et al., 1976 and Hart and Rodriguez, 1978) had been fully commissioned. This had the advantage over a single-cut monolith in that by detuning the one crystal with respect to the other it was possible to reduce the harmonic content of the exiting beam. The degree of harmonic rejection depended on the X-ray energy. For Ti (K-edge = 4966 eV) the harmonic rejection needed to be high, ~ 55%. For Hf, (L_I edge = 11270 eV) this could be lowered to ~ 10%.

For the case of Zr (K-edge = 17998 eV) the rocking curve of the crystal is very narrow and consequently the instrument becomes sensitive to vibrations from the surroundings, e.g. vacuum pumps. This coupled with the effect of crystal heating in the presence of the white beam, which alters the d-spacing, made the instrument's performance very poor at hard wavelengths. It was for this reason that measurements on the Zr edge were

taken elsewhere.

2. The post exit slit consisted of two lead blocks incorporated into a clockwork mechanism that enabled each block to be moved vertically with respect to each other. This arrangement could then be used to select only the monochromatic beam and tailor it accordingly to match the sample size and shape. Fig. 2.6a. shows the diffraction profile immediately after the monochromator, where the intense beam corresponds to the straight-through or primary beam. Fig. 2.6b. is the same diffraction profile but taken after the post exit slit, showing how all the other reflections, apart from the desired monochromatic beam, have been eliminated.

3. Due to the high intensity of synchrotron radiation, ionization chambers were used for the detector system. The ion chambers absorb an amount of radiation which is proportional to the X-ray energy. Therefore, the total absorption at the first ion chamber should be sufficient to obtain a good signal to noise ratio, but should not be so much as to prevent enough flux reaching the sample and second ion chamber.

4. All room temperature measurements were performed in air at atmospheric pressure. Low temperature measurements (77 K) were taken at SSRL (Stanford) for the ZrO_2-containing system. Samples were wrapped in 'aluminium foil' to produce a good thermal contact and housed in a "cold finger" cryostat. This technique was also attempted at the SRS for TiO_2-containing glasses. Unfortunately, the presence of the milar windows appreciably attenuated the X-ray intensity in the second ion chamber and made EXAFS measurements impractical.

a)

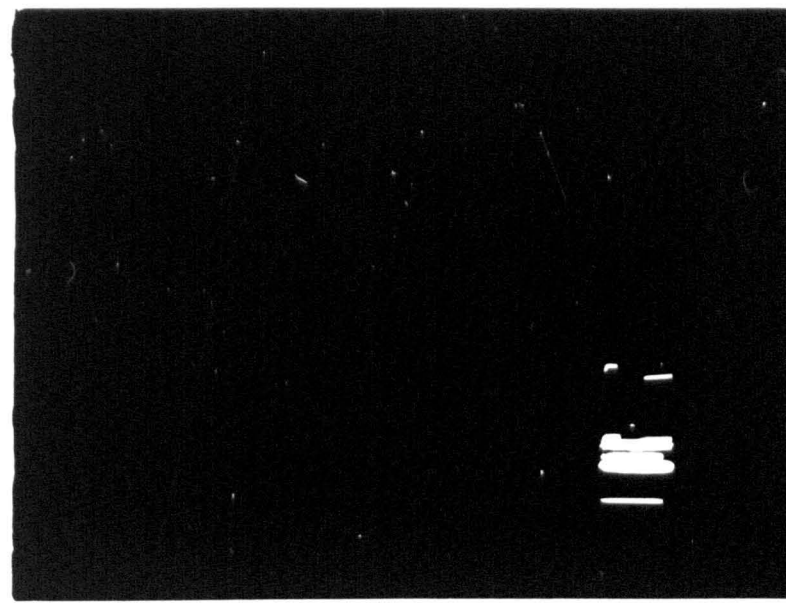

b)

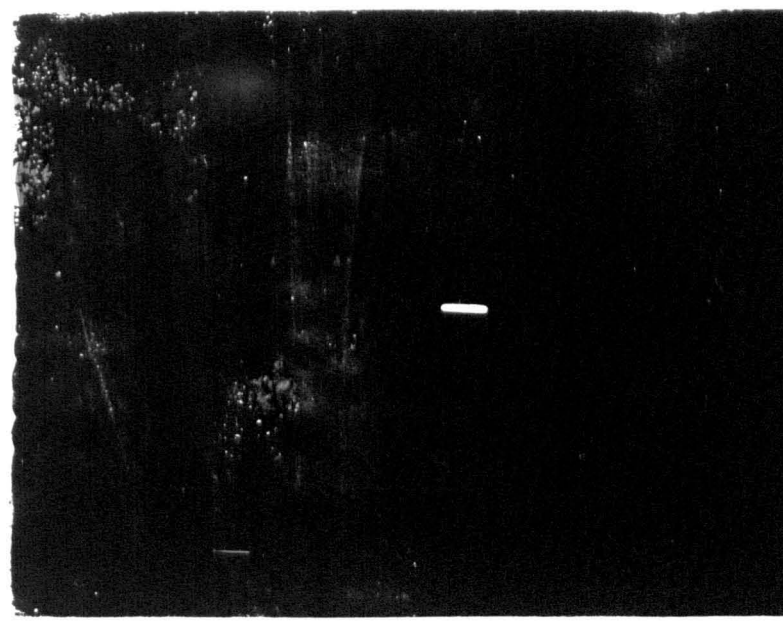

Fig.2.6 Polaroid photographs showing the synchrotron beam profile:

a) immediately after the monochromator and:

b) after the post exit slit.

5. Data acquisition and instrument control were achieved via a PDP 11 mini-computer. The current from the ionization chambers was passed through amplifiers operating at typically 10^9 gain. The output voltages were then directed through a voltage to frequency converter (v-f) and registered by a scaler, operating at a time gate specified by the output signal. At zero voltage the v-f converters produce a minimum frequency which must be offset from the data taken to obtain the true absorption.

The monochromator position was controlled by means of a stepping motor and the degree of increment pre-set before the experiment. This enabled the user to select different energy resolution requirements for particular regions of the spectrum. For example, near the edge, the monochromator would be set for energy intervals of 1 eV whilst at the high energy side this would be increased to say, 5 eV.

The table height was also adjusted so as to keep the sample area exposed to the beam constant. The table height h is given by,

$$h = 2D \cos\theta$$

where D is the inter cyrstal spacing and θ the crystal angle from the horizontal.

2.3.6. Normalization

A typical X-ray absorption spectrum is shown in Fig. 2.7. for the L-edges of Hf in HfO_2, taken using the double crystal monochromator (10% harmonic rejection) with the electron beam of the synchrotron operating at 170 mA at 2G eV. Data collection time for the whole spectrum was around 1 hr and allowance was made for the decay of the beam within this period. Preliminary data reduction has been performed on this spectrum in order to remove background effects from the measuring system, such as absorption of

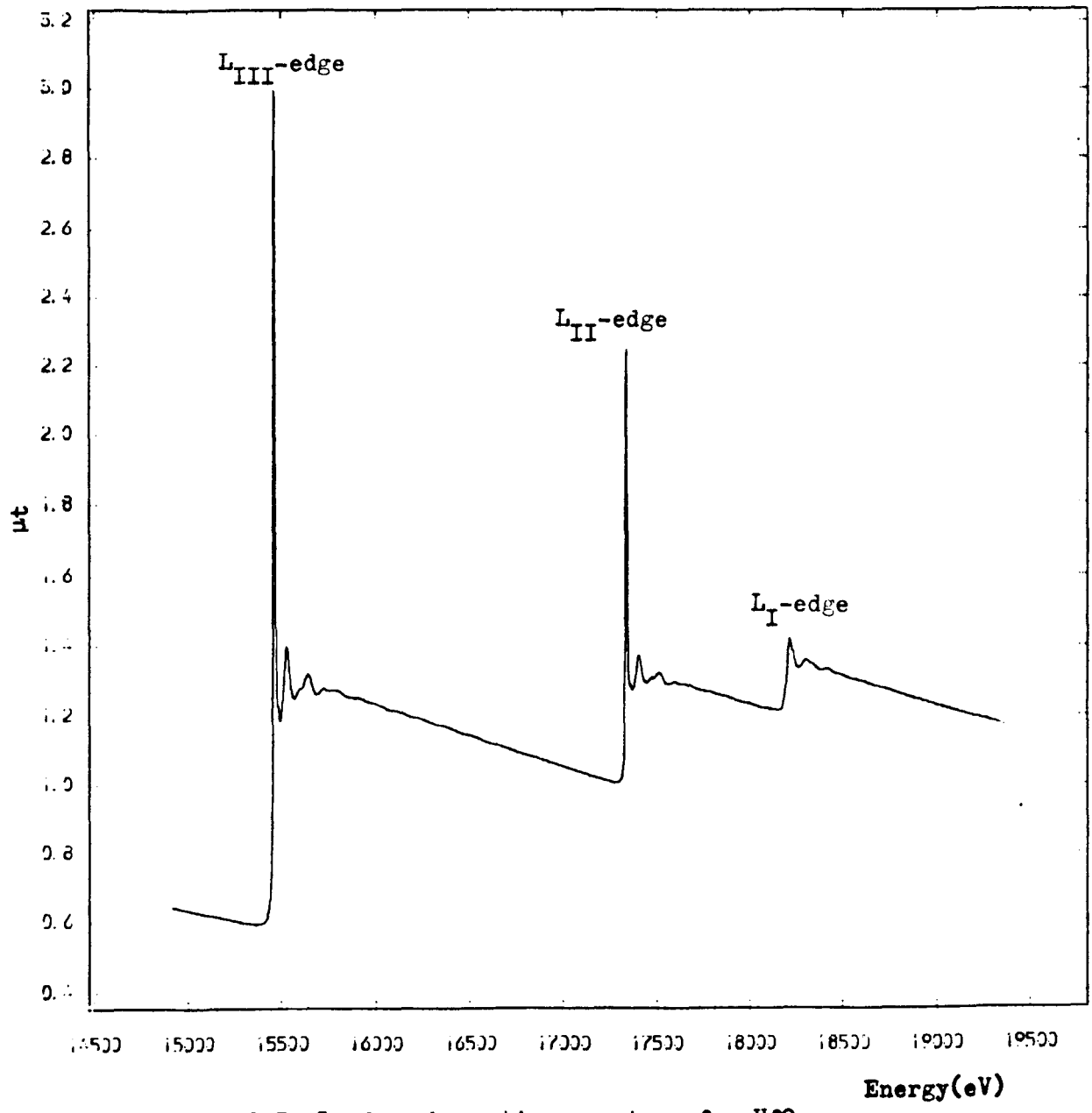

Figure 2.7. L-edge absorption spectrum for HfO_2.

the air or He. To do this, ionization chamber signals are measured over the same range of photon energy with no sample present. This normalization spectrum is then subtracted from the sample spectrum to give a true measure of μt.

Chapter 3

THEORY AND INTERPRETATION OF EXAFS

3.1. THEORY OF EXAFS

The X-ray absorption spectrum of a material is characterized by a series of abrupt rises in absorption due to the excitation of core electrons. For photon energies sufficient to eject such an electron from the confines of its parent atom, the annihilated photon energy $h\omega$ (ω is the frequency of the incident X-ray photon) is given up as kinetic energy to the photoelectron, i.e.

$$E_{K.E} = \hbar\omega - E_b \qquad (3.1.)$$

where E_b is the binding energy of the core electron.

For nearly all materials, on the high energy side of the edge, the absorption is characterized by oscillations that extend for several hundred eV - so-called EXAFS - (Fig. 3.1.). In order to understand this phenomenon, eqn. 3.2. gives the probability of X-ray absorption under the dipole approximation,

$$P = \frac{2\pi e^2}{mc^2\omega} |M_{fi}|^2 \rho(E_f) \qquad (3.2.)$$

where M_{fi} is the matrix element $\langle f|\underline{\varepsilon}.\underline{r}|i\rangle$, $\underline{\varepsilon}$ being the electric field polarization vector and $\rho(E_f)$ is the density of states at the final state energy, E_f. For energies well above the edge $\rho(E_f)$ is approximated by a free electron density of states of energy

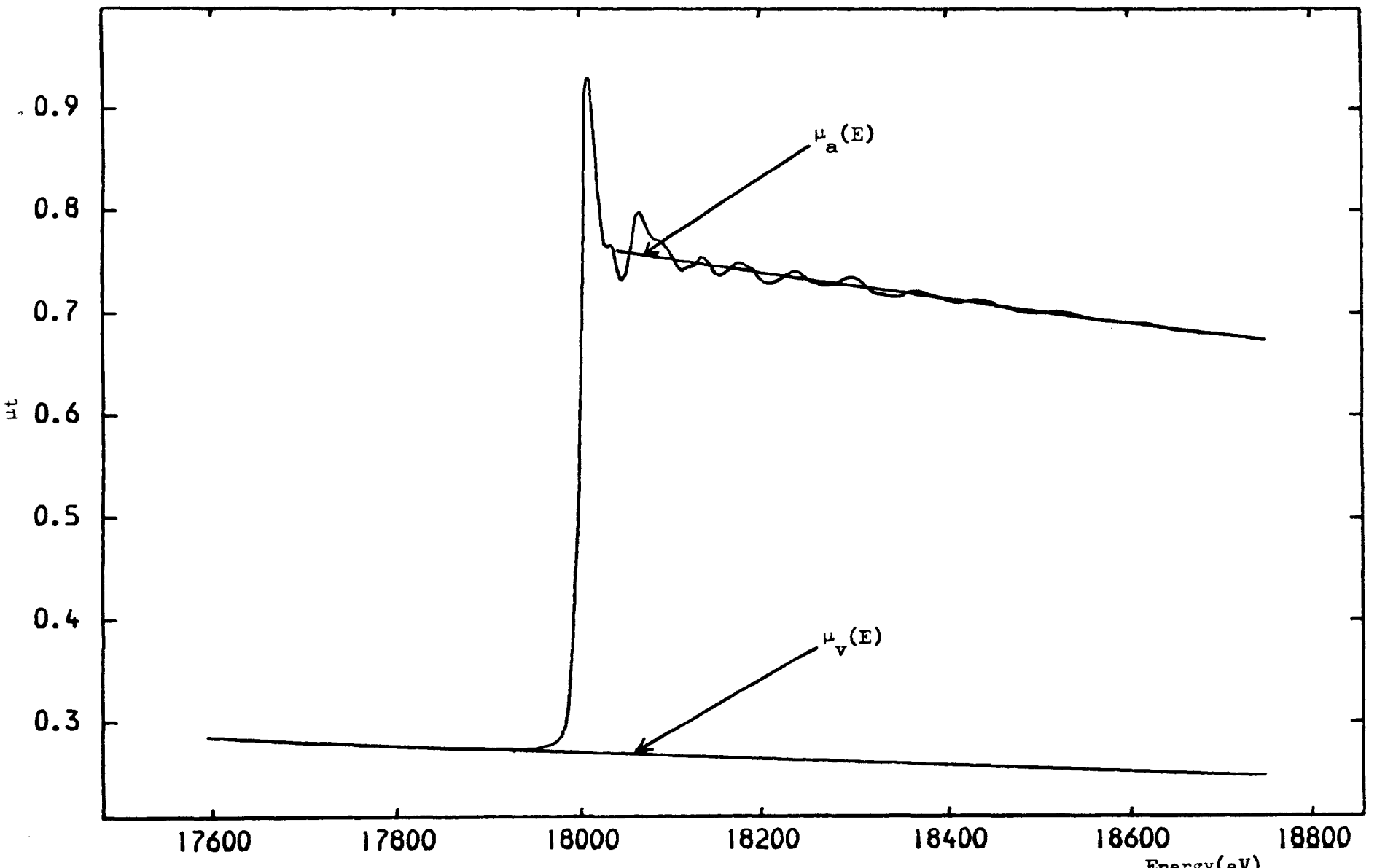

Figure 3.1. Method for extracting the EXAFS from the total absorption coefficent according to equ. 3.3.

$$E = E_0 + \frac{\hbar^2 k^2}{2m} \qquad (3.3.)$$

Under these assumptions the oscillations must arise from variations in the matrix elements. As the initial state has $l = 0$, the variations are inherent in $|f\rangle$ (necessarily of "p-type" character) as a function of ω

It is interesting to note, that the original theory of EXAFS (Kronig, 1931) held that the oscillations were due to a fluctuating density of states between allowed and forbidden energy bands. This theory became known as the long range order (LRO) approach as it is essentially couched in a band structure formulism.

Now, for the cases of condensed matter and some gases, the form of $|f\rangle$ will take on two contributions: an outgoing wave from the central atom and a back-scattered contribution from the surrounding atoms. If these two waves interfere constructively, it will give rise to a peak in the EXAFS, if they interfere destructively a trough will appear. Furthermore, due to the highly localized nature of the initial 1-s state the overlap of matrix elements occurs at approximately $r = 0$.

For the particular case of point scattering, these assumptions were used by Sayers et al. (1970) to formulate the first successful EXAFS theory. This has since been revamped and generalized by Lee and Pendry (1975) to the case of amorphous systems. Under successive approximations concerning the curvature of the wave in the asymptotic plane wave limit (APW) the EXAFS function may be written as

$$\chi(k) = \sum_j \frac{N_j}{kr_j^2} |f_j(\pi)| \sin(2kr_j + 2\delta_1 + \psi_j)$$

$$X \exp(-2\sigma_j^2 k^2) \exp(-2r_j \gamma) \qquad (3.4.)$$

where the summation is over j shells at distances r_j from the central atom, containing N_j identical atoms. $f_j(\pi)$ is the back scattering amplitude of the jth shell. The phase term 2δ, results from a contribution of δ_1 in the waves outward and inward trips as it experiences the excited atom's potential. ψ_j is the phase of the back-scattering factor $f_j(\pi)$, defined as

$$f_j(\pi) = |f_j(\pi)|e^{i\psi_j} \qquad (3.5.)$$

and does not appear explicitly in the original theory of Sayers et al. The two exponential terms are: (i) a Debye-Waller factor with σ_j^2 being the mean square relative displacement of absorber and scatterer (Schmidt, 1963) and (ii) a factor which reflects the attenuation of the outgoing wave due to elastic scattering into an incoherent state. γ^{-1} is the inelastic mean free path of the electron. Sayers et al. included this term as an empirical damping factor but in the subsequent theory, this damping is expressed as an imaginary part ζ to the photo-electron energy E such that

$$k = [2(E + i\zeta)]^{\frac{1}{2}} \sim (2E)^{\frac{1}{2}} + i\zeta/(2E)^{\frac{1}{2}} \qquad (3.6.)$$

Thus, it is possible to equate $\zeta/(2E)^{1/2}$ to γ in eqn. 3.4.

Eqn. 3.4. has been formulated using atomic units ($e = m = \hbar = 1$) such that the unit of energy is now the Hartree (1 Hart = 27.20 eV) and the unit of distance is the Bohr radius ($1^c = 0.529177$ Å).

3.2. INTERPRETATION OF EXAFS SPECTRA

Within the EXAFS function lies a whole wealth of information about

the local environment of particular atoms. In order to evaluate these highly desirable parameters there are three routes which may be followed, these are: (1) a real space formalism to produce a radial distribution function by means of a Fourier transform; (2) least squares fitting of eqn. 3.4. using theoretically determined scattering data; and (3) a combination of (1) and (2) in which individual peaks in the FT are transformed back into k-space and parameterized expressions for the phase and amplitude functions, for that shell, are determined by comparison with suitable model compounds

3.2.1. Isolation of the EXAFS

From Section 3.1. it was shown that the true absorption $\mu(k)$ above the edge may be thought of as modifications of the monotonically decreasing absorption of an isolated atom $\mu_a(k)$, due to the interference effect, that is

$$\mu(k) = \mu_a(k) \, [1 + \chi(k)] + \mu_v(k) \qquad (3.7)$$

where $\mu_v(k)$ represents absorption due to events other than K-shell excitation. This may be approximated by a Victoreen (1962) (eqn. 3.8.) polynomial. $\mu_a(k)$ is modelled by a further polynomial passing through the EXAFS and defines the zero of the fine structure.

$$\mu_v(k) = A\lambda^3 + B\lambda^4 \qquad (3.8.)$$

The fitting range for eqn. 3.8. was typically taken from about -150 to -30 eV below the edge and extrapolated to higher energies. For the polynomial above the edge, the range was ~ 35 eV to the end of the data. This procedure is shown in Fig. 3.1. Using eqn. 3.7. we may now define the

EXAFS function as

$$\chi(k) = \frac{\mu(k) - \mu_a(k) - \mu_v(k)}{\mu_a(k)} \qquad (3.9.)$$

The background subtraction and normalization procedure results in $\chi(k)$ being the fractional change in absorption and is independent of specimen thickness.

3.2.2. Fourier Transform

The Fourier transform (FT) of eqn. 3.4. will, in the absence of any phase shift, result in a series of Gaussians - see eqn. 3.10. - that peak at the bond distance $r = r_j$, the amplitude of which is a measure of $N_j/r_j 2$ attenuated by the degree of disorder σ_j^2, whether dynamic (thermal) or static (glassy). The width and shape of the peak results from a convolution of the distribution function with an amplitude function containing the back scattering and mean free path terms. The FT is broadened further by the necessity to restrict the data due to inadequacies in the theory for low energy data and disorder effects at high energies. The choice of the window function is not unique. There are typically three main forms used: the square window, the Gaussian window and the Hanning window. The latter two are more commonly used as these suppress the side lobes produced by the convolution of a square window, making interpretation easier. For the purposes of this work, the Hanning function was preferred (see Section 4.2.). Varying the limits of the window will also affect the height and position of the peaks. (This underlines the importance of keeping the range of data constant when comparing FT's).

The decay of the EXAFS amplitude is an additional problem as damped sine waves have extra sidebands that will further broaden the peaks. To

sharpen the FT an attempt is usually made to compensate for this attenuation by weighting the experimental spectrum by a factor of k^n, so biasing the high energy region. The weighting parameter n is usually chosen as

	3	for 1st and 2nd rows of the periodic table
	2	for row 3
and	1	for rows > 3.

Therefore the FT that is actually taken is

$$F(r) = \frac{1}{\sqrt{2\pi}} \int W(k)\ k^n \chi(k)\ e^{2ikr} dk$$
$$= \frac{1}{2} \sum_j \frac{N_j}{r_j^2 \sigma_j} \exp \frac{(r - r_j)^2}{\sigma_j^2} \qquad (3.10)$$

For the case of a non-zero phase shift, Sayers et al. (1972) showed that if the total phase parameter $\alpha_j(k)$ can be expressed thus:

$$\alpha_j(k) = 2\delta_1 + \psi_j = -ak + b \qquad (3.11.)$$

a form first used by Mott (1963), then structural features will be shifted in real space by an amount a/2.

Thus, it is now possible to extract structural information from unkown compounds by a direct comparison of the quasi-RDF's for each material with a known or model compound. From the latter it is possible to determine the bond-distances in the unknown by evaluating the parameter a. Relative measures of N_j and σ_j^2 are also possible in systems where there is additional structural information through temperature dependent EXAFS measurements

Hayes (1978) has presented a formalism for interpretation of EXAFS data in real space, beneficial in its application to disordered systems. $\chi(k)$ is separated in to two terms containing: (1) structural information couched in $\rho(r)$; and (2) the complicated energy dependent terms within the parameter $\Omega(k)$. Thus for an absorber α and scatterer β.

$$k\chi_\alpha(k) = \sum_\beta \int \frac{dr}{r^2} \rho_{\alpha\beta}(r) 2Re[e^{2ikr}\Omega_{\alpha\beta}(k,r)] \qquad (3.12.)$$

where

$$\Omega_{\alpha\beta} = (-2i\pi^2)t_\beta(k,-k)\exp[-2\mu(k)r + 2i\delta_\alpha(k)] \qquad (3.13.)$$

$\rho_{\alpha\beta}$ is the RDF of atomic species β relative to atoms of type α. Comparison of eqn. 3.12. with eqn. 3.4. shows that $t_\beta(k, -k) = f(\pi)$ and $\mu = \gamma$.

Using the convolution theorem eqn 3.12. can be written as

$$F(r) = \sum_\beta \int \frac{dr'}{r'^2} \rho_{\alpha\beta}(r')\xi_{\alpha\beta}(r - r') \qquad (3.14.)$$

where $\xi_{\alpha\beta}(r-r')$ is the FT of $W(k)k^n\Omega(k',r)$

From eqn 3.14. it is easy to see why EXAFS has a distinct advantage over diffraction techniques (eqn. 1.7.) for which the spectra contain all atom-atom correlations. In EXAFS, the local environment about one particular α is sampled and thus for multi-component systems partial quasi-RDF's are readily available.

As was mentioned earlier, to obtain structural information, direct comparison with model compounds is essential. Such a procedure is known as the principle of chemical transferability. For the case of disordered systems the justification for invoking such a principle is not readily

apparent as the pair distribution function in these cases may possess asymmetries which will invalidate such a transfer - see Brown and Eisenberger (1979).

Although the FT technique possesses many limitations, its use as a first step in any further curve fitting analysis is invaluable as it gives a real space picture of a system, on the basis of which provisional models may be postulated. The next section will now concern itself with these more accurate techniques.

3.2.3. Curve Fitting

The estimation of structural parameters from the FT suffers from the artefacts inherent in the mathematical interpretation. As will be shown, the particular choice of model compounds in one study (Chapter 4), the overlapping of coordination shells makes interpretation from comparison of FTs difficult. Moreover, for disordered systems in general, the range of data in k-space is of limited extent which significantly affects the height and shape of the peaks in the FT further decreasing the resolution.

However, curve fitting techniques offer a considerable increase in resolution in the determination of structural parameters although computational requirements are greatly enlarged. The methodology is simple: an initial guess is made (usually from an examination of the FT) from which the corresponding theoretical equation given in eqn. 3.4. is calculated and compared with the experimental EXAFS. This initial guess is then refined to make a further estimation; and so it carries on, in an iterative procedure, until a minimum in the sum of the squares is reached. The exact procedure is discussed in more detail in Appendix A.

A pre-requisite of the curve fitting algorithm is the knowledge of the phase and amplitude functions. There are two different methods used to obtain this information: either *ab initio* calculations are performed;

or the functions are approximated by a comparison with suitable model compounds.

3.2.4. Calculation of Amplitude and Phase Functions

Theoretical calculations of the phase shift commence with an assumption of the potential experienced by the photoelectron. This can be thought of as being due to the nucleus, other electrons and exchange correlations. To evaluate the phase shift δ_1, it is necessary to compare the solutions of the Schrodinger equation, in the presence of this potential, with those derived in its absence. Lee and Pendry (1975) calculated the matrix element using core wavefunctions after Herman and Skillman (1963). Here the potential is described in a 'muffin-tin' type scheme: a spherically symmetric potential up to a distance $r_{M.T}$, typically half the distance between absorber and scatterer and constant for $r \geq r_{M.T}$, and treating the central atom as neutral. This latter assumption was noted by Lee and Pendry to be a limiting factor in their theory (*vide infra*).

From the central atom phase shifts δ_1, the back-scattering amplitude and phase may be calculated thus

$$f(\pi) = \frac{1}{k} \sum_{0}^{\infty} (2\ell + 1)(-1)^{\ell} \sin(\delta_\ell) e^{i\delta_\ell} \qquad (3.15.)$$

and

$$\psi(k) = \arg[f(\pi)] \qquad (3.16)$$

In order to circumvent the complicated process of the calculation of phase and amplitude functions for each material, Teo and Lee (1979), on the basis of an electron scattering theory formulated by Lee and Beni

N.B. $\delta_\ell \equiv \delta_1$ in eqn. 3.15. and has been changed for reasons of clarity.

(1977) have tabulated this data for a cross-section of elements: $6 \leq Z \leq 82$. Their results were calculated for a range of photoelectron wavevector $4 < k \leq 15$ A^{-1}. In the theory several assumptions were made: the curvature of the wave was neglected and treated in the APW limit; relaxation effects of the atom were approximated by using an unscreened Z + 1 wavefunction, (for a consistent model low momentum electrons would experience a potential described by a screened Z + 1 ion whilst for high k electrons and unscreened Z (fully relaxed) potential would be more appropriate); and the atomic potentials were treated by overlapping muffin-tins. Lee and Beni point out that many of these approximations may be compensated for by varying E_0 in eqn. 3.3.

It must be noted that the phase shifts are only uniquely defined once the energy threshold has been fixed. Varying E_0 by ΔE_0 will alter the photoelectron momentum by

$$k' = \left[k^2 - \frac{2\Delta E_0}{7.62}\right]^{\frac{1}{2}} \qquad (3.17.)$$

The corresponding phase shift modification will then be

$$\alpha(k') = \alpha(k) - 2(k' - k)r$$

$$\simeq \alpha(k) + 2r\Delta E_0/7.62\ k \qquad (3.18.)$$

This shows that phase shifts are more sensitive to a change in E_0 at low k rather than at high k.

The above description has been shown by Pettifer (1977) to be seriously in error for heavy scatterers, below 200 eV. Thus it is essential to use the full theory (curved-wave) of Lee and Pendry at low energies.

So far in this theory only single scattering has been discussed. Due to the similarity between the EXAFS process and low energy electron diffraction (Pendry, 1973) it is expected that at low photoelectron energies, multiple scattering effects will contribute to the fine structure. Furthermore, the strong forward scattering component becomes important when one atom shadows an outerlying atom in another shell. Lee and Pendry do discuss multiple scattering effects although they are computationally difficult to evaluate. One alternative method used by Ashley and Doniach (1975) introduces, on an *ad hoc* basis, a parameter W_j which partially accommodates multiple scattering into a single scattering scheme. W_j is described as a shell penetration factor to account for the electron flux that is scattered when passing through a shell j.

3.2.5. Approximations of the Phase and Amplitude Functions

Eqn. 3.4. may be expressed simply as a sinusoidal term modulated by an envelope function thus:-

$$\chi(k) = \sum_j A_j(k)\sin(2kr_j + \phi_j) \qquad (3.19.)$$

where, as a matter of convention ϕ_j is defined as

$$\phi_j(k) = \alpha_j(k) - \pi \qquad (3.20.)$$

and

$$A_j(k) = \frac{N_j}{r_j^2} |f_j(\pi)| \exp(-2\sigma_j^2 k^2) \exp(-\gamma r_j) \qquad (3.21.)$$

In this scheme, structural parameters are deduced by approximating $A_j(k)$ and $\phi_j(k)$ by some parameterized expression and using these in

the least squares fitting of the experimental data. They are calculated with reference to a model compound and the approximations are then transferred to an unknown, but chemically similar, system. The justification for utilizing the concept of chemical transferability is based on the premise that, to a good approximation, the form of the phase and amplitude function is governed by the core electron densities of the absorber and scatterers and is not affected by the valence electrons which ultimately determine the chemistry. Citrin et al. (1976) demonstrated the validity of the concept of chemical transferability for a whole range of materials.

In this work, rather than expressing all the amplitude factors in the function A(k), they are explicitly expressed in the theoretical equation and only the back-scattering function is approximated. As a result it is not possible to extract the value of σ_j^2 *per se* but rather a relative measure of $\Delta\sigma_j^2$ is calculated with respect to the model compound. Two forms for f(k) have been used in the past; firstly it can be expressed by means of a Lorentzian function,

$$f(k) = \frac{B}{C + (k - D)^2} \qquad (3.22.)$$

a form found by Teo et al. (1977) to be applicable for atoms with $Z \leq 36$. However, for light atoms Cramer and Hodgson (1977) preferred the more rapidly decreasing form:-

$$f(k) = \frac{c_0 \exp(-c_1 k^2)}{k^{c_2}} \qquad (3.23.)$$

where the $1/k^c$ factor models the electron back-scattering from such atoms, whilst the exponential term parallels the Debye-Waller factor.

The most general form for the phase shift has been offered by Citrin

et al., namely,

$$\phi(k) = a_0 + a_1 k + a_2 k^2 \qquad (3.24.)$$

For the purposes of this work, the majority of the EXAFS contribution is due to oxygen scattering. In this case eqn. 3.23. is more applicable and Fig. 3.2. compares the theoretical data of Teo and Lee (1979) with the parameterized amplitude function, as can be seen the fit is well matched. Similarly, it is possible to test the quadratic form of eqn. 3.24. with the corresponding data for the central atom phase shift (Zr) and the scatterer phase (O), together with the combined phase, $2\delta_1 + \psi$. The result is shown in Fig. 3.3. and the results for the floated parameters are given in Table III.

a_0	11.892
a_1	-1.698
a_2	0.044
C_0	0.12
C_1	0.026
C_2	1.97

TABLE III

Calculated coefficients for the parameterized amplitude (Oxygen) and phase (Zr-O) functions using theoretical data obtained by Teo and Lee (1979)

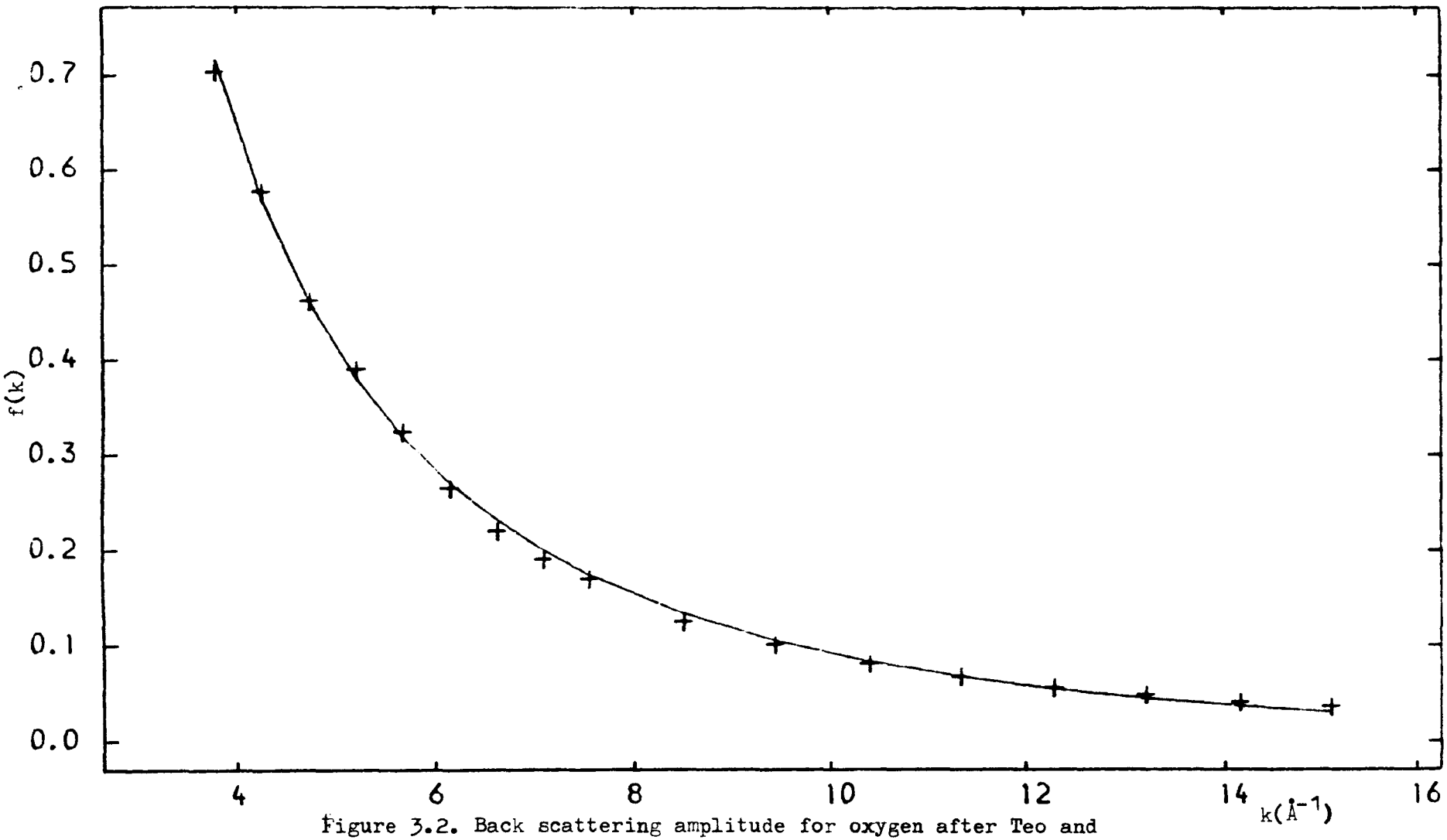

Figure 3.2. Back scattering amplitude for oxygen after Teo and Lee (+), solid line is the least squares fit using equ. 3.23.

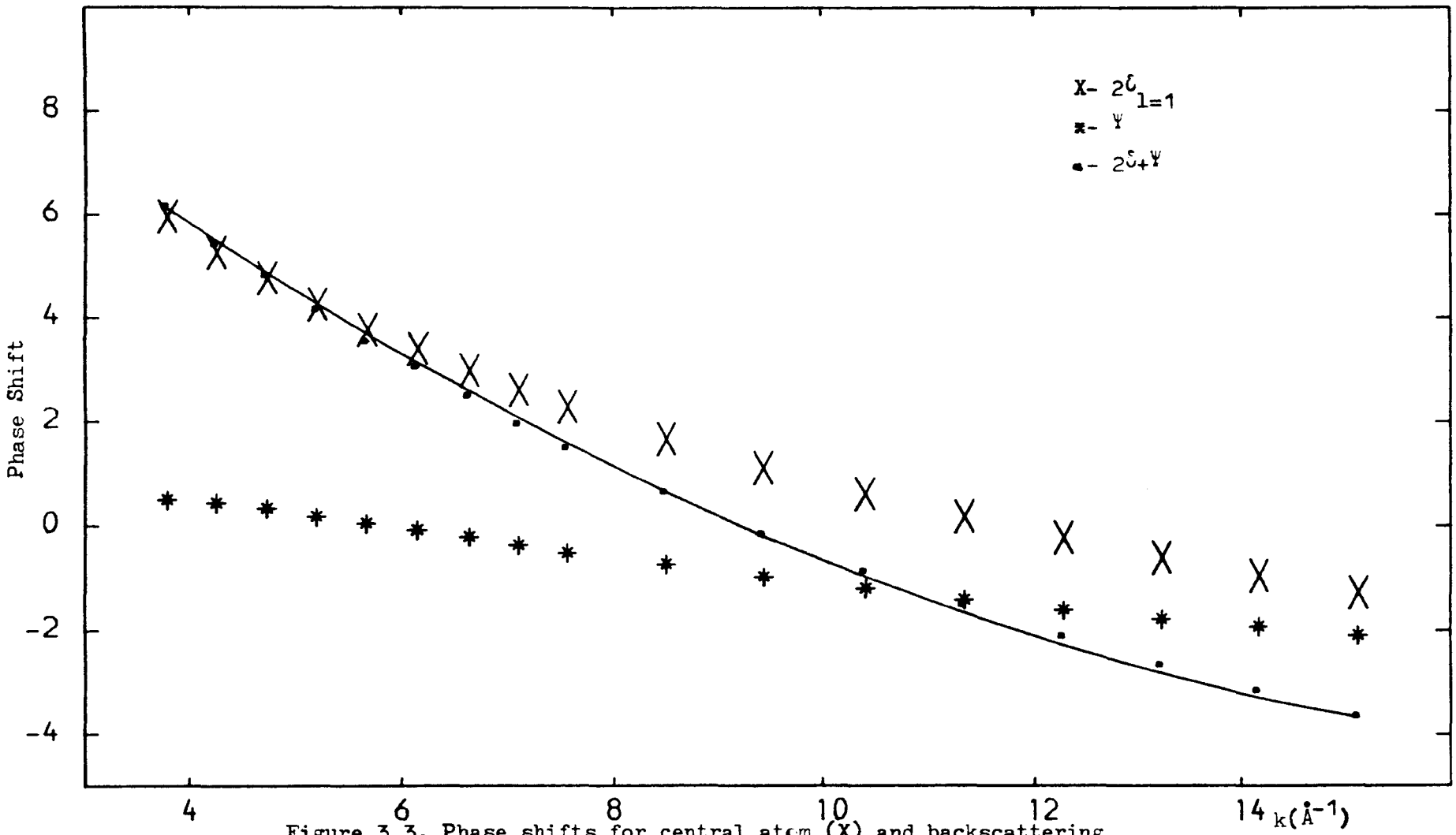

Figure 3.3. Phase shifts for central atom (X) and backscattering atoms (*) after Teo and Lee. Solid line is the least squares fit to their sum.

Finally it should be noted that one serious limitation of using eqn. 3.21. is that no explicit account is taken of the mean path free term or of many body effects. In general these terms are a function of k but for the purposes of this work, they will be assumed to be constant and as such may be included via C_0. Furthermore, the accuracy of structural information is clearly dependent on the validity of the initial premise (chemical transferability) and the approximations of the phase and amplitude functions. These effects will be discussed where relevant.

3.2.6. Curve Fitting by Fourier Filtering

In the studies that follow, two techniques proved to be beneficial. As a preliminary structural investigation the FT of the EXAFS was taken and the data obtained from that used as an initial guess for bond distances in the curve-fitting routines. *Ab initio* calculations were attempted although this was abandoned in favour of less time-consuming procedures.

The most rewarding technique proved to be the method of Fourier filtering. Here, the EXAFS from one particular shell in the FT is extracted from the rest by back-transforming the r-space data into k-space. This requires the added complication of another FT over a restricted data range and so particular care must be taken in the choice of window functions.

Chapter 4

EXAFS STUDIES OF THE K-EDGE OF Zr IN SODA-LIME-SILICA GLASSES

4.1. INTRODUCTION

The results presented in this chapter are for the glass compositions listed in Table IV. Table V gives the thermal treatments. Together with these results, infrared data will also be shown. These were obtained using a Perkin Elmer 983 spectrometer in the transmission mode and data acquisition was achieved by means of a PE 3600 data station. Infra red specimens were prepared by a standard technique of pressing thin discs of the powdered glass with dry KBr, a material which is known to be transparent in the wavelength range of interest.

The glasses were chosen in order to obtain structural information on the atomic arrangement around Zr under compositional variation. From experience with simple binary silicates, these may be induced by the change in concentration or by the isostructural substitution of the alkali cation, e.g. Li for Na. Furthermore, structural changes may also occur on heat treatment of the specimen below the glass transition temperature. To monitor this effect, the rapidly quenched counterpart of sample ZrA was also measured.

As shall be shown, qualitative information on the structure may be obtained by FT techniques in conjunction with a known model compound, chosen in this study to be $ZrSiO_4$. However, to obtain a higher degree of accuracy, the study was extended to a curve fitting analysis using the same model compound.

On the basis of the structural theory presented, infrared data will be reappraised and a short study of the L-edges of Hf, known to act in a

chemically similar way to Zr, in the same soda-lime-silica base glass will be presented to support the overall model.

Sample	ZrO_2	CaO	SiO_2	Na_2O	Li_2O	K_2O
ZrA	8.9	6.3	68.5	16.3	0	0
ZrB	8.9	6.3	68.5	0	16.3	0
ZrC	8.9	6.3	68.5	0	0	16.3
ZrD	8.9	6.1	63.6	21.4	0	0
ZrE	8.9	6.5	73.0	11.6	0	0

TABLE IV

Compositions of ZrO_2-containing glasses studied by EXAFS
(Values are in mole %)

Sample	Sintering Temp (°C)	Melting Temp (°C)	Annealing Temp (°C)	Annealing Time (hrs)
ZrA	750	1550	680	2
ZrB	750	1450	680	2
ZrC	750	1650	680	2
ZrD	750	1500	638	2
ZrE	750	1640	735	2
ZrA2	-	1550		

TABLE V

Thermal history of glasses given in Table IV
(Sample A2 corresponds to the quenched form of A)

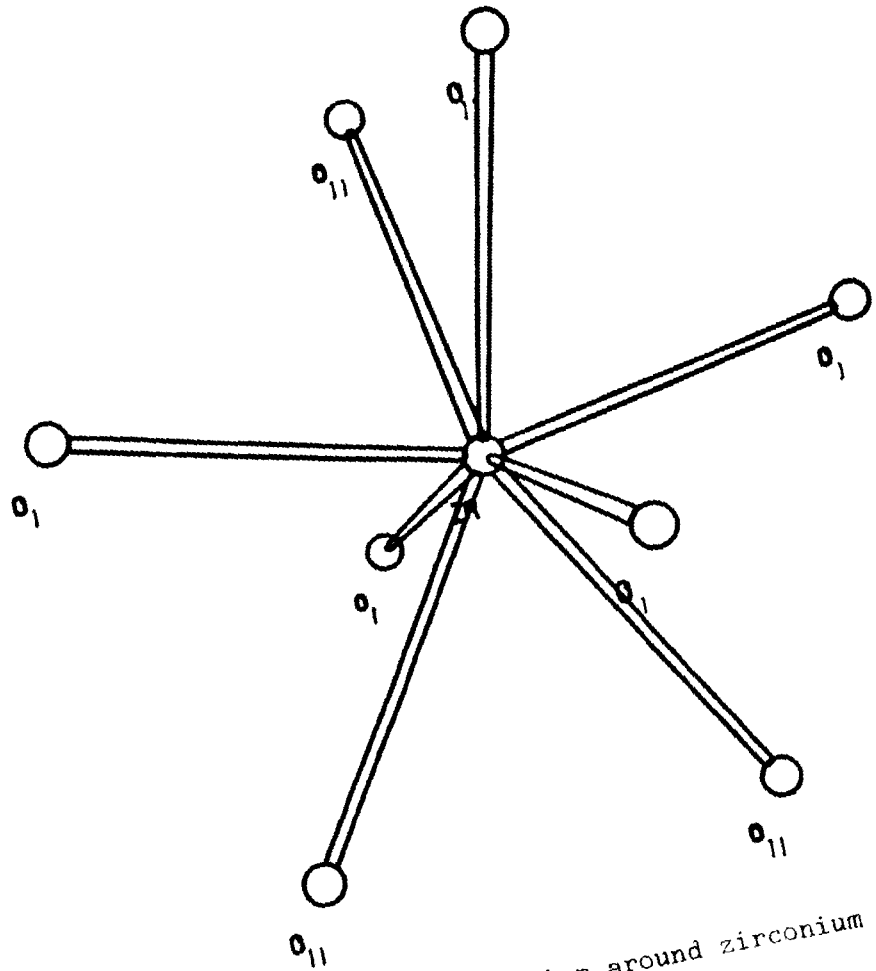

Figure 4.1 Oxygen coordination around zirconium in $ZrSiO_4$. $Zr\text{-}O_I$=2.13Å, $Zr\text{-}O_{II}$=2.27Å.

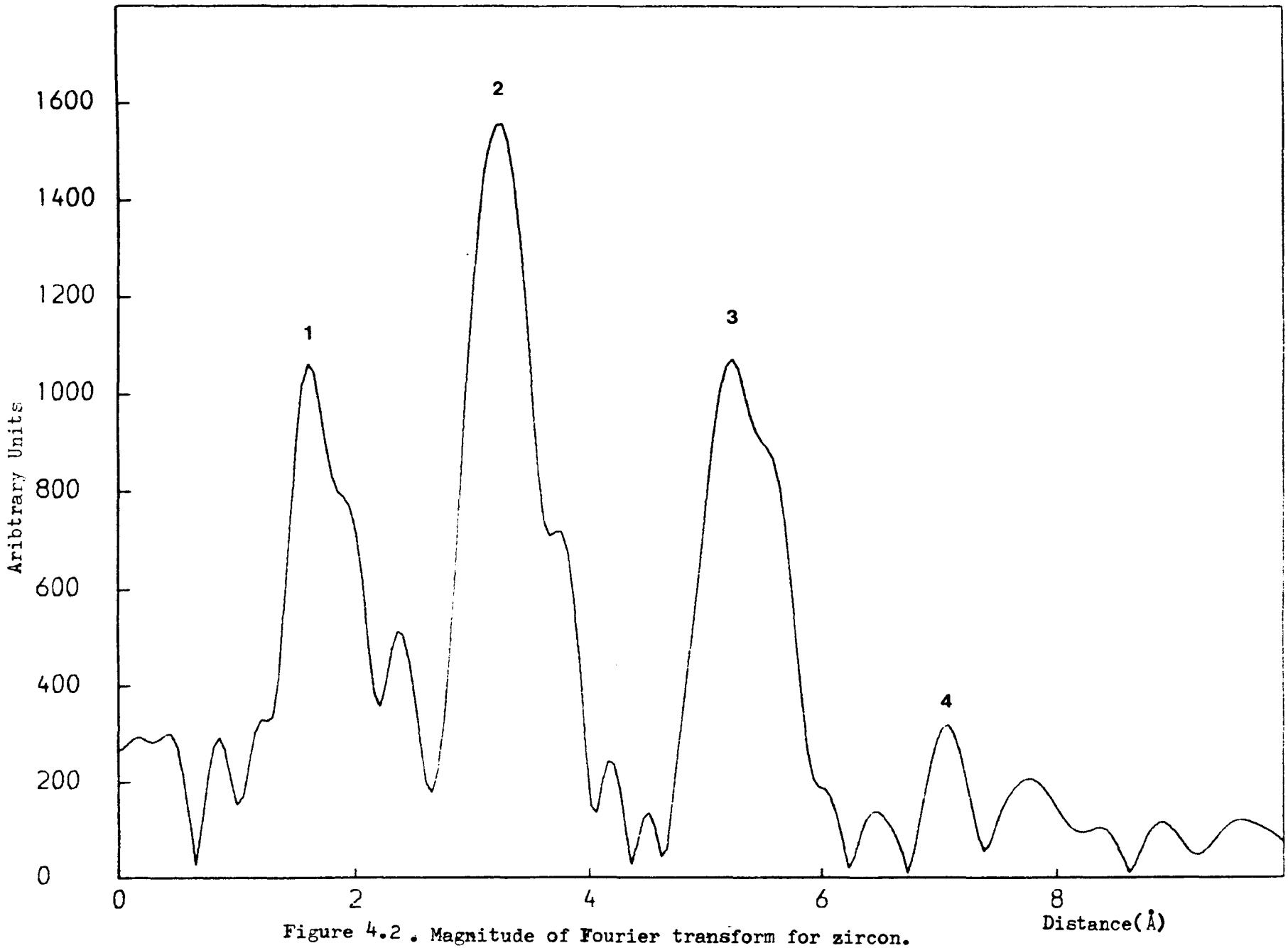

Figure 4.2 . Magnitude of Fourier transform for zircon.

4.2. THE MODEL COMPOUND: $ZrSiO_4$

4.2.1. Fourier Transform

As a model compound for the comparison of ZrO_2-containing glasses, $ZrSiO_4$ was chosen. The radial distances about a Zr atom are given in Table VI after Wyckoff (1927) and Krstanovic (1958). The oxygen first shell coordination, of particular interest in the study of oxide glasses, consists of two zirconium-oxygen tetrahedra as shown in Fig. 4.1. The disposition is similar to that found by Teufer (1962) in tetragonal ZrO_2. The specimen was prepared in the way described in Section 2.1. as a thin film of the powdered material.

The magnitude of the FT of the EXAFS for zircon (Fig. 4.8.) is shown in Fig. 4.2. The transformation was performed over a range in energy space of 40-720 eV with a Hanning window function of the form:

$$W(k) = \begin{cases} \frac{1}{2}\,(1 - \cos(k - k_{min})\pi/2\alpha) & \text{for} \quad k \le k_{min} + \alpha \\ \frac{1}{2}\,(1 - \cos(k_{max} - k)\pi/2\alpha) & \text{for} \quad k \ge k_{max} + \alpha \\ 1 & \text{for} \quad k_{max} - \alpha > k > k_{min} + \alpha \\ 0 & \text{elsewhere} \end{cases}$$

where $\alpha = \gamma\delta k$, γ being the fraction of the data range which is smoothed; $\delta k = k_{max} - k_{min}$, $\gamma = 0.1$.

As can be seen the FT shows 4 distinct peaks which all exhibit some kind of distortion from the Gaussian form predicted by eqn. 3.10., due to the inability of the technique to resolve scatterer distances that are close to each other and scattering from atoms of different species at the same distance. Both effects are present in $ZrSiO_4$. The characteristic

SHELL	NUMBER	DISTANCE	TYPE
1a	4	2.13	Oxygen
1b	4	2.27	Oxygen
2	2	2.99	Silicon
3a	4	3.63	Silicon
3b	4	3.63	Zirconium
4b	8	4.05	Oxygen
4b	4	4.24	Oxygen
4c	8	4.36	Oxygen
4a	4	4.54	Oxygen
5	4	4.67	Silicon
6	8	4.9	Oxygen
7	8	5.55	Zirconium
8a	4	5.57	Zirconium
8b	4	5.57	Silicon
9	2	5.98	Zirconium

TABLE VI

Radial Distances about a Zr atom in $ZrSiO_4$

shoulder at 1.98 Å is indicative of a split shell. As Fig. 4.3. shows, peak 1 may be schematically represented by the sum of two Gaussians of differing width. The FT is shown without any phase correction α_j. Assuming the crystal structure values to be correct this gives a value for a/2 of 0.42 Å (see eqn. 3.11.).

4.2.2. Curve Fitting of the Experimental Spectrum

Clearly the accuracy of this method is unacceptable. Thus, as a first approach to least squares fitting, the tabulated values for the phase and amplitude function of Teo and Lee as expressed by eqns. 3.23. and 3.24. respectively, were used through a refinement of E_0, as the effects of electronic configuration and charge can be compensated by varying the threshold energy. The mean square relative displacement σ_j^2 was also allowed to vary. The result of this was not wholly conclusive and it was considered necessary to adopt a Fourier filtering technique.

4.2.3. Curve Fitting by Fourier Filtering

Of particular importance in the study of disordered systems is the contribution to the EXAFS from the first shell only. To calculate the phase and amplitude parameters for oxygen scattering in zircon, the EXAFS for the first shell was filtered from the total scattering contribution by back-transforming the restricted FT. This was achieved by "masking-off" the first peak in r-space, between 1 and 2.3 Å. This procedure is shown in Fig. 4.4a. with the resultant oxygen EXAFS plotted in Fig. 4.4b by the solid line. The EXAFS shows a distinctive kink at 10.5 $Å^{-1}$ which can be attributed to a split oxygen distance: Martens et al. (1977) showed that for a material possessing a split first shell the following equations may be derived.

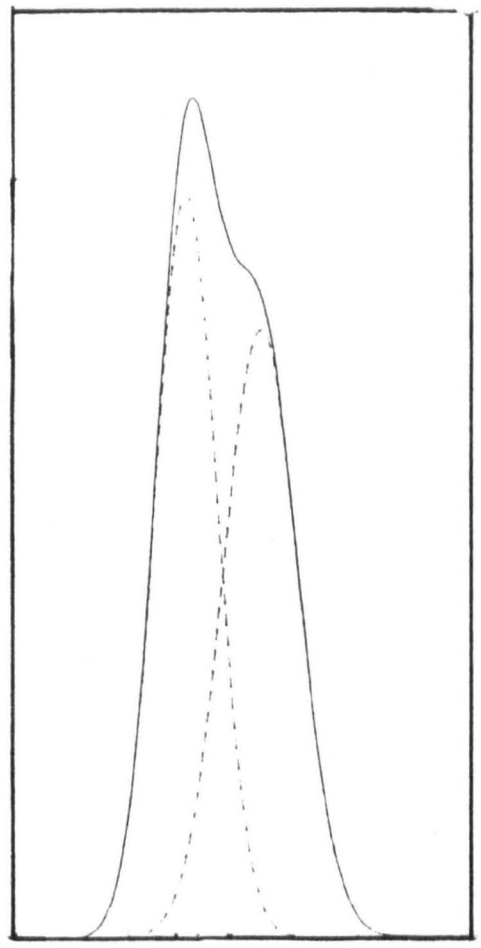

Figure 4.3 Schematic representation of peak 1 in Fig. 4.2

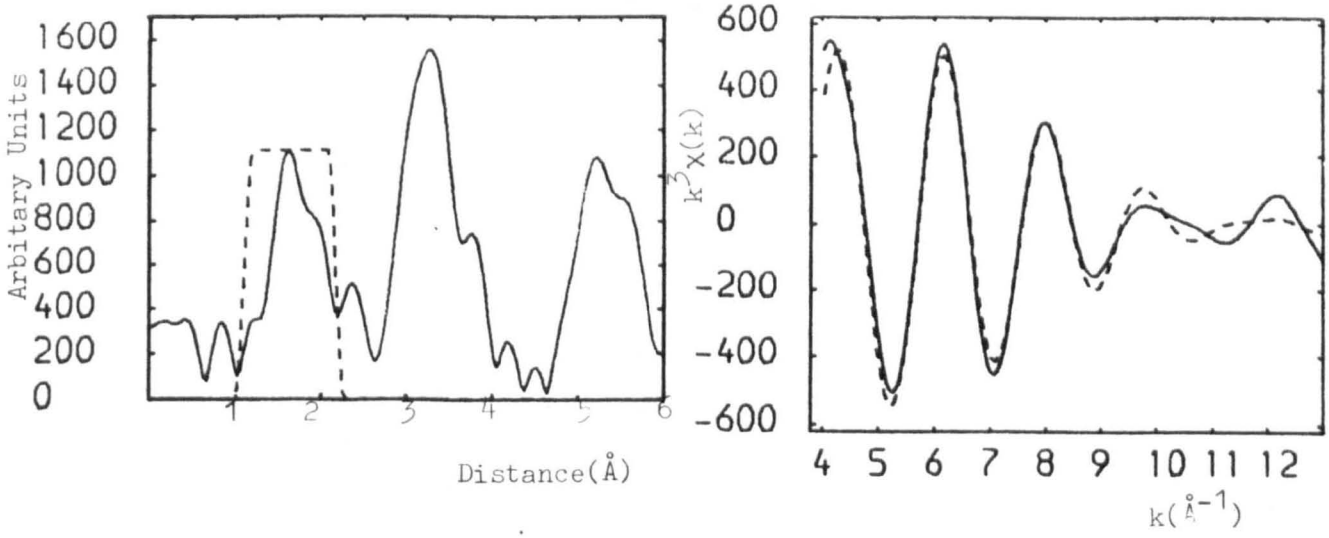

Figure 4.4 The oxygen Fourier filtered EXAFS, $\chi_j(k)$, b) obtained by isolating peak 1 in the FT a), by means of a Hanning function.

$$\chi = A_1(k)\sin(2kr_1 + \phi(k)) + A_2(k)\sin(2kr_2 + \phi(k))$$

$$= A_1(k)[(C + 1)\sin(2k\tilde{r} + \phi)\cos k\Delta r +$$

$$(C - 1)\cos(2k\tilde{r} + \phi)\sin k\Delta R)]$$

$$= \tilde{A}\sin(2k\tilde{r} + \tilde{\phi}(k))$$

where

$$\Delta r = r_2 - r_1$$

$$\tilde{r} = (r_1 + r_2)/2$$

$$\tilde{A} = A_1(1 + C^2 + 2C\cos 2k\Delta r)^{\frac{1}{2}} \qquad (4.1.)$$

$$\tilde{\phi} = \phi - \tan^{-1}\{(1 - C)\tan(k/\Delta r)/1 + C\}$$

and

$$C = A_2/A_1 = \left(\frac{N_2 r_1^2}{N_1 r_2^2}\right) + \exp(2\Delta\sigma_{12}^2 k^2) \qquad (4.2.)$$

where $\Delta\sigma_{12}^2 = \sigma_1^2 - \sigma_2^2$

Eqn. 4.1. predicts that the amplitude function has an oscillatory nature of period $k = \pi/2\Delta r$. Fig. 4.5a. shows the amplitude function for zircon weighted by k^3. The minimum at $k = 10.5$ Å^{-1} agrees well with the split distance $\Delta r = 0.15$ Å.

Using the paramaterized expressions for the amplitude and phase functions described earlier, a least squares refinement procedure was performed. To compensate for amplitude attenuation, the EXAFS spectrum

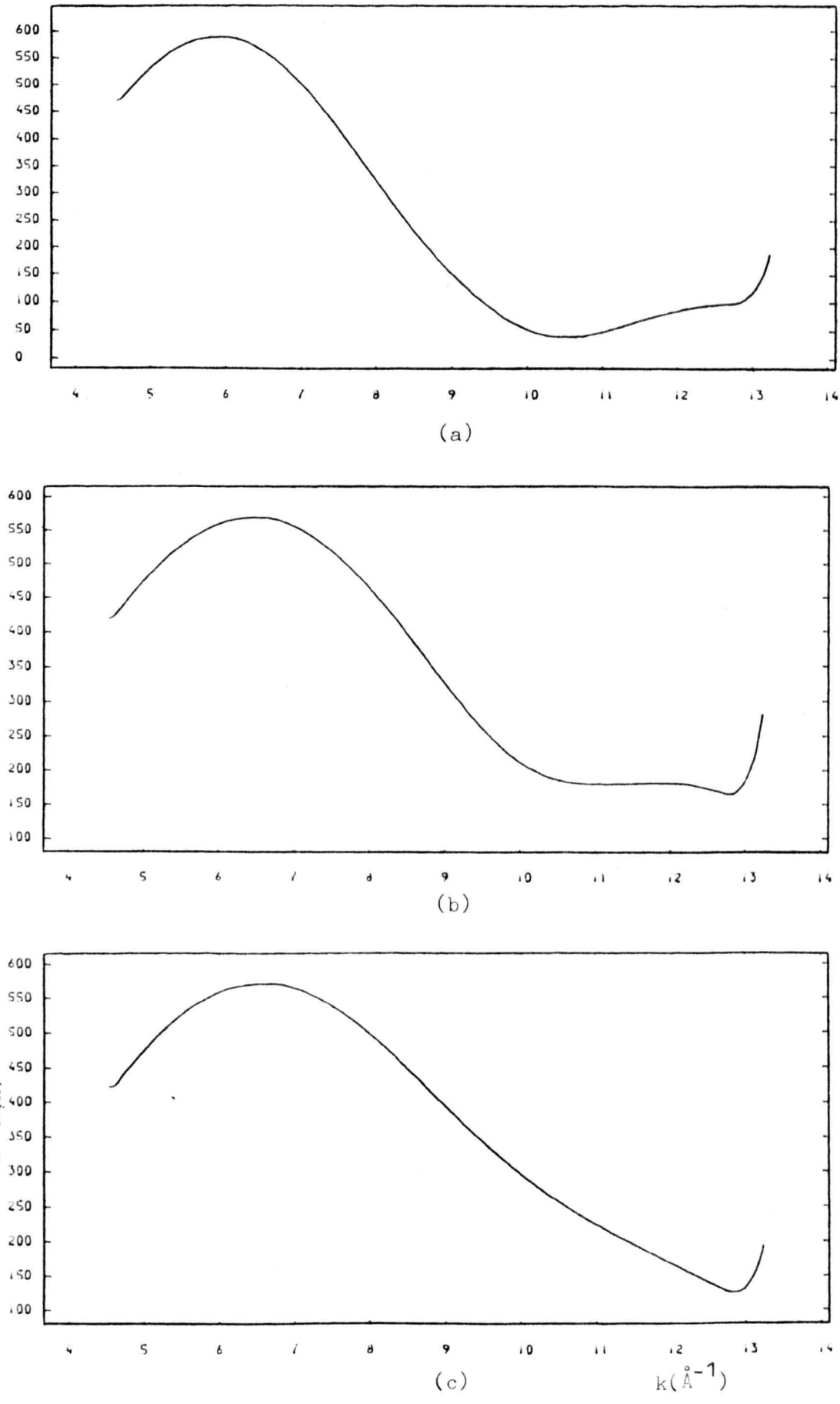

Figure 4.5. Amplitude of the first shell (see eqn. 4.1) for:- a) $ZrSiO_4$, b) sample ZrA2 and, c) sample ZrA1.

was weighted by k^3. Results showed that the parameters defined in eqns. 3.23. and 3.24. were dependent on the range of fitting and also on the degree of weighting and as such bear no real physical significance. However, this does underline the neccessity for keeping the fitting range constant in comparative techniques. Table VII gives a list of these parameters and the least squares fit is shown in Fig. 4.4b. by the dashed line.

a_0	3.759
a_1	-1.434
a_2	0.0314
c_0	0.65
c_1	10.13×10^{-3}
c_2	0.99

TABLE VII

Phase (a_n) and amplitude (c_n) parameters for the first shell contribution to the EXAFS of $ZrSiO_4$. Fitting range was from 4 to 13.5 $\mathring{A}^{-1}$ with a k^3 weighting.

In the refinement of these parameters it has been assumed that the value of σ_j^2 is the same for both oxygen distances. In a recent paper by Morinaga et al. (1983) the degree of ordering of the Zr-O bond was shown to be greater in the shorter oxygen bond as the degree of covalency increases due to an increasing overlap of wavefunctions. Because of this

ambiguity in the value of σ_j^2 , coupled with high correlation between it and the floated parameter c_1, the best that can be achieved will be relative measures of the mean square relative displacement.

In order to alleviate the problem of termination effects and errors that are generated on back transformation (these are particularly prevalent at the extreme of the k-space data), considerable effort was put into the refinement of phase and amplitude parameters directly in energy space. Unfortunately, due to the nature of the model compound, the beat at 10.5 A^{-1} could not be adequately matched as noise in the original spectrum tended to obscure this contribution, especially when weighted by k^3. However using the parameters listed in Table VII, a least squares fit is shown in Fig. 4.6. for the experimental spectrum, together with a plot of the FT of the residuals (inset of Fig. 4.6.), showing that the oxygen contribution has been properly matched. Furthermore, poor background subtraction may distort the EXAFS away from the true oscillatory base-line. To compensate for this a polynomial of the form:-

$$P(E) = \alpha E + \beta E^2 + \gamma E^2 \qquad (4.3.)$$

was used to manoeuvre the actual position of this base-line.

4.2.4. Curve fitting the whole spectrum

Once the contribution to the first shell has been successfully matched, it is theoretically feasible to proceed in the same manner and fit all the shells that arise in the FT by a Fourier-filtering technique. For $ZrSiO_4$, this is not possible as next nearest neighbours are poorly resolved in real space. However, from the preceeding section it was found that oxygen scattering could be adequately fitted using, as initial guesses, data obtained from the least squares refinement described in

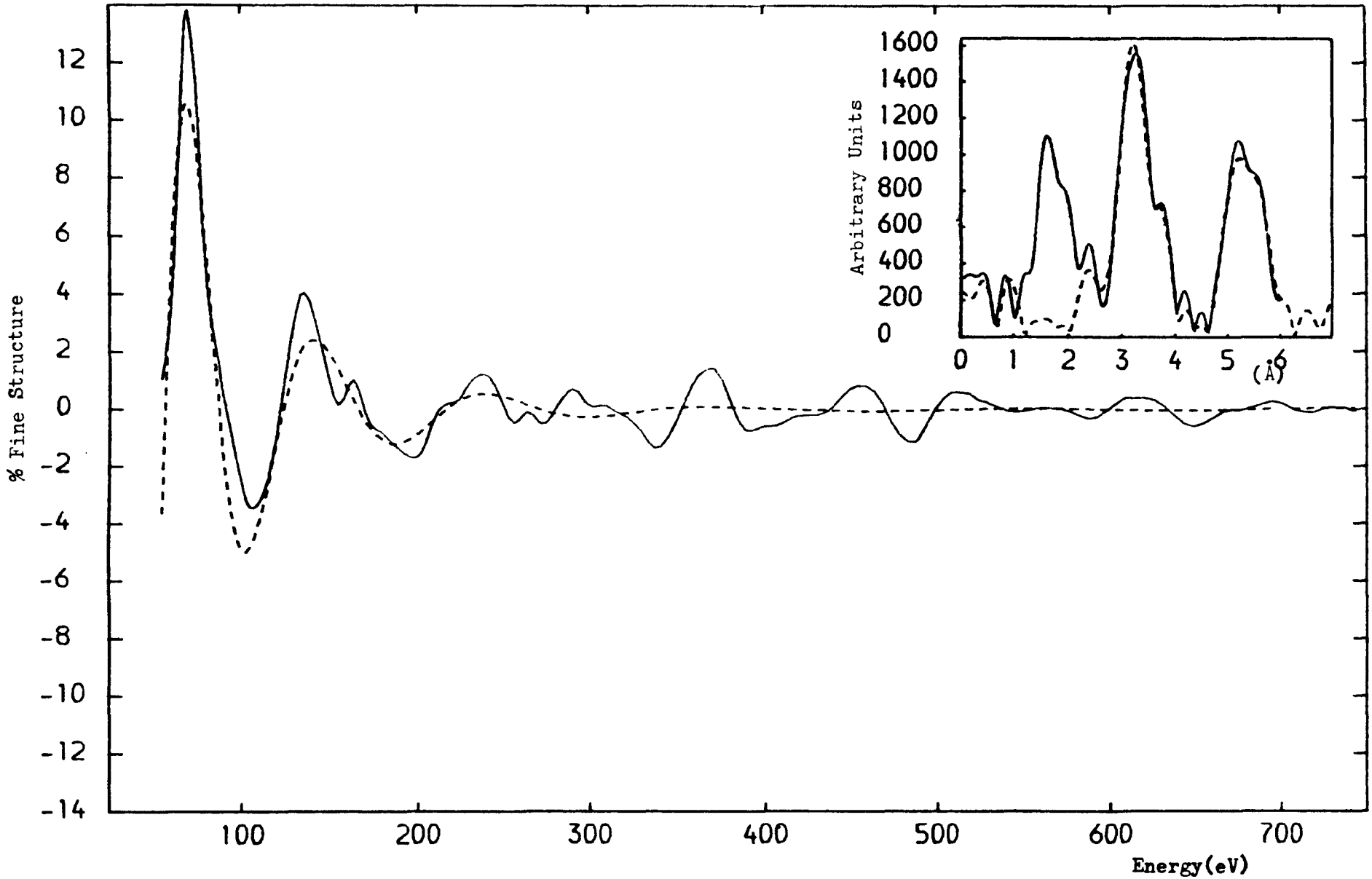

Figure 4.6. Least squares fit of oxygen EXAFS for the original experimental spectrum. Inset is the FT of the residuals.

Section 4.2.3. Thus by fixing the first shell parameters, the whole spectrum was fitted using coordination and radial distance data from Table VI and allowing the phase and σ_j^2 parameters to vary. The amplitude functions were, for the case of silicon scattering, parameterized by a similar expression as for that of oxygen, but for zirconium (Z = 40) scattering, the amplitude peaks strongly at ~ 9 Å and cannot be adequately matched by either an exponential or Lorentzian amplitude function. Thus in this case, the Teo and Lee data was smoothed by a cubic spline approximation (Fig. 4.7.). The initial guesses for the phase coefficients for Zr-Si and Zr-Zr scattering were chosen to be the values obtained by a least squares refinement to the data of Teo and Lee. The resultant fit is shown in Fig. 4.8., for 8 shells. A reasonable fit could only be obtained with an "error-exit" from the minimization algorithm, such that a local minimum could not be found to satisfy the fitting conditions. This was discernible in the final values for the phase and σ_j^2 values, which were adjudged to be unreasonable, presumably due to the high correlation between neighbouring shells.

4.3. ZrO_2-CONTAINING GLASSES

4.3.1. EXAFS

Fig. 4.9 presents the EXAFS spectra for a series of glasses given in Table IV. The measurements were performed at 77 K with an edge energy set at 17998 eV. As such, the absorption data display very little contrast and it is impractical to draw any conclusions between the individual spectra. However, when compared with a crystalline compound, it is possible to infer that the materials are highly disordered due to the fact that very little second shell contribution can be detected. This would be manifested by changes in the periodicity of the oscillations, a trait

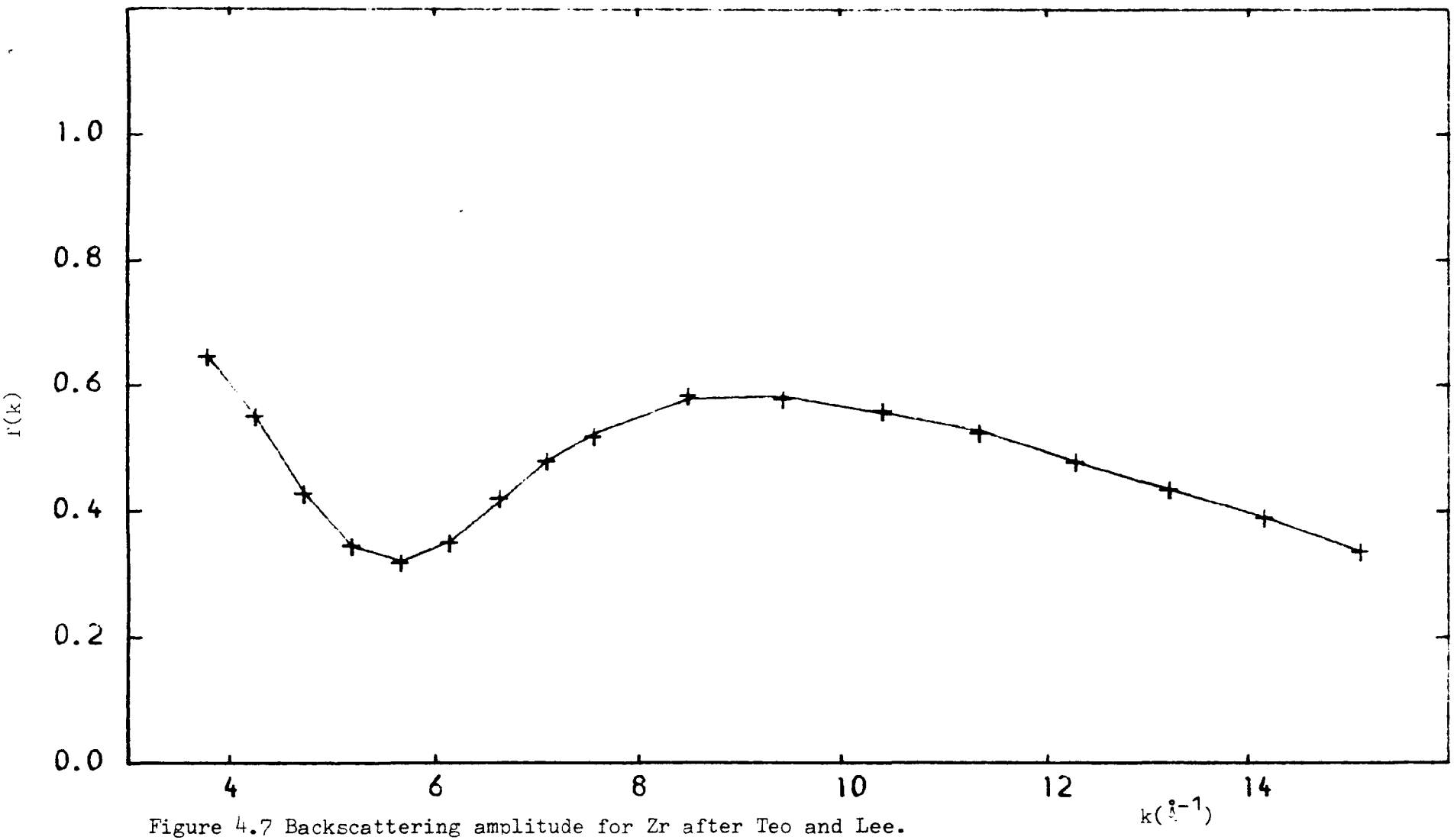

Figure 4.7 Backscattering amplitude for Zr after Teo and Lee.

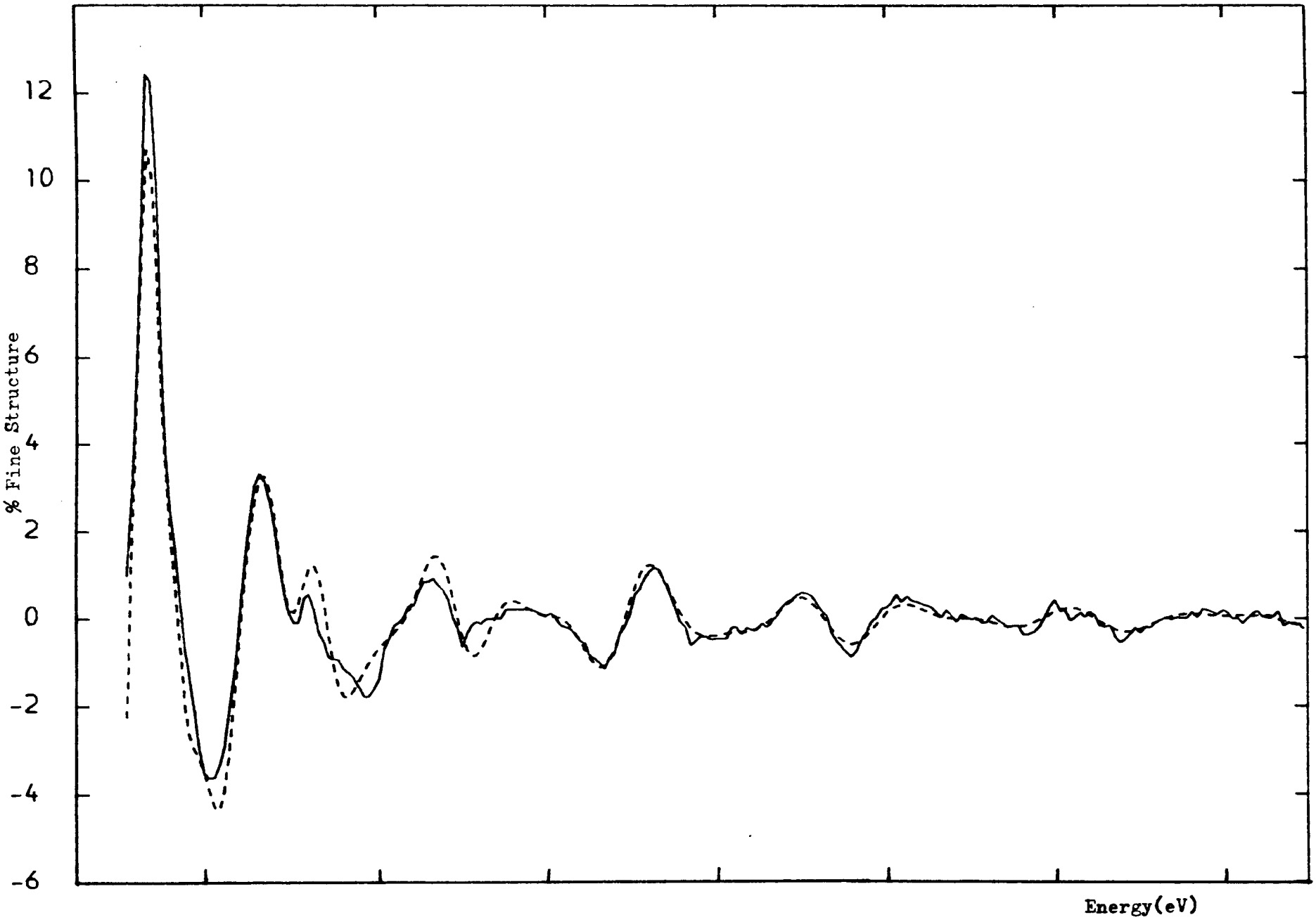

Figure 4.8. Eight shell fit to the EXAFS of zircon.

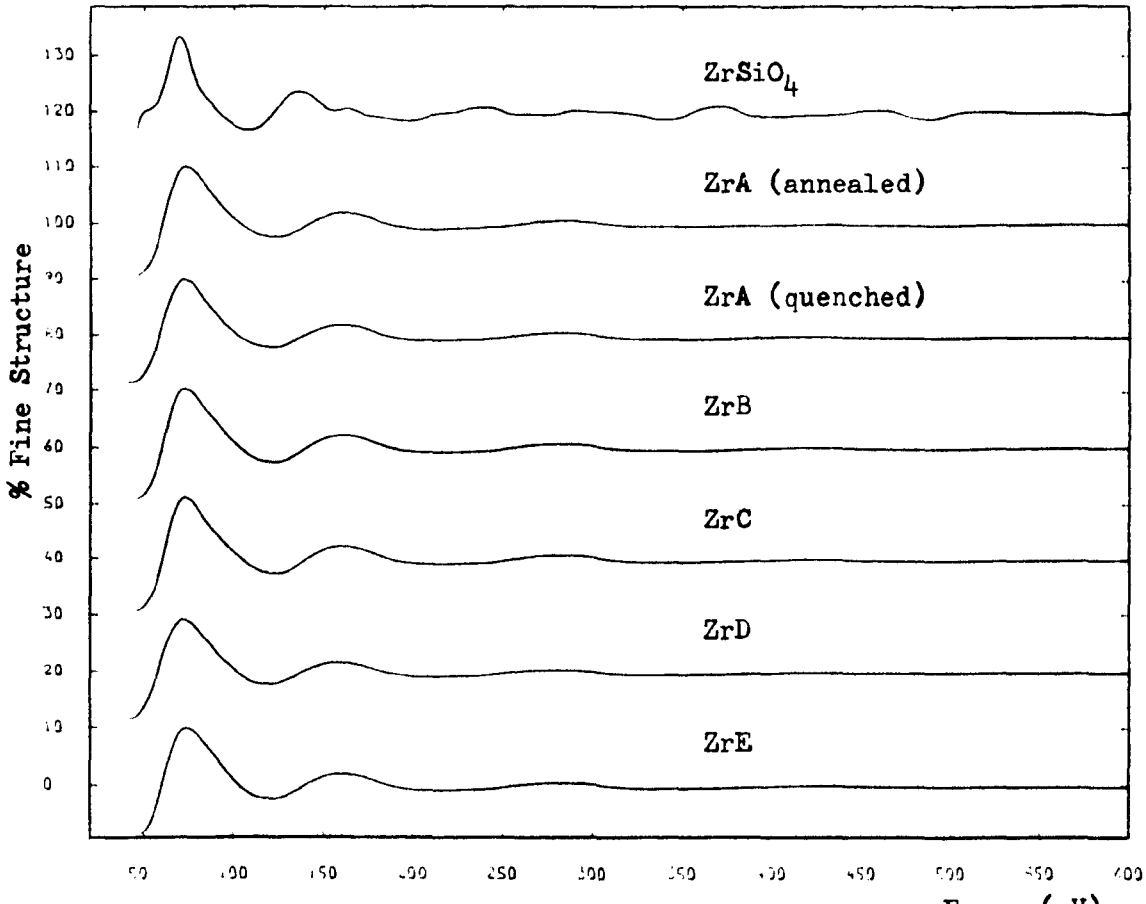

Figure 4.9. EXAFS spectra for the glasses given in Table IV.

which is very apparent in the EXAFS of $ZrSiO_4$. Furthermore, the range of the fine structure extends to only a fraction of the data range for the crystal. Any second shell contribution that may persist will be due to Zr-Si scattering on the basis that the Zr^{4+} ions are distributed uniformly throughout the volume: that is there is no phase separation, borne out by the electron microscopy and X-ray scattering studies discussed in Chapter 2. Furthermore, the lack of Zr-O-Zr infrared modes confirms this postulate.

4.3.2. Infrared Data

The infrared spectra for the ZrO_2-containing glasses are shown in Fig. 4.10. for varying Na_2O content. Fig. 4.11. presents the infrared data for the crystalline compounds SiO_2, $ZrSiO_4$ and ZrO_2. A full account of the assignation of the bands for each sample can be found in works by Wong and Angell (1976), for SiO_2; Phillipi and Mazdiyansi (1971) for ZrO_2; and Farmer (1974) for zircon. The infrared band at 740 cm^{-1} in monoclinic zirconia is indicative of Zr-O-Zr bending vibrations and is not observed in any of the glasses.

For $ZrSiO_4$ (zirconium orthosilicate) the bands in the range 1000 - 600 cm^{-1} are due to the vibrational modes of $[SiO_4]^{4-}$ tetrahedra in isolation, whilst at low frequencies, the bands are due to deformation of the O-Si-O bond angles which, in the presence of the large Zr ion, are necessary to avoid changes in Si-O bond lengths. Due to the range of the KBr pellet technique there is no information below 300 cm^{-1}, however it is reported (Farmer, 1974) that there is no significant translatory displacement of the heavy Zr^{4+} ions within this range. Therefore the glassy spectra presented in Fig. 4.10. can only be discussed in relation to modifications of the vitreous silica spectrum due to depolymerization of that network by the addition of particular oxides (see for instance,

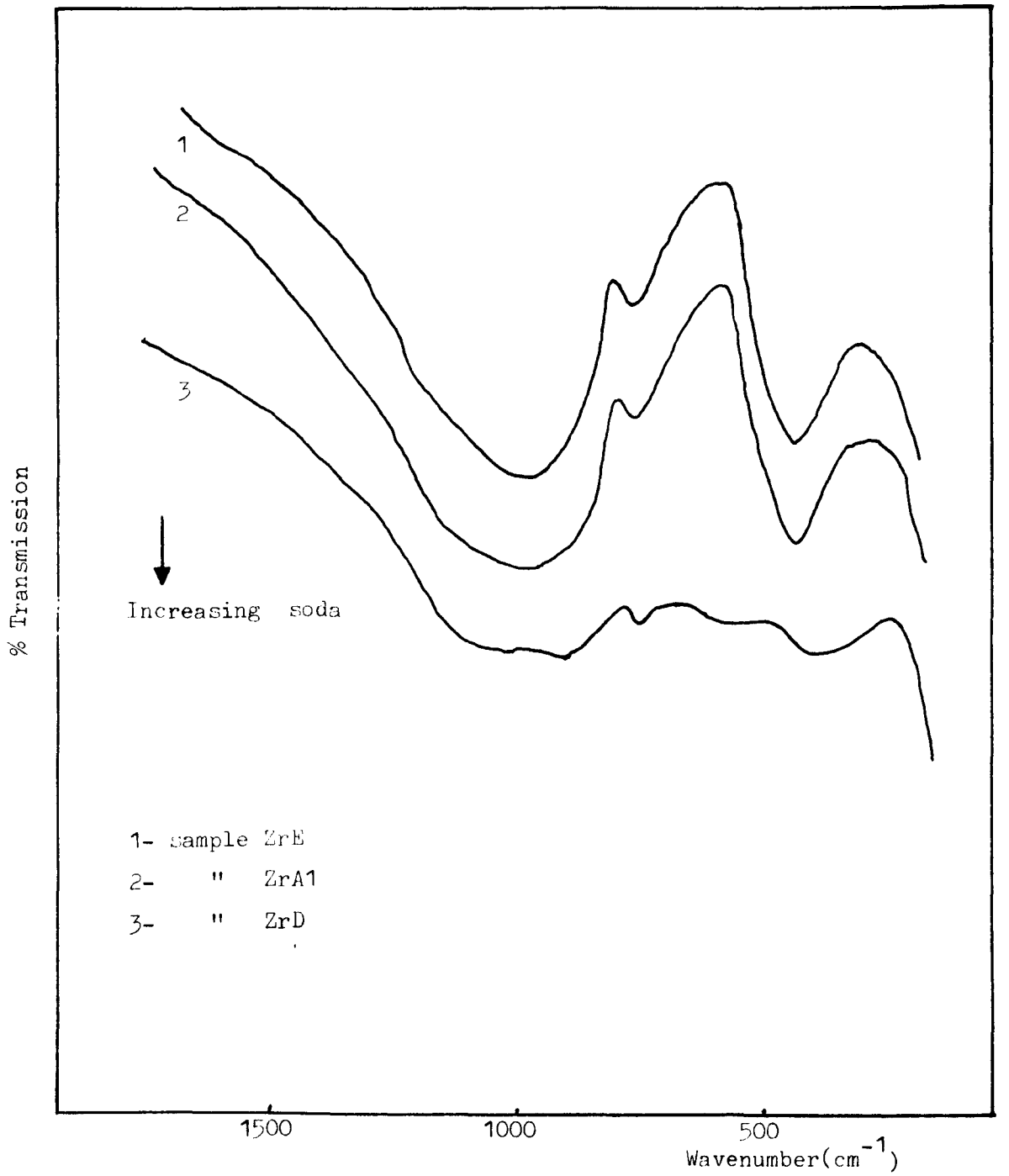

Figure 4.10 Infra red transmission data for three glasse containing varying Na_2O content. Spectra are displaced on the ordinate scale.

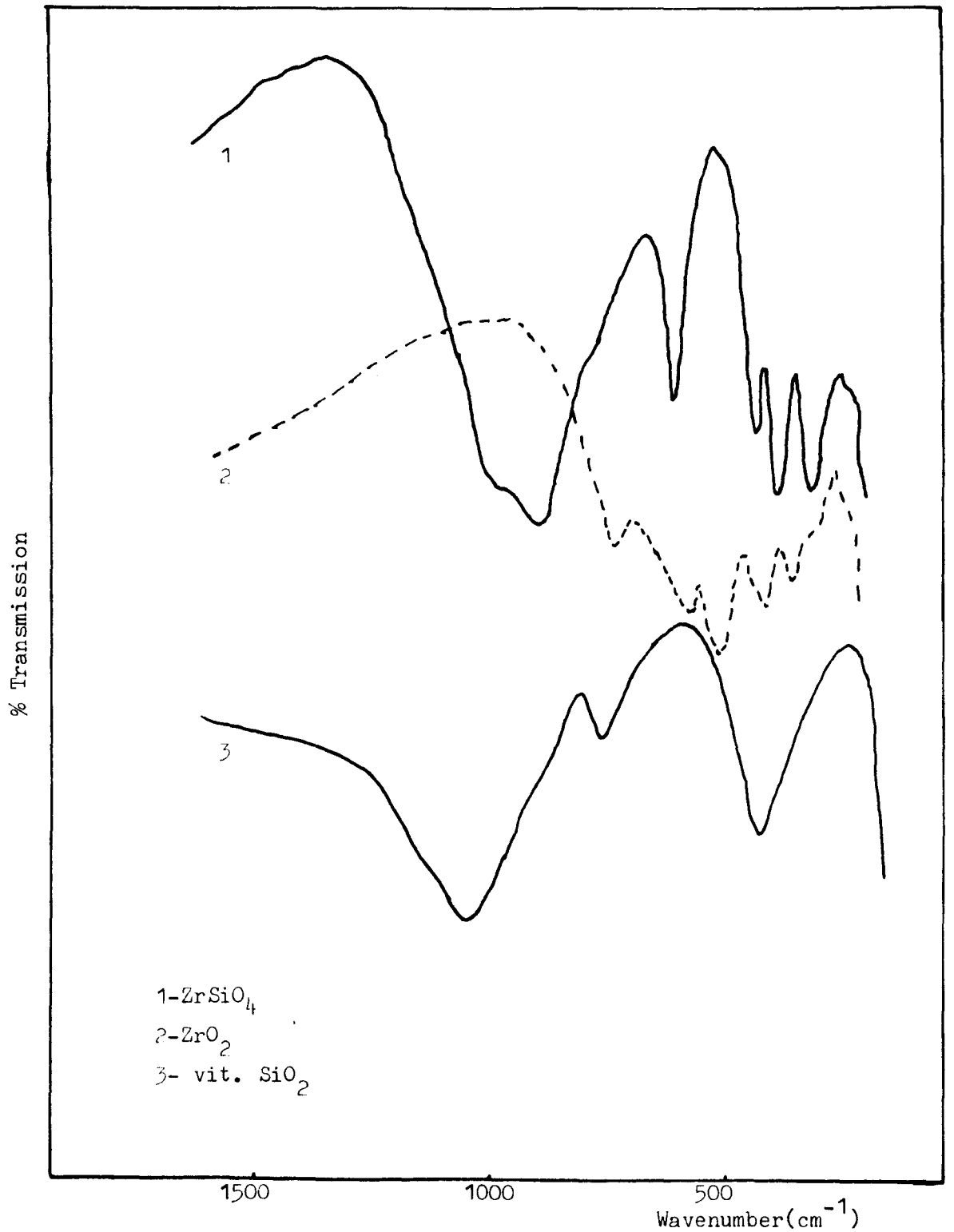

Figure 4.11 Infra red transmission data for three comparative solids.

Hannu and Su, 1964). The band at 1100 cm^{-1}, due to Si-O stretching, is shifted to lower frequencies (decreasing force constant) as the alkali content is increased, due to the formation of non-bridging oxygens (NBO). This effect also manifests itself in the broadening and shifting to lower frequencies of the band at 780 cm^{-1} which is assigned to Si-O-Si stretching vibrations. The band at 480 cm^{-1} appears to be insensitive to modifier content.

4.4. ANALYSIS OF EXAFS DATA

4.4.1. Fourier Transform

The magnitude of the FT's for some of the glassy specimens shown in Fig. 4.9. are presented in Fig. 4.12. The dominant scattering contribution is confirmed to be that of oxygen. Given that the magnitude of the first peak is related to the CRN, mean square relative displacement σ_j^2, and bond length, the relative differences in these parameters may be calculated using eqn. 4.2.

The quantity σ_j^2 can be considered to be made up of two components: one due to thermal disorder; the other due to glassy disorder. This can be expressed as:-

$$\sigma_j^2 = \sigma_{j,T}^2 + \sigma_{j,S}^2 \qquad (4.4.)$$

For two glasses, say 1 and 2, that possess the same fictive temperature, $\Delta\sigma_{21}^2$ (eqn. 4.5.) will be just the difference in the static disorder, i.e.

$$\Delta\sigma_{21}^2 = \sigma_2^2 - \sigma_1^2 \qquad (4.5.)$$

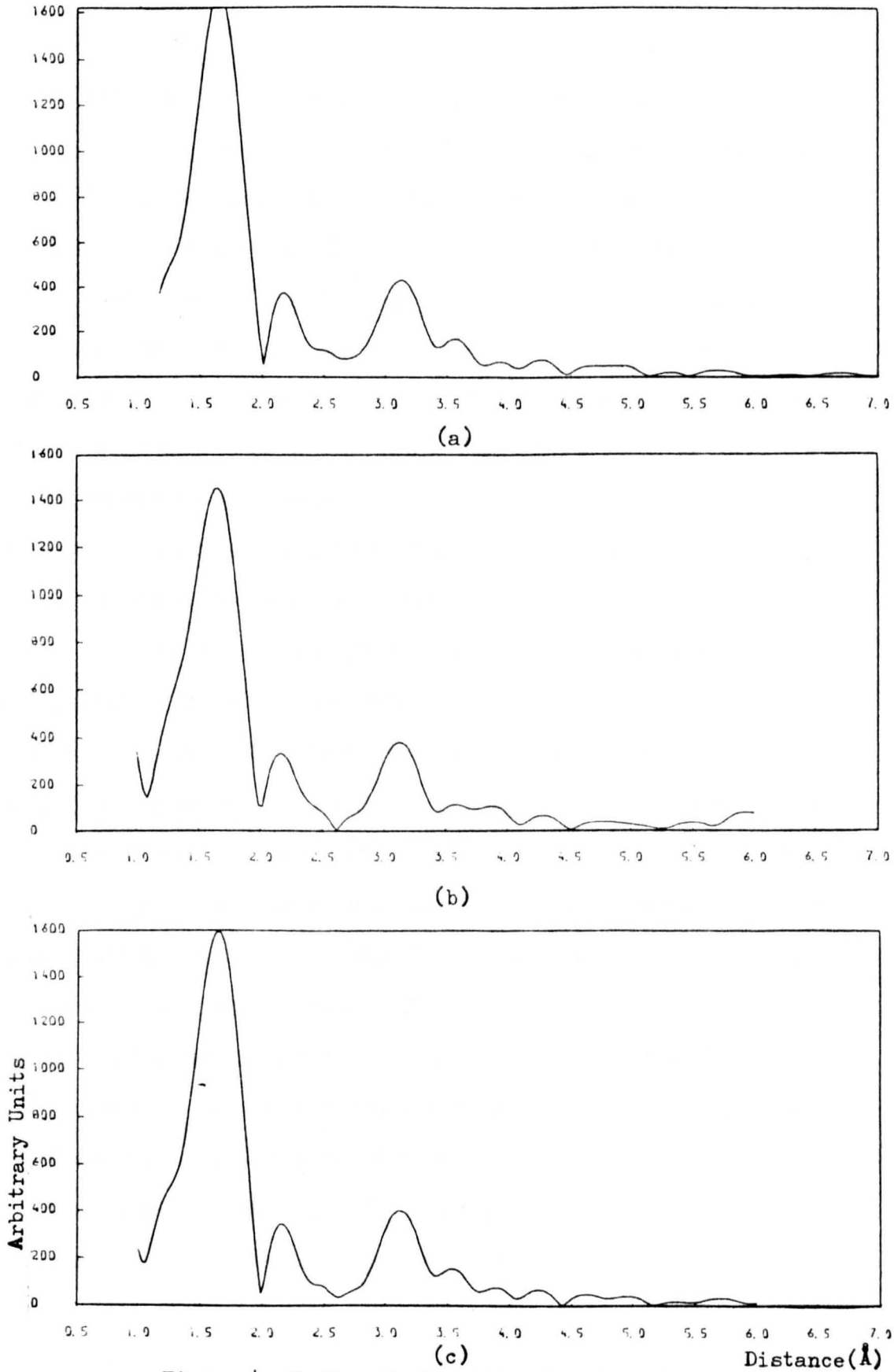

Figure 4.12. Magnitude of Fourier transform for three ZrO_2-containing glasses: (a) ZrA; (b) ZrD; and (c) ZrE.

Thus a plot of $\ln(A_1/A_2)$ should be a straight line, the gradient of which will be $2\Delta\sigma_{21}^2$. If the CRN and bond-length are unchanged the intercept will be zero. Fig. 4.13. compares the ratio of the first shell amplitudes for samples ZrA and ZrC and samples ZrA and ZrB. Fig. 4.14 presents a similar plot for the case of varying Na_2O content, although the annealing temperatures were different and as a result may effect the analysis. Extrapolating back to $k^2 = 0$, gives a value of approximately zero. Error bars were calculated on a statistical basis and are weighted by k^3. For clarity only a few points are shown.

Unfortunately it was not possible to compare crystalline and glassy compounds in a similar manner because of the split oxygen distance present in the former. As shall be seen later, the same rule applies for the comparison of quenched and annealed specimens.

The most striking difference between the FT's appears in the comparison of the annealed and quenched samples - Fig. 4.15. It is believed that the production of rapidly quenched fibres "freezes-in" the structure of the melt and any subsequent heat treatment below T_g will tend to relax the structure and find an equilibrium (this gives rise to the so-called fictive temperature, T_f). This relaxation process can be observed by the stress relief given to glasses and also by the changes in density of the glass, which was recorded for these two glasses to be ~ 10% increase on annealing. The characteristic shoulder on the oxygen peak of glass ZrA2 (quenched) is indicative of another Zr-O bond distance. To verify this, the same procedure was repeated as for the two Zr-O distances in zircon.

Fig. 4.5b. shows the amplitude function $\tilde{A}(k)$ for the quenched sample and Fig. 4.5c. presents the same function for the annealed specimen, ZrA2. The former exhibits a minimum in the amplitude indicative of a split oxygen shell, with $\Delta r = 0.16$ A. No such beat is found in the annealed

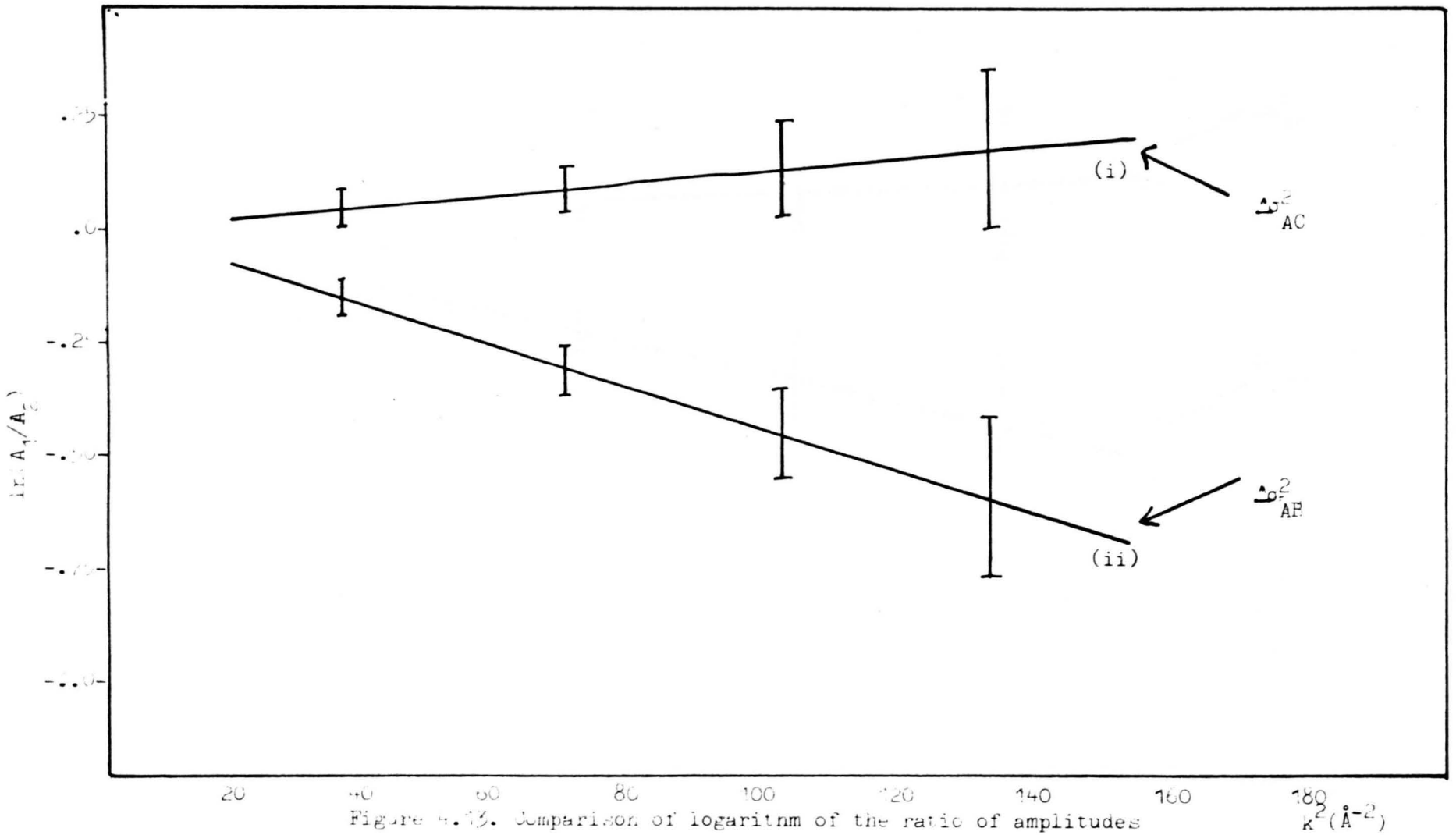

Figure 4.13. Comparison of logarithm of the ratio of amplitudes for the first shell in samples: (i)ZrA and ZrC; (ii)ZrA and ZrB.

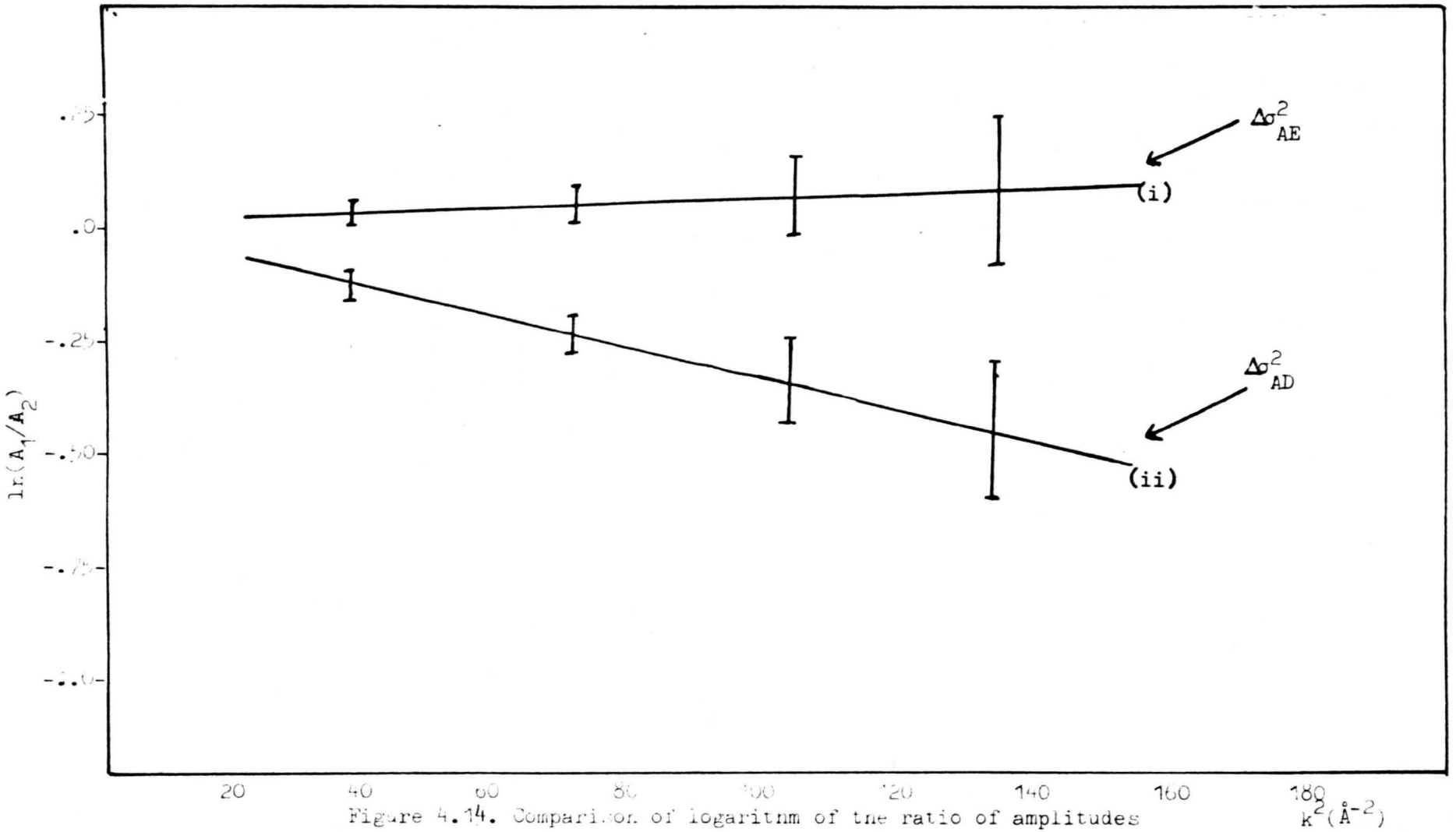

Figure 4.14. Comparison of logarithm of the ratio of amplitudes for the first shell in samples: (i)ZrA and ZrE; (ii)ZrA and ZrD.

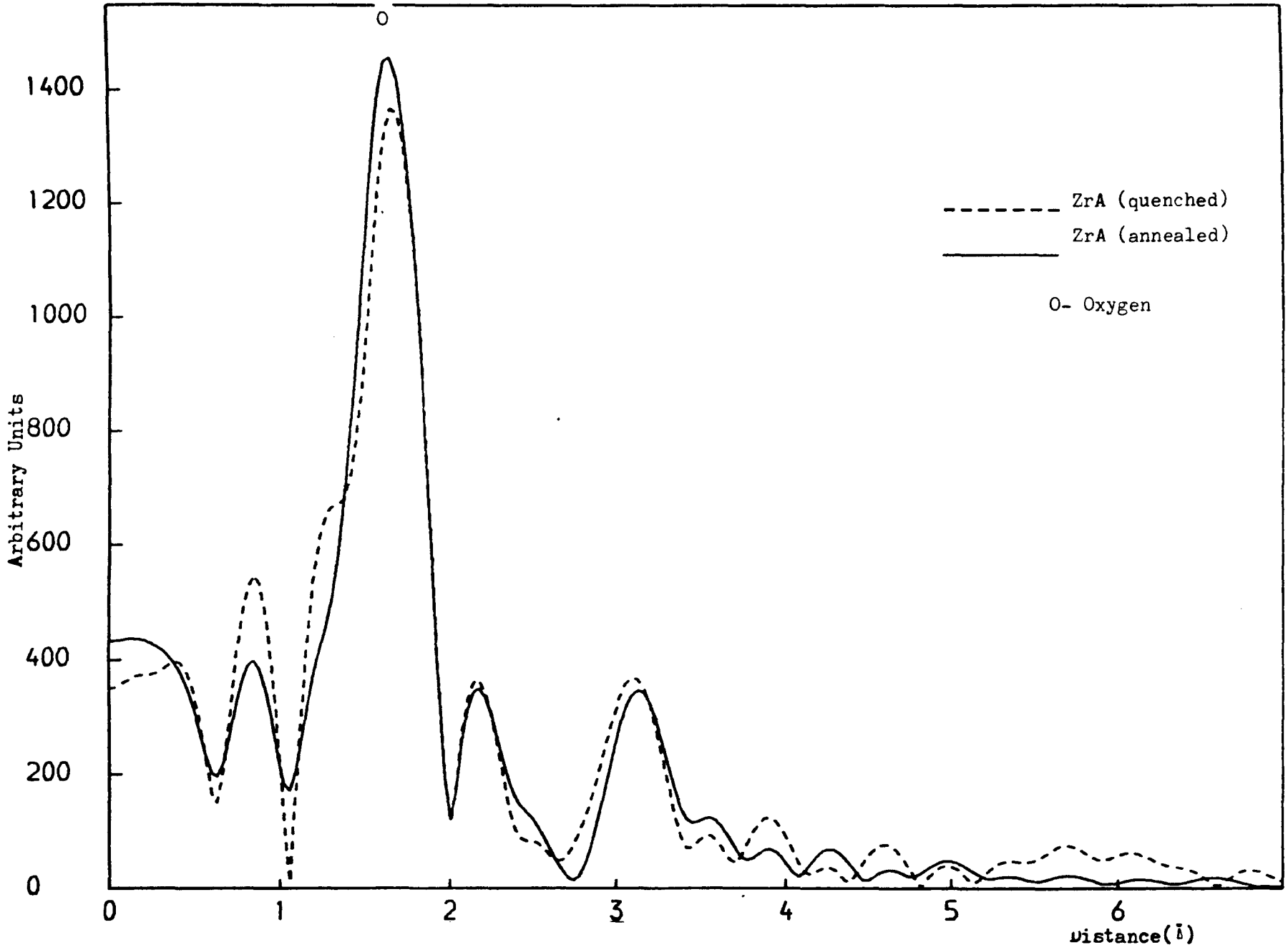

Figure 4.15. Magnitude of Fourier transforms for ZrA composition having undergone differing heat treatment.

specimen.

Comparison of the magnitude of the FT's with that of zircon, shows that the amplitudes are larger in the former. This is partly due to the method of sample preparation as finite-size-particle effects can lead to discrepancies of - 10% in CRN determination. However, this would still not account for all the amplitude reduction. Bond lengths in the annealed specimens appear to be unchanged. Using the value for the phase shift parameter defined in eqn. 3.11., the Zr-O distance is estimated at 2.09 ± 0.13 Å.

The contribution to the EXAFS from outerlying shells is minimal, confirming the disordered nature of the glass. As was shown from the study of $ZrSiO_4$, no accurate information could be obtained for Zr-Si scattering. Therefore, it is of little worth to discuss further any possible intermediate ordering in these glasses.

This study has shown that although the resolution of the technique is limited, qualitative information may be gathered on the atomic arrangement, which will now be used in a more accurate analysis via least squares fitting of the EXAFS data.

4.4.2. Least Square Fitting

Using the phase and amplitude parameters established from the study of the model compound, least squares refinements of the inverse Fourier transformed data were performed. The floated parameters were N_j, r_j and $\Delta\sigma_j^2$ together with E_0. These results are summarized in Table VIII and the fits (broken lines) are compared to the first shell EXAFS in Figs. 4.16. to 4.21. Errors have been estimated by a combination of the uncertainties in the floated value and the phase and amplitude data (see Appendix A).

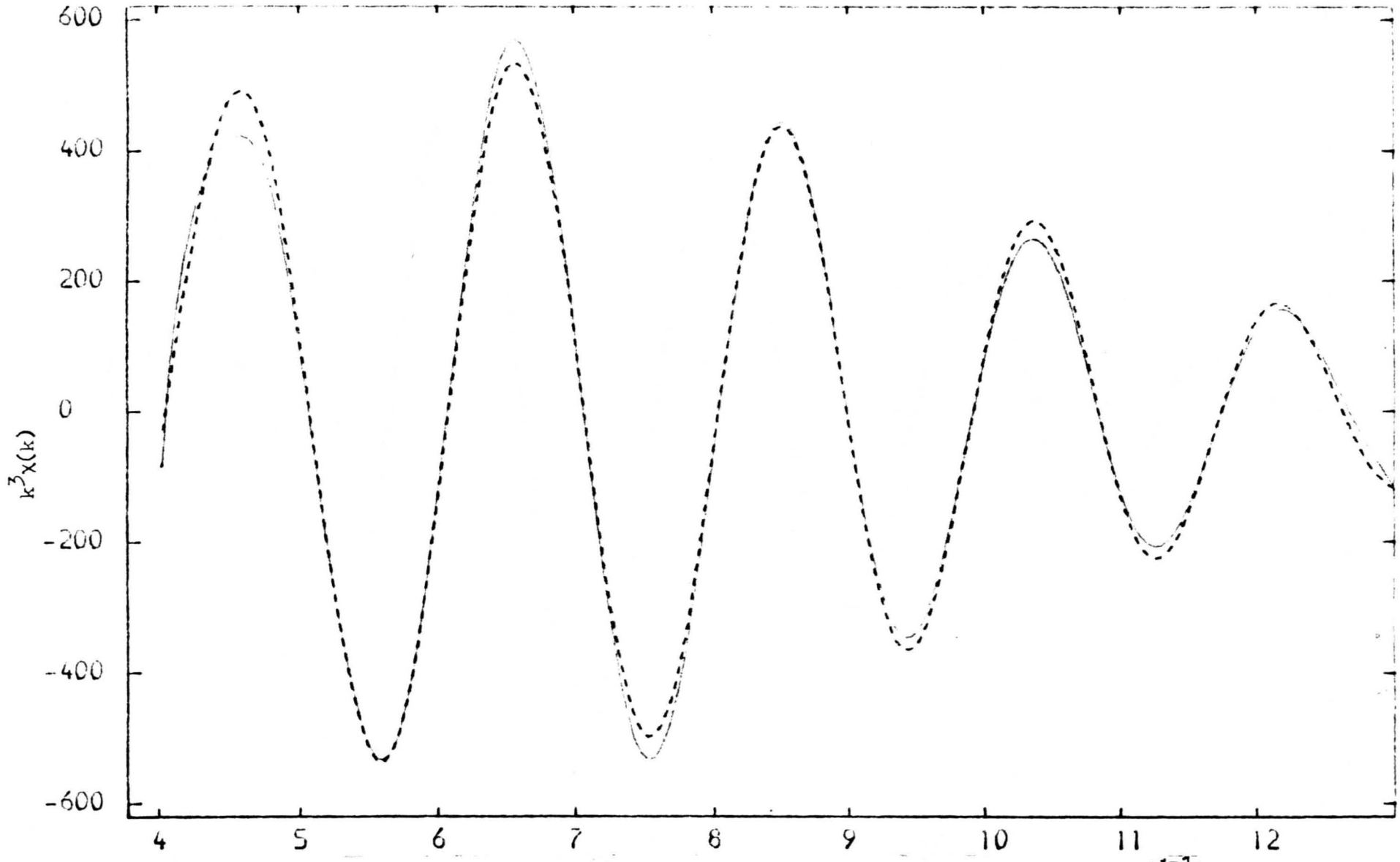

Figure 4.16. Inverse Fourier transform (solid line) and least squares fit of the oxygen shell in ZrA.

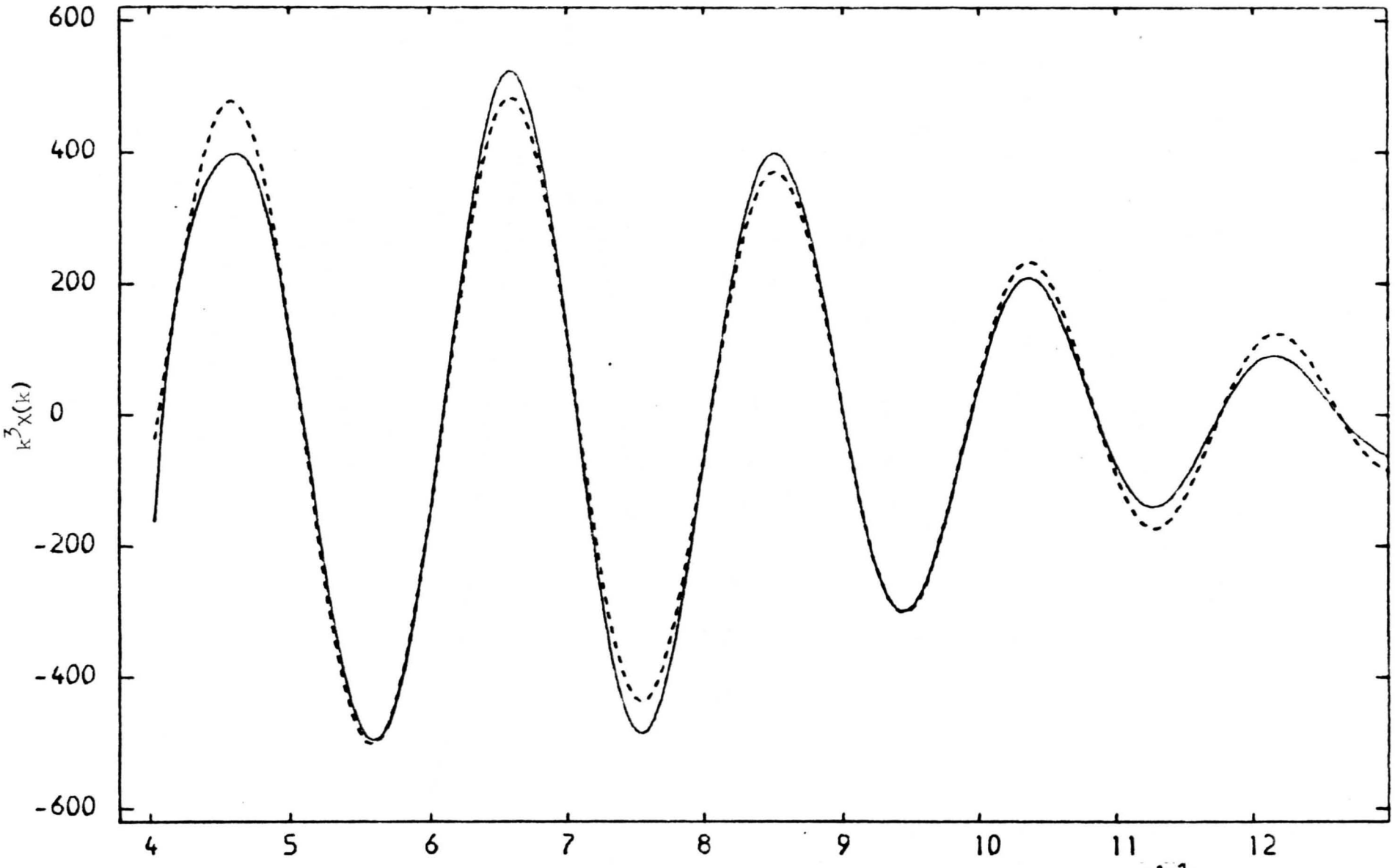

Figure 4.17. Inverse Fourier transform (solid line) and least squares fit of the first shell in ZrB.

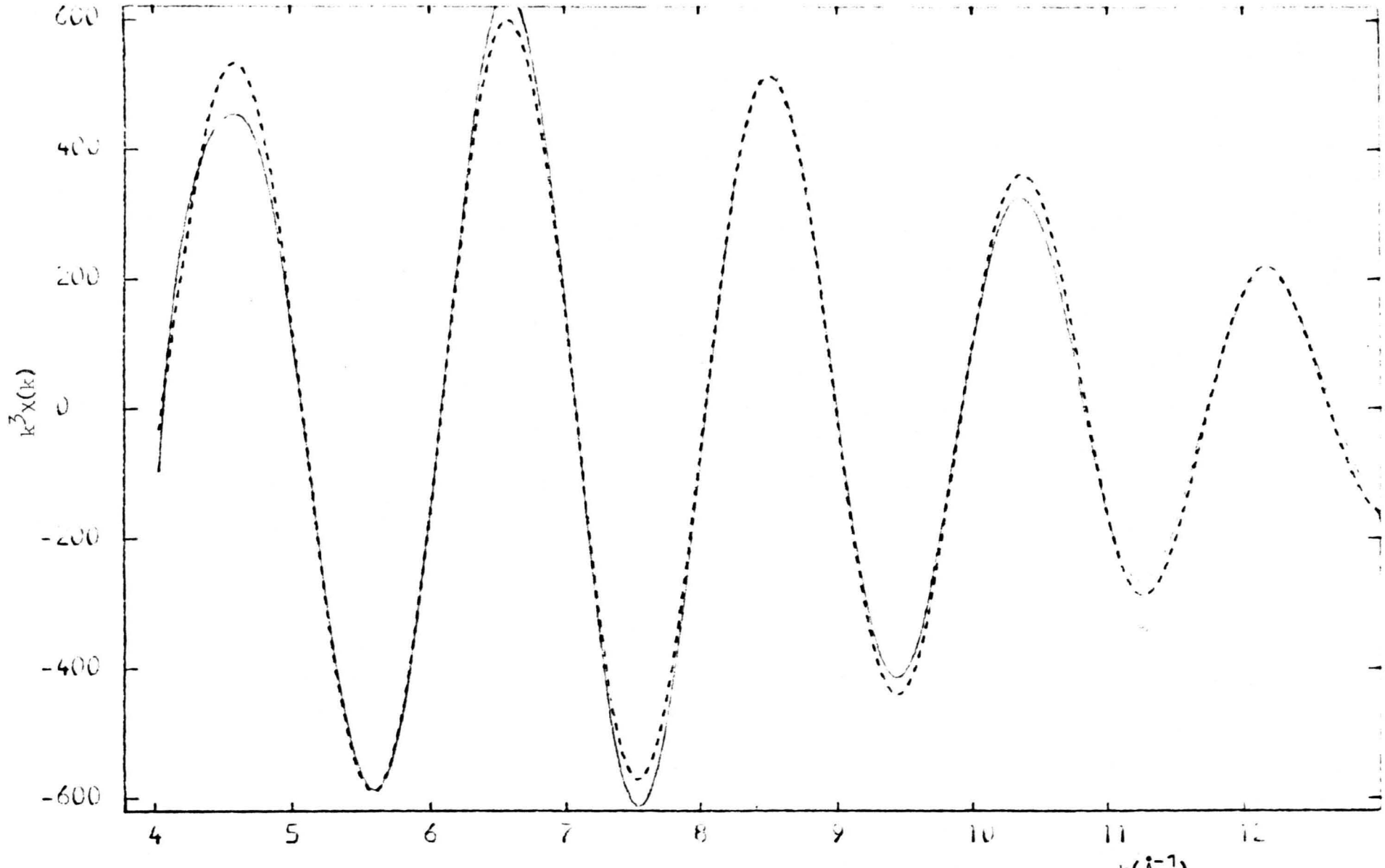

Figure 4.18. Inverse Fourier transform (solid line) and least squares fit of the oxygen shell in ZrC.

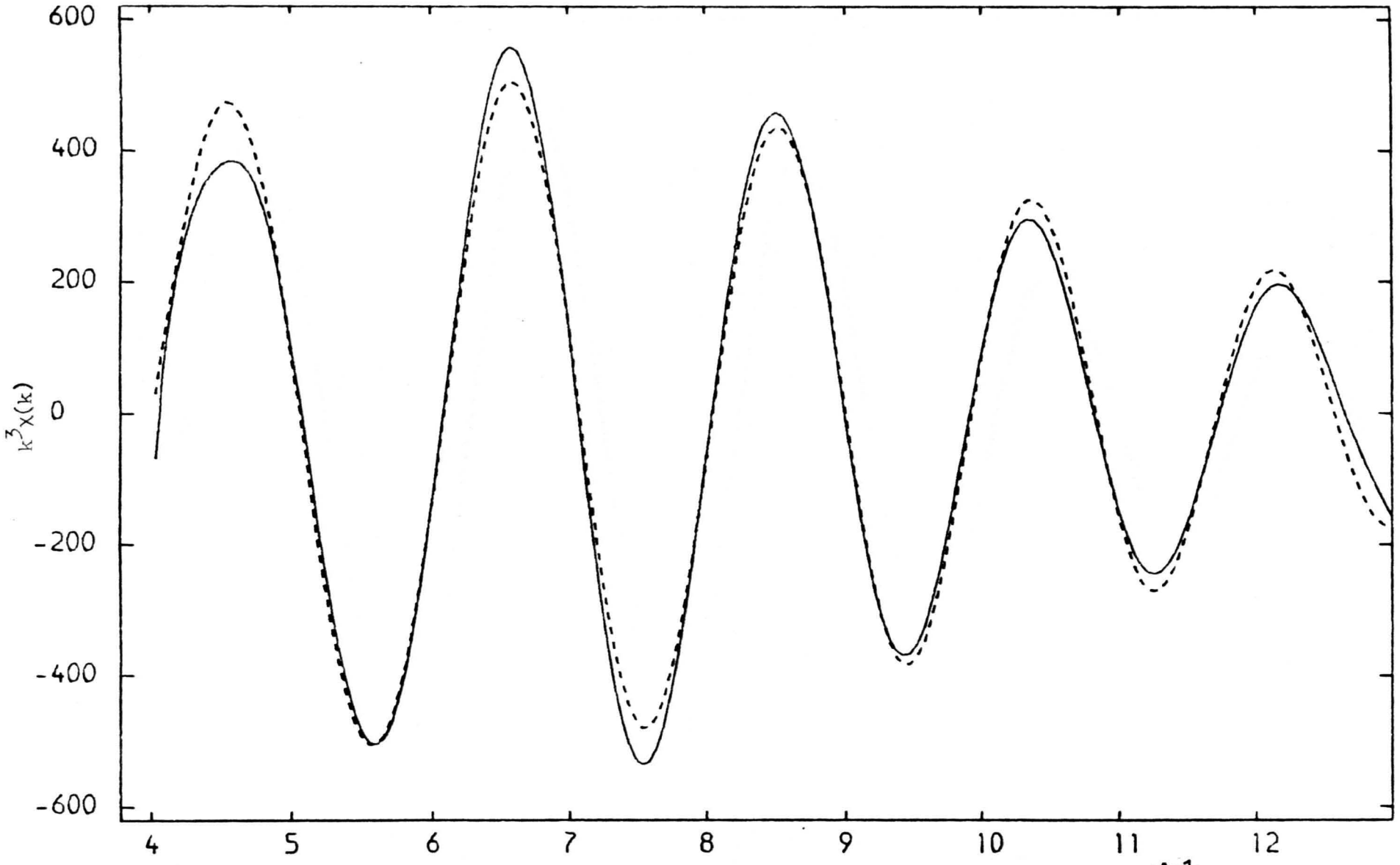

Figure 4.19. Inverse Fourier transform (solid line) and least squares fit of the oxygen shell in ZrD.

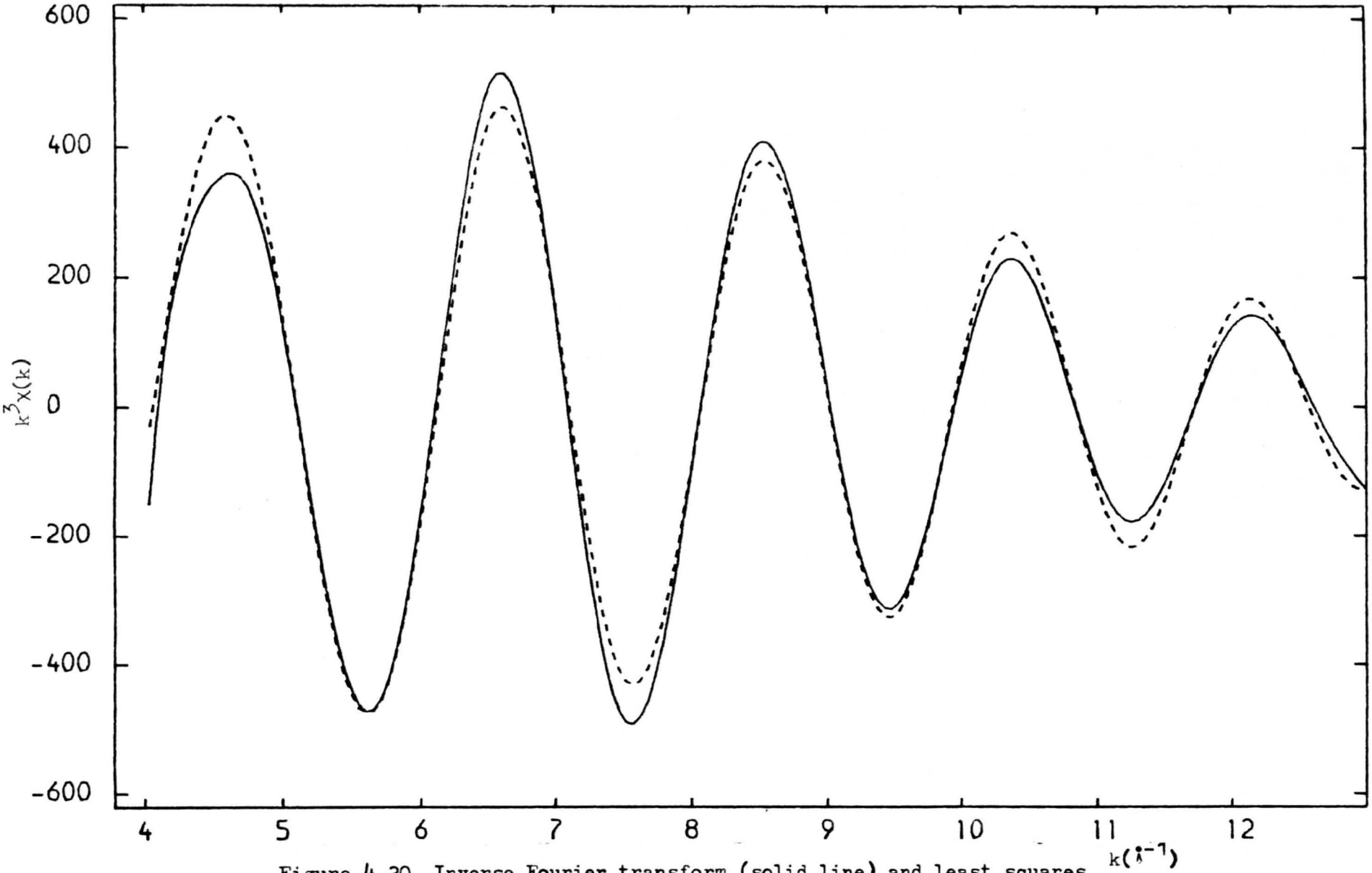

Figure 4.20. Inverse Fourier transform (solid line) and least squares fit of the oxygen shell in ZrE.

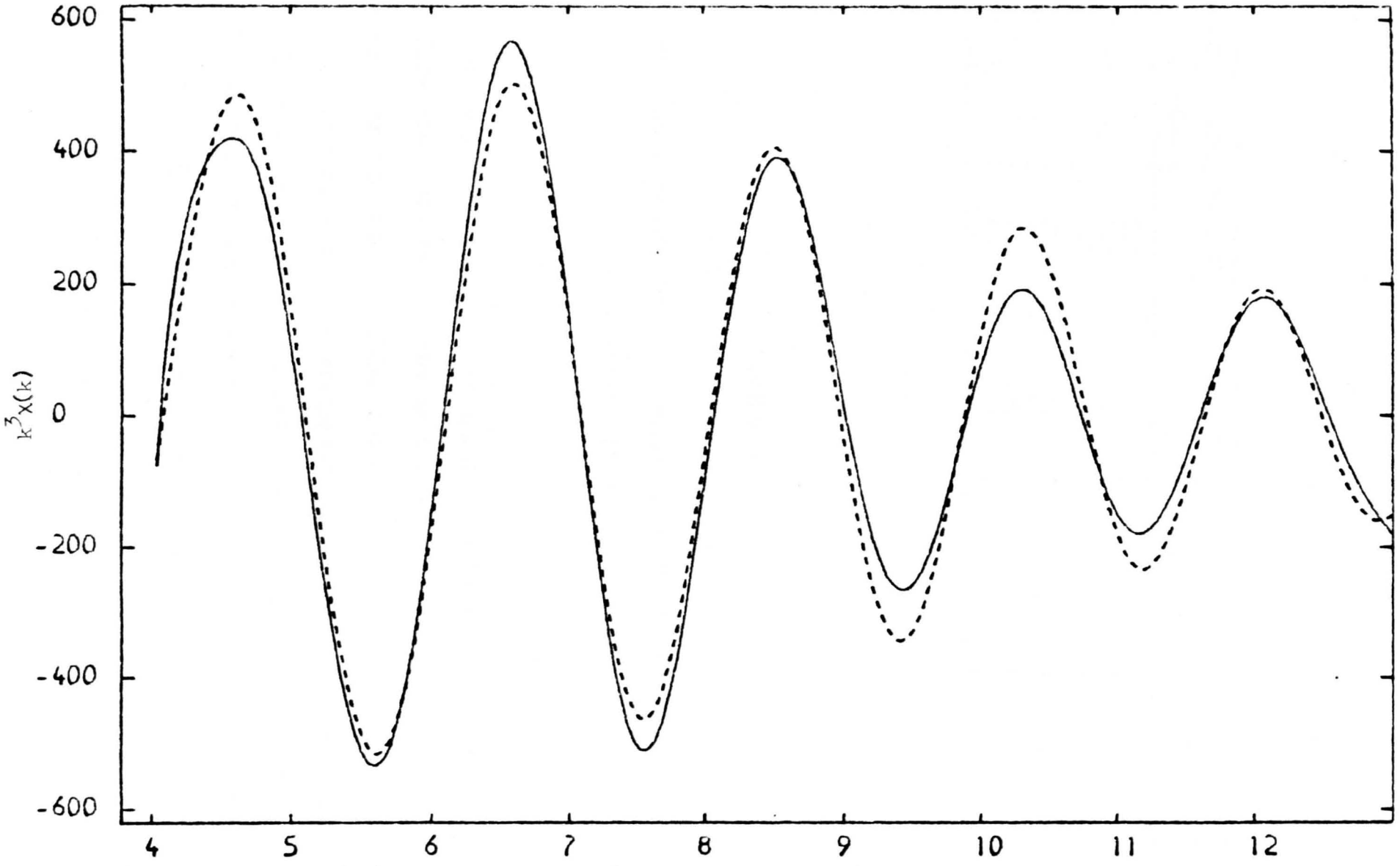

Figure 4.21. Inverse Fourier transform(solid line) and least squares fit of the oxygen shell in ZrA2.

SAMPLE	COORD. SHELL	N_j (± 1)	r_j (± 0.05) (Å)	$\Delta\sigma_j^2$ (± 5) (x 10^{-3} Å^2	E_0 (± 1) (eV)
ZrA	1	5.6	2.09	-16	5
ZrB	1	5.8	2.09	-7	5
ZrC	1	5.6	2.09	-23	5
ZrD	1	5.4	2.08	-10	5
ZrE	1	5.6	2.09	-14	5
ZrA2	1	0.4	1.95	-35	5
ZrA2	2	4.6	2.11	-5	5

TABLE VIII

Results of fitting EXAFS data

($\Delta\sigma_j^2$ values are compared to the value for $ZrSiO_4$: σ_j^2 = 0.005 A^2;

edge energy = 17998 eV)

For the particular case of the quenched samples - Figure 4.21. - no reasonable fit could be obtained on the assumption of a single Zr-O distance. On the basis of this, and supported by the study in the previous section, a further refinement was pursued in which two cation-anion distances (r_1 and r_2) were allowed to vary together with N_1, N_2, $\Delta\sigma_1^2$ and $\Delta\sigma_2^2$. This procedure gives a value for Δr (r_2-r_1) of 0.16 ± 0.1 A which agrees with the earlier result (Section 4.4.1.). Here it is anticipated that correlation effects may distort the values given in Table VIII. To serve as a check, this procedure was repeated for the annealed

specimens for which it was found that no resolvable two shell distances could be obtained.

4.5. THE ROLE OF Zr

4.5.1. Previous Studies

Much of the work on the structure of ZrO_2-containing glasses in the past has been performed using infrared and/or Raman spectroscopy. For instance, in a sodium borosilicate glass system, Roganzin (1973) attributed the broadening of the 1082 cm^{-1} (Si-O stretching vibration) and 470 cm^{-1} infra red bands with increasing ZrO_2 content, to be due to the depolymerization of the silica network with Zr^{4+} ions occupying an interstitial (modifying) site. On the other hand, Botvinkin et al. (1964), working on the sodium-silicate system, drew conclusions on the role of Zr by way of inference from the devitrification products. They observed that $NaZrO_3$ and $NaSiO_3$ phases both crystallized on heat treatment and by analogy with binary silicates, postulated that the Zr environment within the parent glass was similar to that of the crystal and thus behaves as a network former with a CRN of 6. Other models have been suggested on the basis of bonding and crystallochemical characteristics of zirconium and oxygen via comparisons with known silicate structures. Belov (1963) considered the zirconium environment to be similar to that observed in minerals such as lovenite and seidzorite, where the basic structural units consist of mixtures of $[SiO_4]$ and $[Si_2O_7]$ anions with Zr being octahedrally coordinated.

4.5.2. Determination from EXAFS Studies

The EXAFS results summarized in Table VIII indicate that the Zr^{4+} ions occupy a well-defined site within the glass with an average CRN of

approximately 6, situated at a distance of 2.09 ± 0.05 Å. Comparison of these results with values obtained from crystalline compounds show that the oxygen arrangement may be similar to that found in perovskite, $CaZrO_3$ - Megraw (1947). The degree of ordering, reflected by the negative $\Delta\sigma_j^2$ values, is larger than that found in $ZrSiO_4$, although with hindsight this may have not been the most suitable of standards. This decrease can be attributed to the first shell domination of the ordering process at the expense of outerlying shells, a criterion that has to be fulfilled for crystals, but is not a prerequisite in glasses. This is quite clearly shown by the weak second shell signal (silicon). This effect has been shown to occur in other glass systems (see Chapter 1).

Such a description lends support to the theory that Zr^{4+} behaves as a glass former in this particular glass system (cf Taylor and McMillan, Appendix C) and substitutes for Si. The substitution is clearly not isostructural as is the case for Al^{3+} and Ti^{4+} ions. The structural unit may be schematically represented as:-

$$\equiv Si - O - \underset{Na^+}{Zr} - O - Si \equiv$$

The dictate of electrical neutrality requires the presence of modifying cations occupying the interstices between neighbouring polyhedra.

Using this model, the structural information given in Table VIII can be explained in much the same manner as for binary and tenary silicates. There is no change in the oxygen coordination of Zr by the isostructural replacement of the major modifying constituent, however this does effect the degree of ordering. This effect is shown in Fig. 4.13., indicated by the decreasing $\Delta\sigma^2$ value as the alkali ion increases in size and decreases in ionic field strength, that is, oxygen atoms are donated more readily by K^+ ions than by Li^+, making the competition for oxygen on cooling

considerably more favourable.

The same idealized model can also be applied to the case of varying alkali content (Fig. 4.14.). For low concentration (~ 17 mole % total modifier content) there seems little change compared to the ZrA composition. It would be expected that there exists a minimum modifier content to the glass forming region simply on the grounds of electrical neutrality. For large modifier contents (~ 28 mole %) more and more oxygens are donated and the depolymerization of the network lowers the viscosity. With analogy to the case of binary and ternary silicates the Zr-O bond shortens by ~ 0.01 Å, but the static disorder increases as more NBO's are produced. The necessary requirement that either two Na^+ ions or one Ca^{2+} ion must be located within the interstices or in the vicinity of the NBO, to preserve electrical neutrality in even an idealized (infinite chain) $[ZrO_6]$ - $[SiO_4]$ network, imposes severe constraints on the amount of modifying cations that can be incorporated before the interstices around the zirconium octahedra become saturated and the glass phase separates, as these ions preferentially occupy sites around the silica tetrahedra. This idealized model explains why there is a relatively small region of glass formation for this system.

The above conclusions have been drawn with respect to results obtained for the annealed specimens. It is known that the physical properties of glasses depend to a large extent on their thermal history. It has been noted already that density changes occur on annealing indicating a certain amount of ordering prior to any observable crystallization. The results for the quenched and annealed samples do indeed show such an effect with respect to the occurrence of two metal-ligand distances in the former. This implies changes in structure of the glass on subsequent heat treatments, an effect which has hitherto been thought to be unobservable on the atomic scale. However, caution

must be taken in the reliability of the fitted parameters for the quenched sample as the two shells will be highly correlated.

4.5.3. **Infrared Studies**

In the light of this theory of ZrO_2-containing glasses, the infrared data presented in Section 4.3.2. may be explained. As has been mentioned, the Zr^{4+} ion does not take part in translatory vibrational modes within the spectral range covered (1500 cm^{-1} - 300 cm^{-1}) and it is therefore expected that the only way to monitor the behaviour of Zr^{4+} is by its effect on the SiO_2 network. Caution must be taken in attributing the non-existence of Zr-O modes to be a result of a loosely bound Zr cation, implying that it may act similarly to Na^+ as a modifier cation.

Infrared results presented in Fig. 4.10. place the main Si-O stretching frequency at ~ 1000 cm^{-1} due to the contribution from both bridging and non-bridging oxygens, a shift to lower frequency far in excess of that due to the breaking up of the [SiO_4] network by the modifying agents (Na_2O and CaO) alone. This modifying effect can be schematically represented as

$$\rightarrow Si - O - Si \leftarrow + Na_2O \rightarrow \rightarrow Si - O^- \; O^- - Si \leftarrow + 2Na^+$$

or

$$\rightarrow Si - O - Si \leftarrow + CaO \rightarrow \rightarrow Si - O^- \; O^- - Si \leftarrow + Ca^{2+}$$

This shift to lower frequencies may be a consequence of a further

depolymerization of the silica network or, as will be shown, may be due to Zr^{4+} ions acting as network formers. This latter effect would cause the Si-O stretching frequency to be shifted and broadened by the existence of Si-O-Zr correlations as is observed in the case of zircon. Furthermore there is no evidence to suggest the splitting of the Si-O band at the pseudo-disilicate composition of the glasses.

Such a model for Zr acting as a network former is supported by monitoring the Si-O-Si stretching frequency at 780 cm^{-1}. The shift observed here is less than the shift observed with 25% Na_2O, in a binary silicate, however, the band is broader. Again, this may be attributed to variation in Si-O-Si bond angles as a result of Zr^{4+} ions replacing Si^{4+}.

4.6. HfO_2-CONTAINING GLASSES

The chemical behaviour of Hf and Zr is almost identical. The size of the respective ions differs only by ~ 0.01 Å and the stereochemistries they exhibit are so similar, that within all naturally occuring minerals containing ZrO_2, HfO_2 is present in small concentrations. The geochemical arrangements of Hf-based compounds are given by Macdermott (1973). In this review the bonding characteristics are suggested as being due to electrostatic interaction and there is no ligand-field stabilization of atomic orbitals reported.

In view of this similarity, it may be anticipated that the structural behaviour of Hf^{4+} ions in glasses resembles, or is even identical to, that of Zr^{4+}. Until now, no structural work has been performed on HfO_2-containing glasses, probably in view of the above reason and also their full technological potential has, as yet, to be fully realized, although they have found use in alkali-resistant fibres.

The glass compositions studied are similar to those given in Table IV. All the glasses were annealed at the same temperature ~ 700°C.

4.6.1. EXAFS Analysis

The major difference in the interpretation of EXAFS data for Hf is that it involves analysis of the L-edges, as the K-edge falls within the region of hard X-ray wavelengths, far too inaccessible by conventional equipment. This in itself presents very little difficulty as only the radial distribution through the FT technique will be discussed.

As a standard, HfO_2 was chosen which is iosmorphous with ZrO_2. Here the metal ion is seven coordinate with an array of irregular Hf-O bond lengths. Fig. 4.22. presents the magnitude of the FT of the EXAFS data for both HfO_2 and ZrO_2 and as can be seen, the qualitative features of both FT's are similar.

The EXAFS for one of the glass samples, HfA (≡ ZrA) is shown in Fig. 4.23. and the corresponding magnitude of the FT in Fig. 4.24. The EXAFS data for the L_I edge has been extracted as this constitutes a pure s-d type transition. The L_{II} and L_{III} edges are characterized by an admixture of transitions, the strong 'white lines' typifying such scattering.

The similarities in bond length and ordering of Hf-O are readily apparent by comparing Figs. 4.24. and 4.4. and notwithstanding a thorough investigation by means of a curve-fitting technique, the qualitative features of ZrO_2- and HfO_2-containing glasses are the same, lending support to the theory that both these congeneric cations take part in the forming of a glass network.

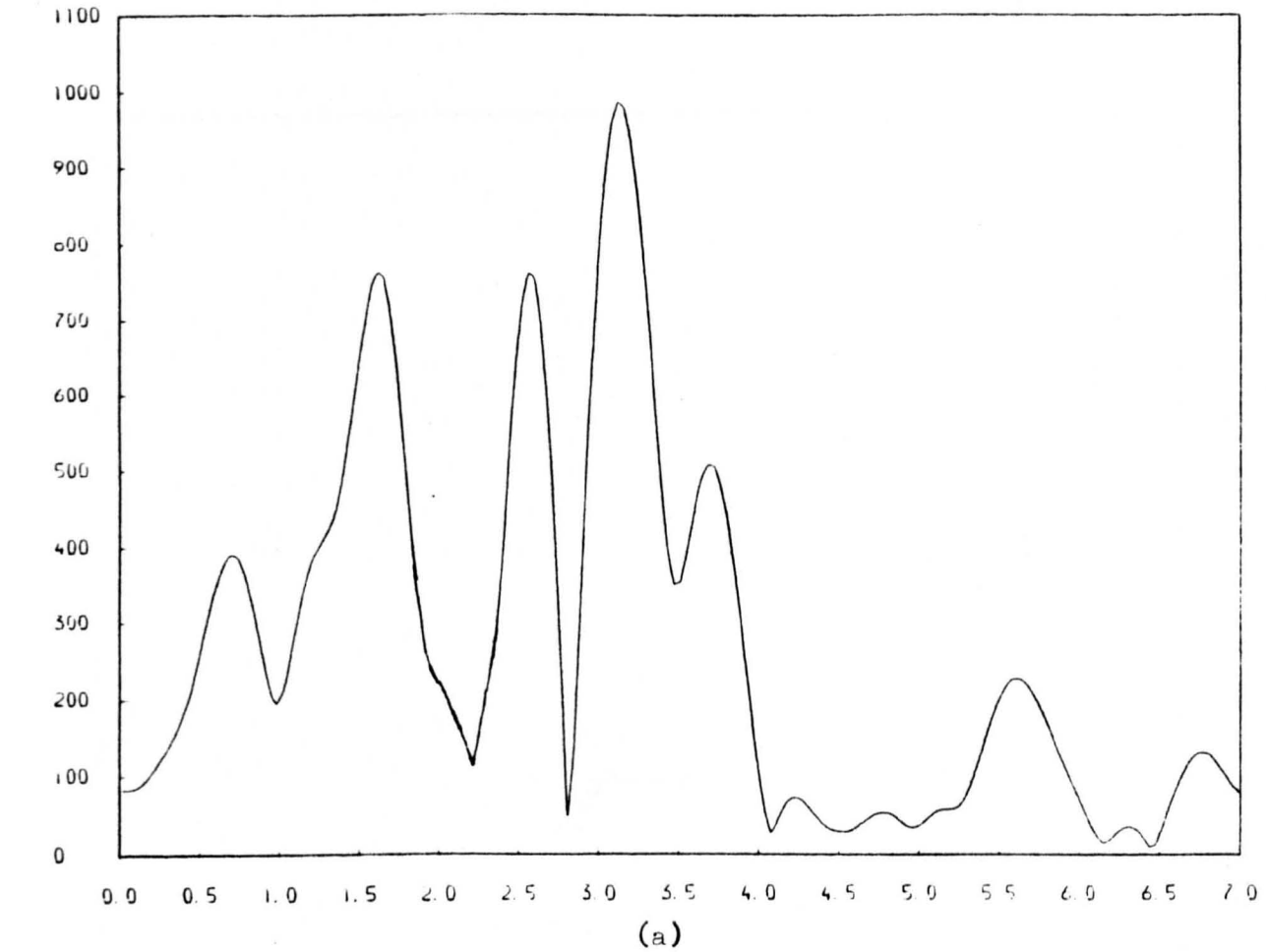

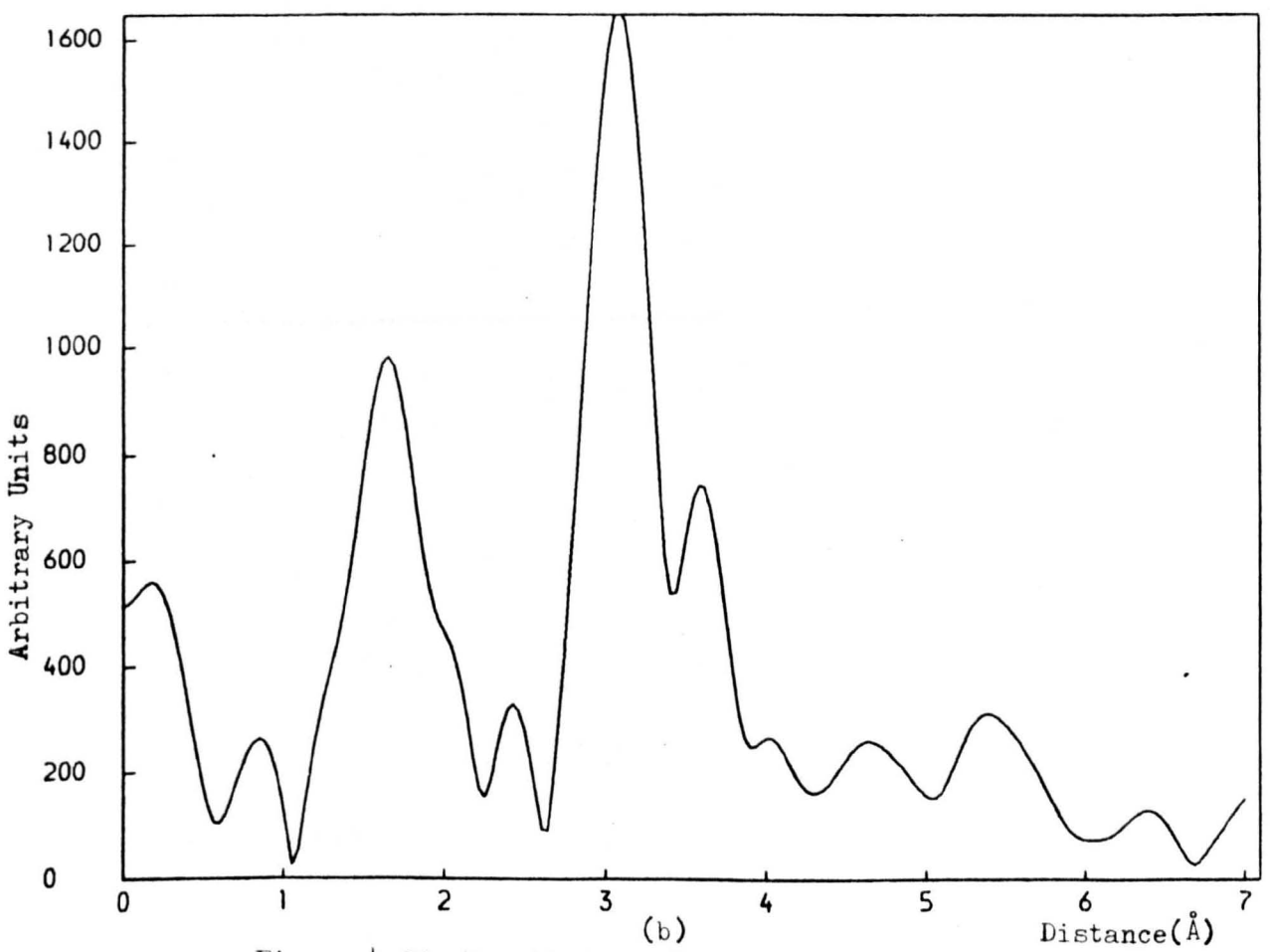

Figure 4.22. Magnitude of Fourier transform for the isostructural compounds:(a) HfO_2 and (b) ZrO_2.

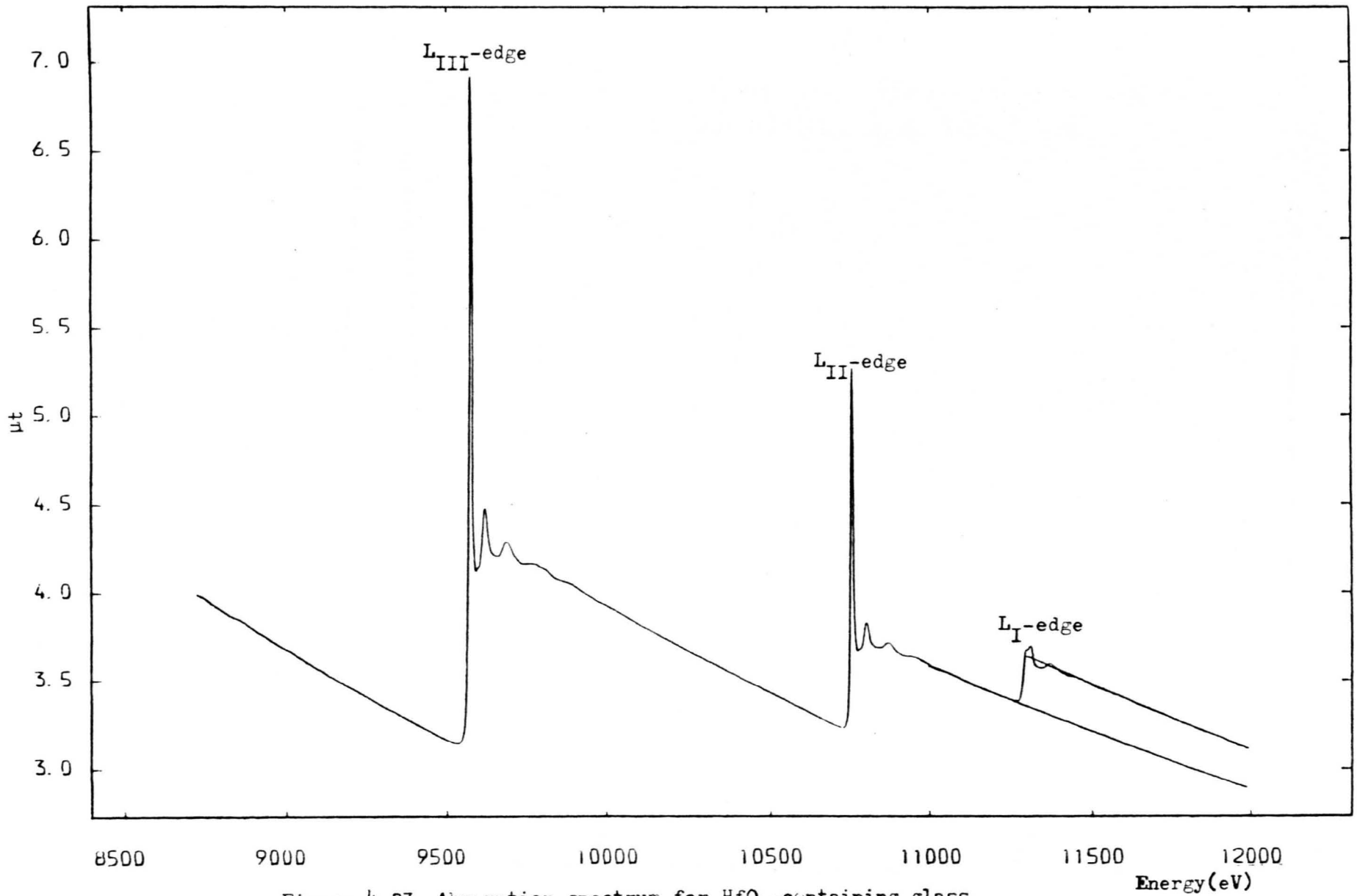

Figure 4.23. Absorption spectrum for HfO_2-containing glass.

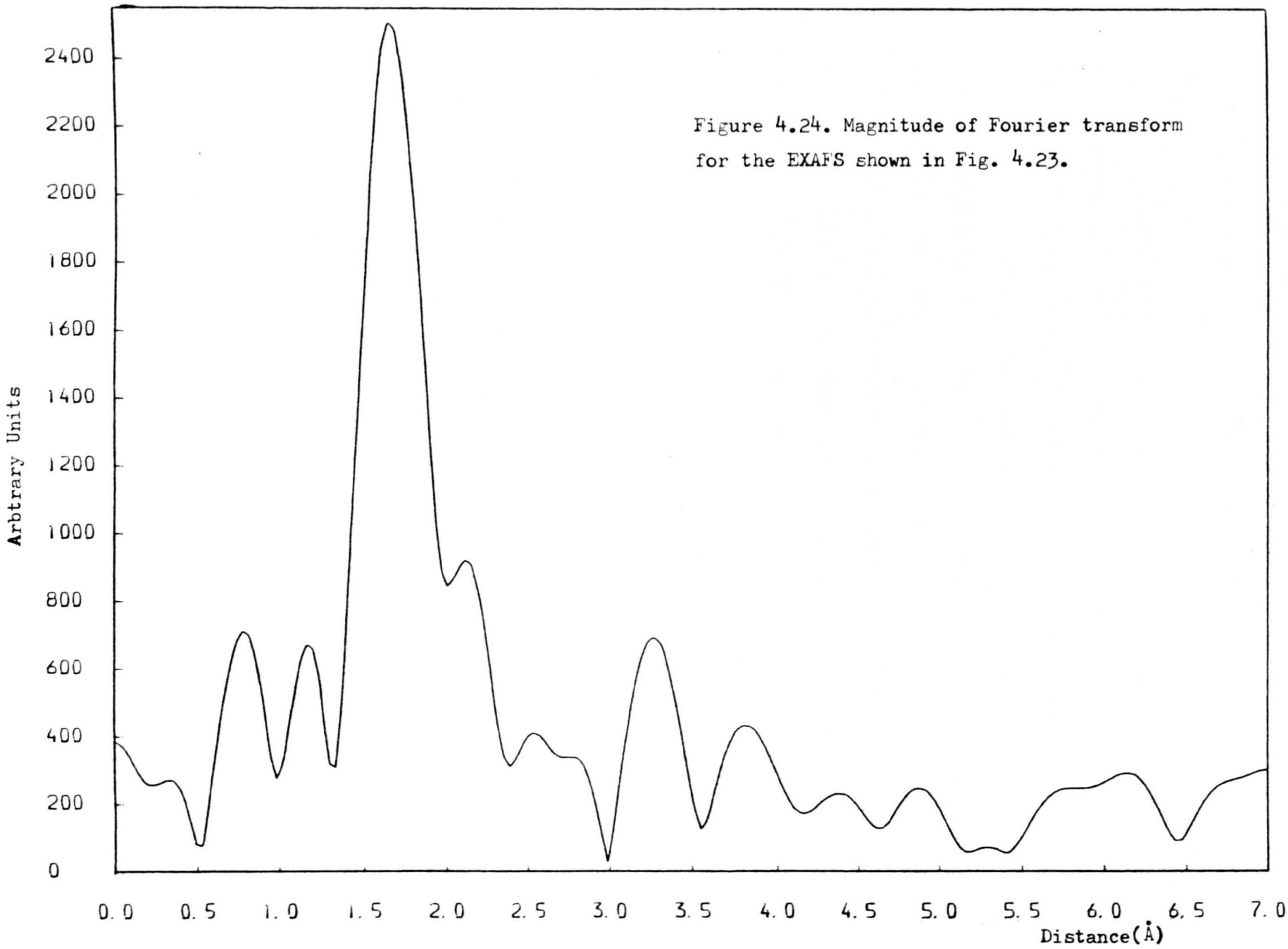

Figure 4.24. Magnitude of Fourier transform for the EXAFS shown in Fig. 4.23.

CONCLUSIONS

The results presented in this chapter have underlined the usefulness of the EXAFS technique for investigating multi-component glass systems. It has proved that Zr^{4+} acts as a network former in this system and occupies a site within the matrix that is more ordered, as far as first shell is concerned, than that of a corresponding crystal. Such a behaviour is not allowed under the prerequisities of the Zachariasen model of glass structure and may therefore lend support to the theory of more complex anionic species being the underlying building blocks of glasses. The results have also shown for the first time that changes in the atomic arrangement due to thermal treatment are observable over atomic dimensions and opens new paths for the study of the mechanism of nucleation and growth. Such a study has already been initiated by the author (Appendix C).

Chapter 5

X-RAY STUDIES OF THE K-EDGE OF Ti IN Na_2O-TiO_2-SiO_2 GLASSES

5.1. INTRODUCTION

The X-ray absorption results presented in this chapter were taken at the Daresbury Laboratory SRS facility. All measurements were performed in air at room temperature on thin film specimens. The compositions of the glasses are given in Table IX. In general the data are of good quality, however for low concentration (~ 5 mole %) counting statistics were poor making EXAFS interpretation very difficult.

A short precis of the previous investigations into the structure and coordination of TiO_2 in glasses is presented. This has been included to serve as a guide to the difficulties that exist in such an investigation and also to justify the choice of glass compositions.

5.2. MODEL COMPOUND ANALYSIS

5.2.1. Choice of Suitable Compounds

As will be discussed in Section 5.3.1. the structural position and coordination of Ti^{4+} ions within glasses is, as yet, not fully understood. Octahedral and tetrahedral environments have been suggested, the ratio of the two sites being a function of composition. To this end, two standards were chosen in which the Ti polyhedra are of one type only. For octahedral symmetry 'analar' grade TiO_2 (anatase) was chosen, and for the tetrahedral case Ba_2TiO_4 (barium orthotitanate) the only four fold oxygen coordinated compound of titanium known to exist. This latter material was prepared by a flux melting technique described by Bland

(1961) and was found to be comprised of 90% Ba_2TiO_4 and an excess 10% TiO_2. The radial distances of the first shell oxygen cage are given in Table X after Cromer and Herrington (1955) for TiO_2 and Bland (1961) and Brown et al. (1973) for Ba_2TiO_4. Both EXAFS specimens were prepared as a thin film as described previously.

Sample	TiO_2	SiO_2	Na_2O
TiA	5	70	25
TiB	10	65	25
TiC	25	50	25
TiD	33	42	25
TiE	40	35	25
TiF	5	61.7	33.3
TiG	26.7	40	33.3
TiH	33.3	33.3	33.3
TiI	40	26.7	33.3

TABLE IX

Compositions of TiO_2 containing glasses in mole %. All glasses were melted in the range 1350-1450 °C and quenched to room temperature.

Compound	N	r_j (Å)	Average Distance
TiO_2	4 2	1.94 1.97	1.95Å
Ba_2TiO_4	4	1.71 1.81 1.82 1.84	1.81 Å

Table X

Oxygen coordination around Ti ions in anatase and Ba_2TiO_4

5.2.2. Raw Absorption Data and EXAFS

The absorption spectrum $\ln(I_0/I)$ for both standards is shown in Fig. 5.1. (TiO_2) and Fig. 5.2. (Ba_2TiO_4). Around the K-edge of Ti, the spectra display two distinct areas of interest. In the region from 50 eV above the edge and beyond the typical EXAFS oscillations are observed, whilst for energies close to the binding energy of the core electron - the so-called XANES (X-ray absorption near-edge structure) - there exists the possibility of electron transitions to bound states of the emitting atom that give rise to characteristic features. Kutzler et al. (1980) and Tossell et al. (1974) suggest that the intensity of the three features observed in TiO_2 are dependent on the degree of anisotropy of the Ti-O bond within the $[TiO_6]$ octahedron. These features are observed in the three phases of TiO_2 (anatase, rutile and brookite) and can be related to the inter-connection of $[TiO_6]$ octahedra: namely in rutile each octahedron shares two edges; in brookite each octahedron shares three edges; and in anatase the common edges are four. The oxygen disposition is characterised by four planar and two axial Ti-O distances. Progressive relaxation of this inversion symmetry will produce finally the one intense pre-edge transition found in titanates possessing a tetrahedral symmetry, e.g. Ba_2TiO_4 and $TiCl_4$ (Sandstrom et al., 1983).

The EXAFS was extracted from the raw absorption data in the manner described previously. One major difficulty with the interpretation of the EXAFS for Ba_2TiO_4 comes from the fact that the Ba L_{III} edge appears some 250-300 eV above the Ti K-edge. This severely affects the resolution of the technique and consequently the amount of structural information is limited. Because of this, Ba_2TiO_4 was chosen as a standard material for comparison of pre-edge features only and not used as a model compound in the least squares fitting analysis.

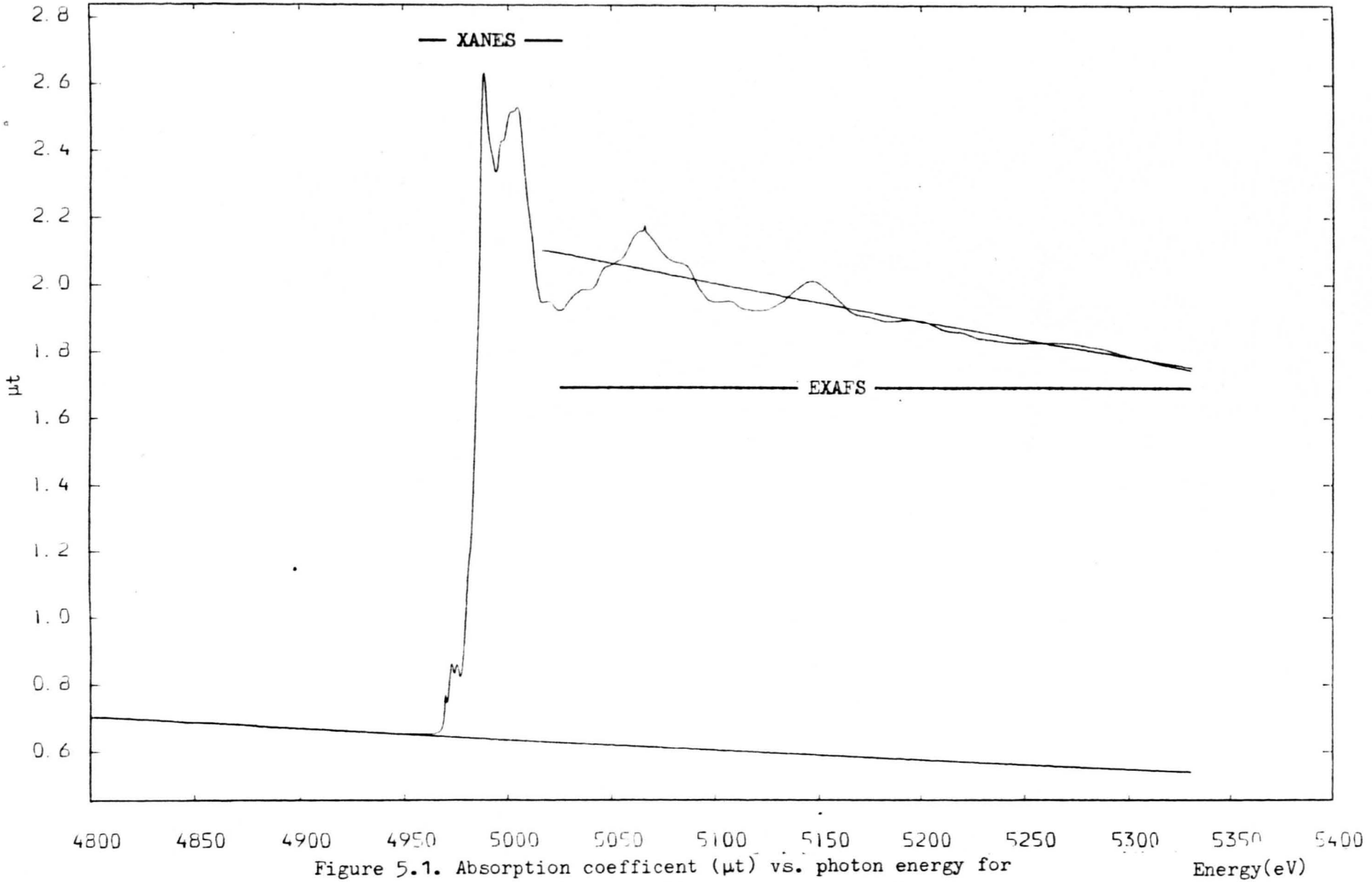

Figure 5.1. Absorption coefficent (μt) vs. photon energy for TiO_2 (anatase). The pre-edge features are charateristic of octahedral coordination.

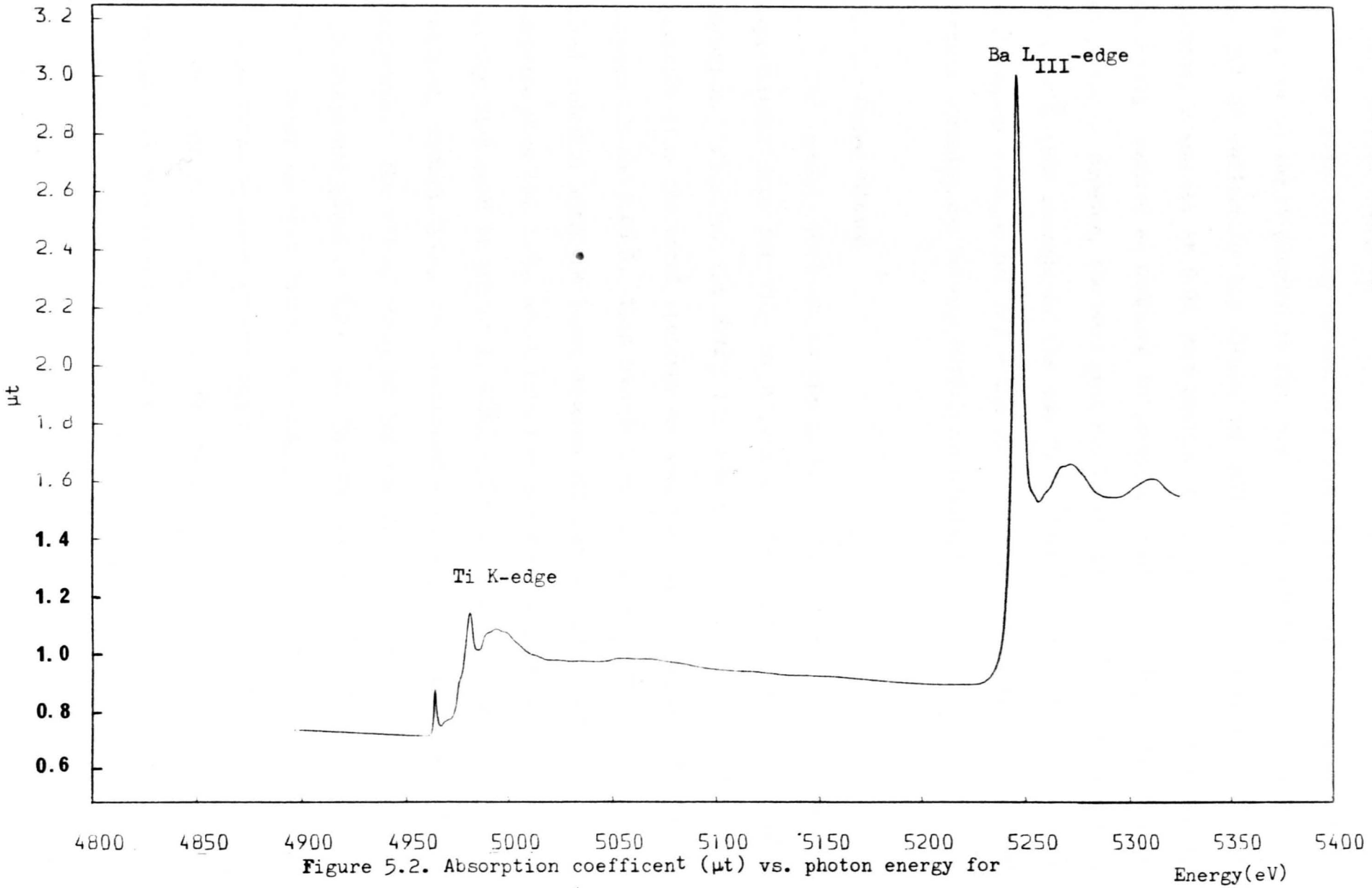

Figure 5.2. Absorption coefficent (μt) vs. photon energy for Ba_2TiO_4. The strong pre-Ti K-edge peak is characteristic of tetrahedral coordination.

5.2.3. Fourier Transform

The EXAFS for TiO_2 is shown in Fig. 5.3a. with the corresponding magnitude of the FT plotted in Fig. 5.4. The FT was taken over a range 40 to 350 eV reflecting the amount of resolvable fine structure in the glasses, γ was set at 0.08 (see Section 4.2.1.). For this reason the FT is poorly resolved as compared to previous studies of TiO_2 (Kozlowski et al., 1983). However, the main peak can be attributed to oxygen scattering at 1.96 Å (the average of the two Ti-O distances observed in anatase) which gives a value for $a/2 = 0.4$ Å. The peaks at higher r represent complex correlations between outerlying octahedra.

5.2.4. Curve Fitting

The method discussed in the previous Chapter was used to fit the experimental data for TiO_2 to a paramaterized expression of the EXAFS equation. Firstly, the EXAFS for the first shell only (oxygen) was filtered from the total spectrum by isolating the first peak in the FT between 1.0 and 2.05 Å. This contribution is plotted in Fig. 5.5a. (solid line) together with the least squares fit (dashed line). This is to be compared with Fig. 5.5b. which fits the same experimental data but with an average Ti-O bond length of 1.96 Å, where at high k the phase is poorly matched, exemplifying the increased accuracy of the curve fitting technique. The values obtained for the amplitude (c_n) and phase (a_n) parameters are given in Table XI. The fitting range was from 4.0 to 10.5 $Å^{-1}$. Prior to this fitting procedure an attempt was made to fit the inverse FT using phase information from Teo and Lee (see Chapter 4). This result is shown in Fig. 5.6. No attempt was made to fit the original experimental data in energy space!

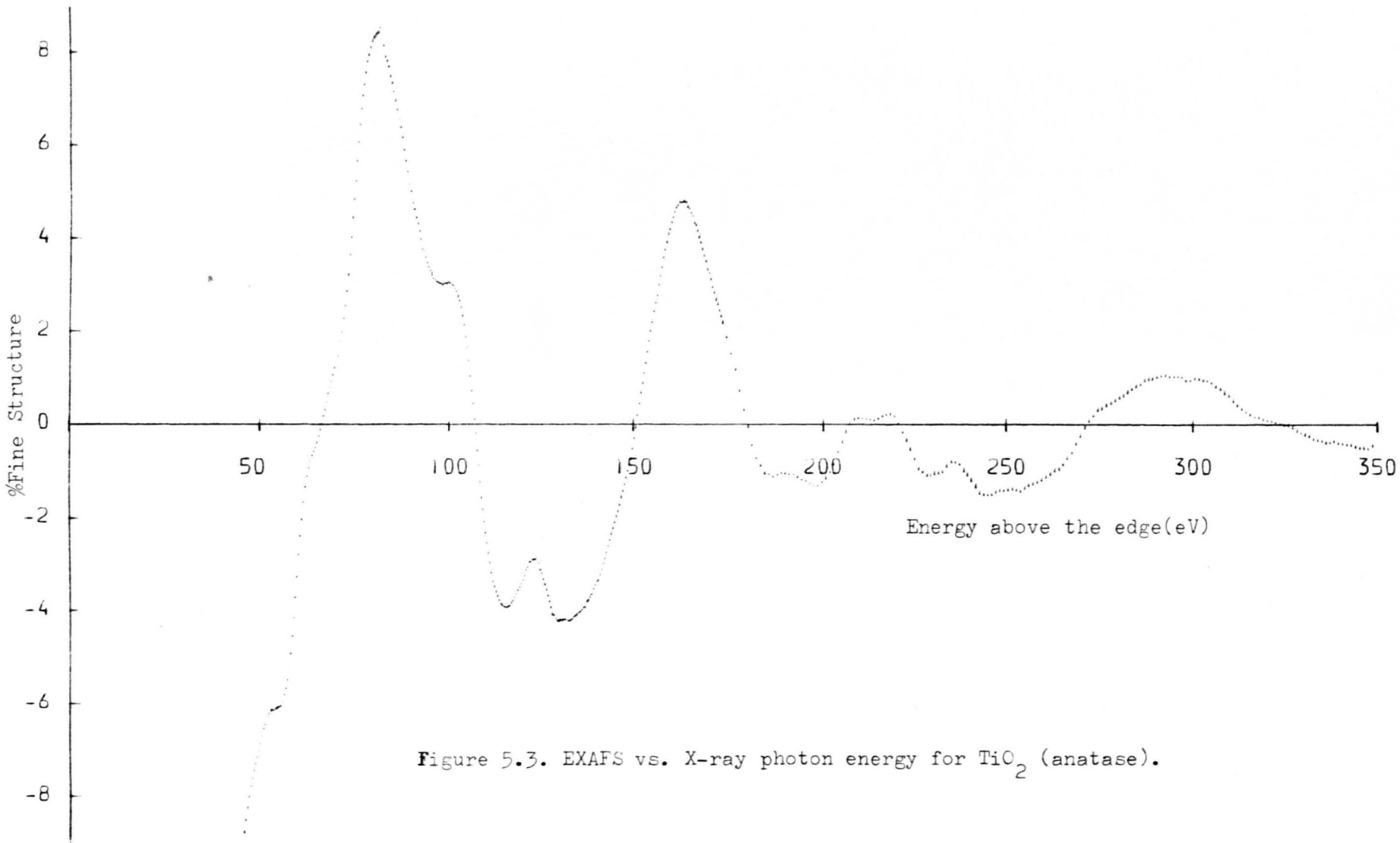

Figure 5.3. EXAFS vs. X-ray photon energy for TiO_2 (anatase).

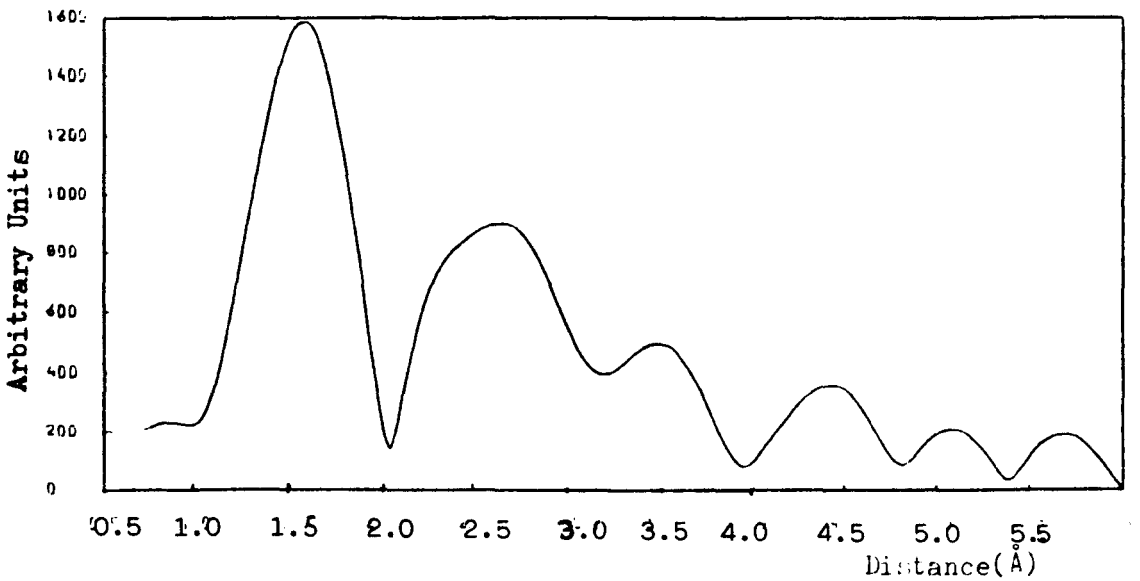

Figure 5.4. Magnitude of Fourier transform for anatase.

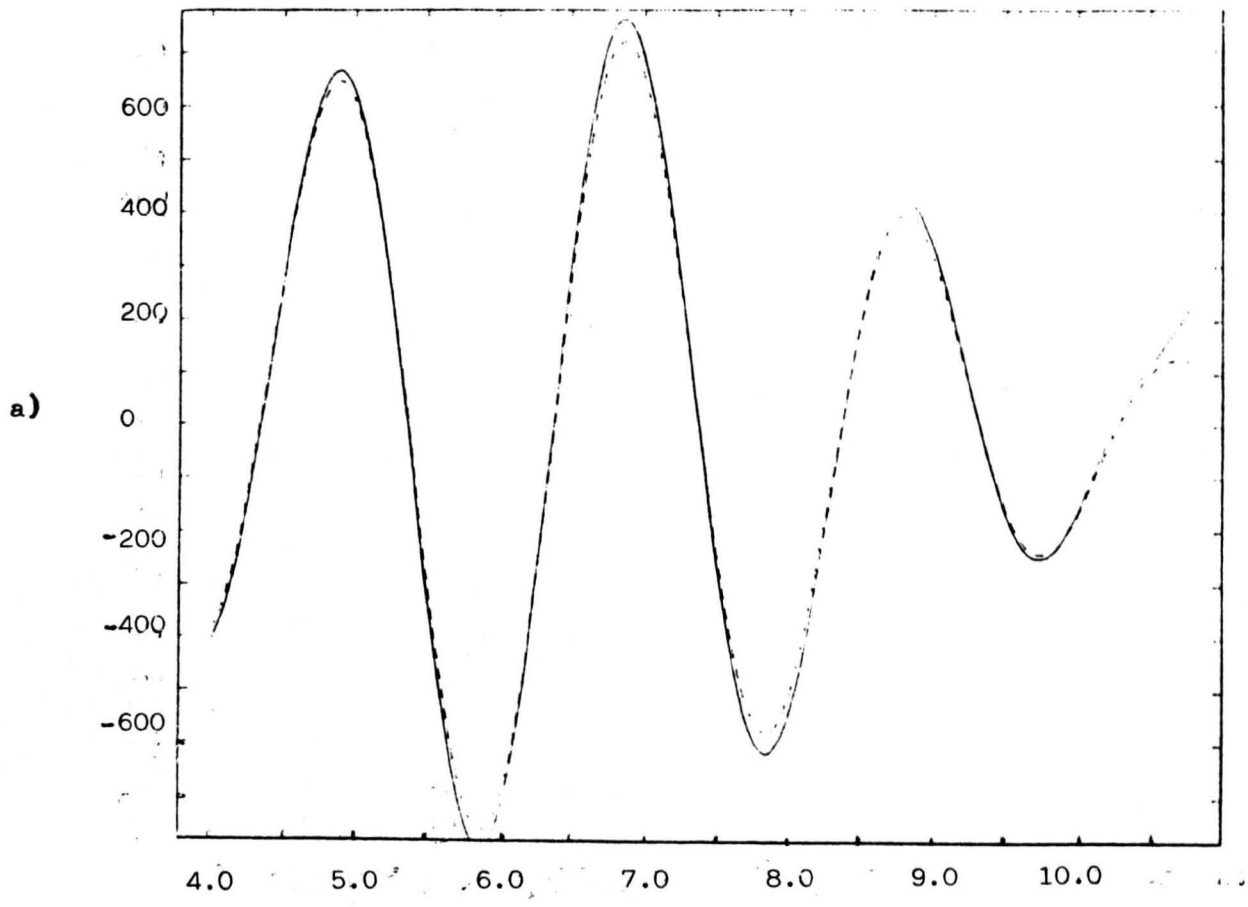

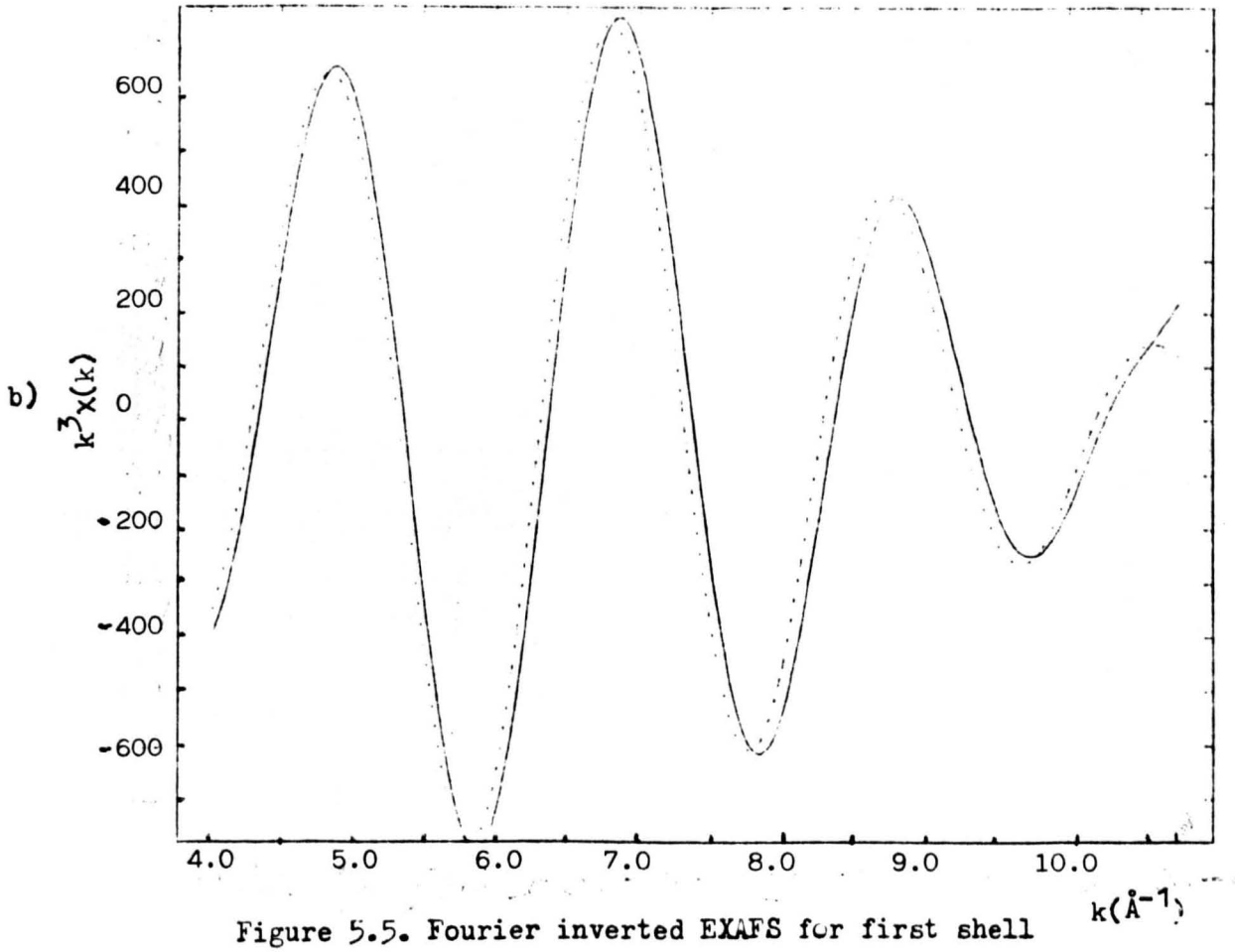

Figure 5.5. Fourier inverted EXAFS for first shell only in TiO_2. Broken line is the least squares fit using (a) data given in Table VIII, and (b) an average Ti-O bond distance.

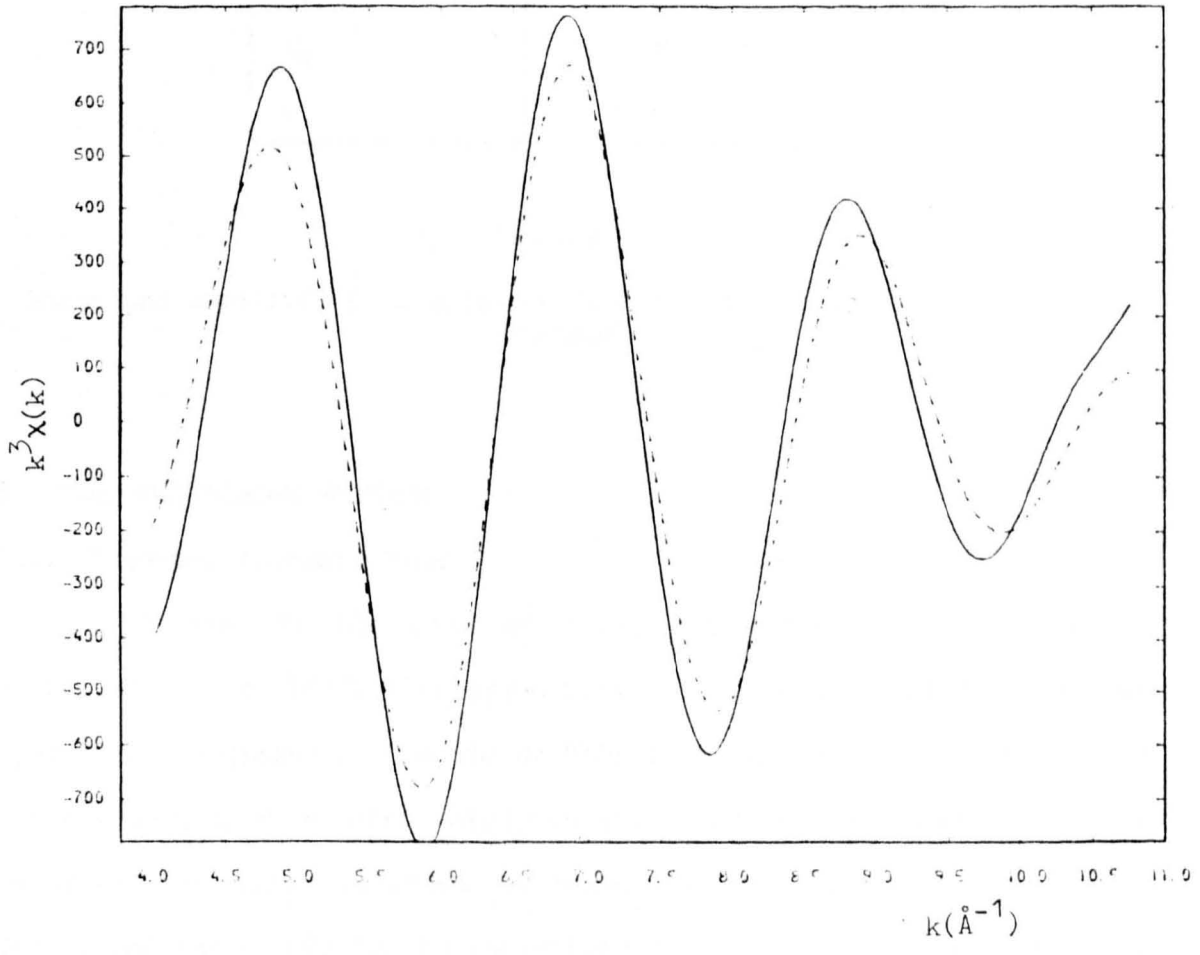

Figure 5.6. Least squares fit (dashed line) to the oxygen EXAFS for anatase using phase information from Teo and Lee.

a_0	3.138
a_1	-1.056
a_2	0.022
c_0	0.03
c_1	26×10^{-3}
c_2	0.76

TABLE XI

Phase and amplitude data obtained from a least squares fit to TiO_2 (anatase)

5.3. TiO_2-CONTAINING GLASSES

5.3.1. Previous Investigations

In contrast to the case of ZrO_2, there has been considerable investigation on both the structure and physical properties of TiO_2-containing glasses. The use of TiO_2 as a nucleating agent by itself or in conjunction with other catalysts (e.g. ZrO_2 - see Chapter 6) in the development of glass ceramics is widely known (Barry et al., 1969) however, the exact role in the nucleation process is far from understood. Recent work by Todhunter (1984) has shown that some ordering of the local Ti environment may be taking place as a precursor to any observable phase separation. This work was carried out on the cordierite system, however, other authors, e.g. Bobovich (1964), have monitored similar trends in other base glasses.

For structural studies *per se* , the wealth of information on the structure is considerable, as is the controversy! Table XII summarizes much of the recent work and the structural tools employed.

AUTHORS	STRUCTURAL	SYSTEM
Manghnani et al. (1971)	IR	Na_2O-TiO_2-SiO_2
Jose and Urnes (1972)	XRD	Na_2O-TiO_2-SiO_2
Loshmanov et al. (1974)	Neutron Diffraction	Na_2O-TiO_2-SiO_2
Hanada and Soga (1980)	X-ray emmission spectroscopy	Na_2O-TiO_2-SiO_2
Chandrasekhar et al. (1979)	Raman	SiO_2-TiO_2
Sandstrom et al. (1980, 1983)	EXAFS	SiO_2-TiO_2
Zarzycki (1971)	XRD	R_2O-TiO_2 (R = Cs, K)
Abradrashitova (1980)	EPR	R_2O-Al_2O_3-SiO_2-TiO_2 (R = Li, Na)

TABLE XII

Structural techniques used to investigate various TiO_2-containing glasses.

In general, these works conclude that Ti^{4+} ions possess a dual character inasmuch as they can occupy two sites within a glass according to the Zachariasen model: either they can enter the network directly and substitute for Si^{4+} ions, or they can break-up or depolymerize the original silica network and as such act as network modifiers. The coordination number they attain is to some extent governed by the particular site they occupy. It has been shown that in binary systems (Zarzycki and Sandstrom et al.) that Ti^{4+} ions may behave as network formers and exhibit either a fourfold or sixfold coordination, depending

on what constituent forms the basic network, the tetrahedral site being an isostructural substitution for Si^{4+} ions.

The evidence for Ti octahedra acting as network formers is also postulated by Abdrashitova, who considered the structural function of titanium to be governed by how polyhedra are connected; either by edge-sharing or corner-sharing, and as such is not a function of the coordination.

The debate over the coordination of Ti is further complicated by the fact that some crystalline titanates and minerals exhibit a 5-fold oxygen environment. For example, K_2TiO_5 (Andersson and Wadsley, 1961) is comprised of $[TiO_5]$ polyhedra grouped in a distorted trigonal bypyramid, and the mineral innelite (Chernov, et al. 1971) has a coordination grouped in distorted pyramids with the possibility of titanyl bonding (Ti = 0) with the apical oxygen. Such a disposition has been suggested by Loshmanov, et al. to exist in TiO_2-containing glasses. They conclude that for high silica contents, Ti exhibits octahedral coordination and as the TiO_2 content is increased, both $[TiO_6]$ and $[TiO_5]$ polyhedra are present, there being no Ti in tetrahedral coordination.

This latter result is of immediate concern in this work. The choice of compositions for the Na_2O-TiO_2-SiO_2 glasses given in Table IX was made in an attempt to observe the intermediate behaviour of Ti^{4+} ions and to identify their role and coordination. It is anticipated that the ratio of sites within the glass would be a function not only of TiO_2 content but also of the amount of modifying cations present.

5.3.2. Raw Absorption Data and EXAFS

As an example of a typical absorption spectrum for this system of glasses, the data for sample TiE is presented in Fig. 5.7. The spectrum possesses two interesting features which require some explanation. At

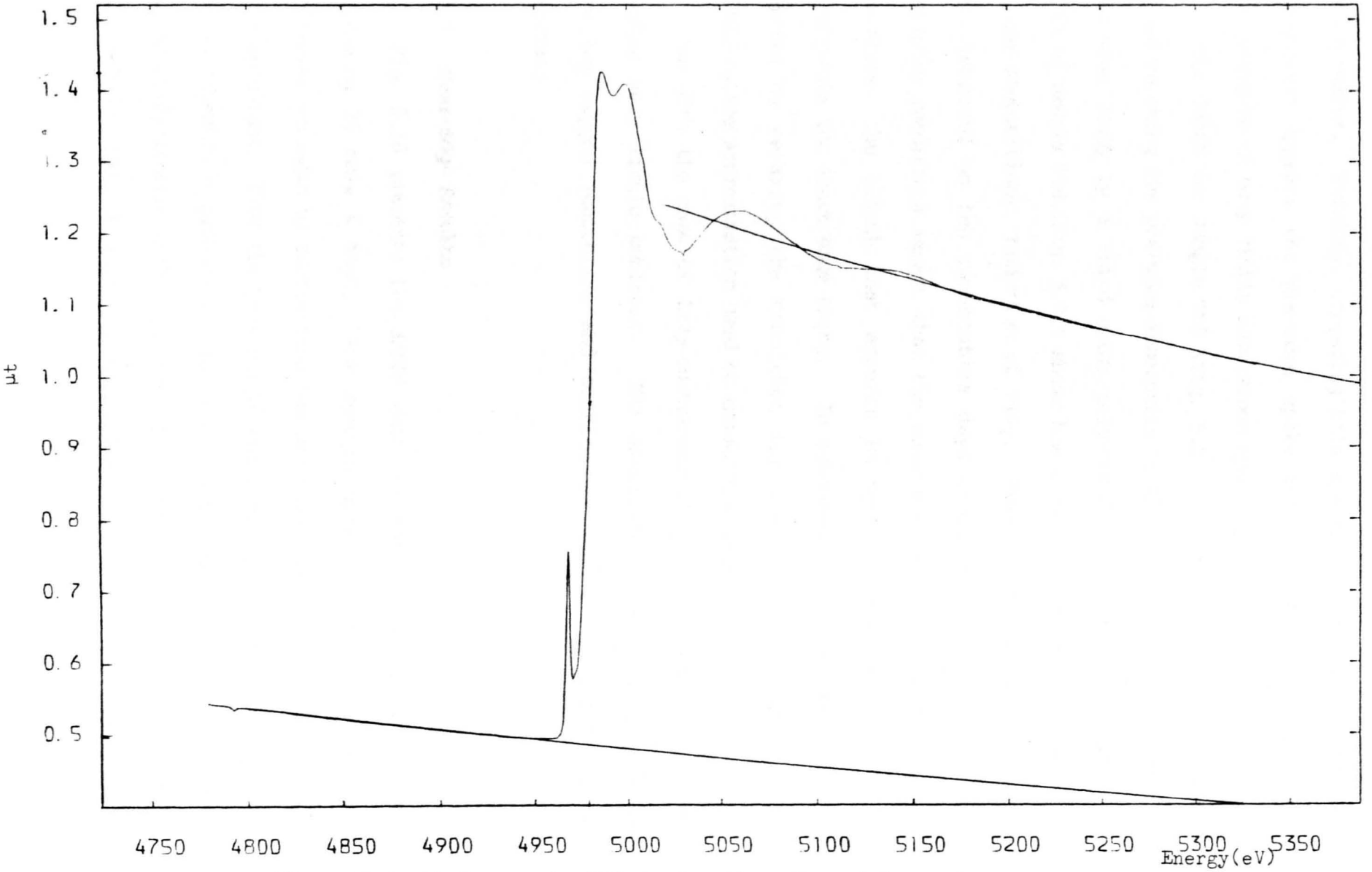

Figure 5.7. μt for sample TiE showing the polynomials used for extracting the EXAFS.

approximately 50 eV above the edge there exists a distinctive kink or 'glitch' in absorption due to spurious reflections emanating from the monochromator. Secondly, comparing this spectrum with that for Ba_2TiO_4, there also appears the pre-edge spike intrinsic to $[TiO_n]$ polyhedra possessing no or very little inversions symmetry.

The EXAFS for sample TiE (Fig. 5.8.) was extracted in the standard way of matching the pre-edge absorption to a Victoreen expression and the post-edge decay by a third order polynomial. Comparing this with the EXAFS of sample TiB (Fig. 5.9.) shows how counting statistics are affected by the compositional variation of TiO_2. Furthermore, these two spectra were measured on two consecutive days under approximately the same operating conditions except that the monochromator had lost calibration. Therefore, the glitch that appears in both spectra can be used to recalibrate the exact edge energy. In subsequent analysis the glitch was removed by relaxing the condition for the number of knots in the culbic-spline approximation used to smooth the data.

As with the case of ZrO_2-containing glasses, the EXAFS themselves display very little contrast. The oscillations decay very quickly, implying oxygen scattering and confirm the disordered nature of the materials.

5.3.3. Near-Edge Results

Fig. 5.10 presents the XANES data for the TiO_2-containing glasses possessing 25 mole % Na_2O. The spectra have been normalized to unit oscillator strength by subtracting the pre-edge absorption and dividing by the step height. From the peak height and width at half maximum, the peak area or transition probability for the s-p transition (as a function of the SiO_2:TiO_2 concentration) can be determined and is shown in Fig. 5.11. for both 25 and 33 mole % Na_2O. The same trend with increasing

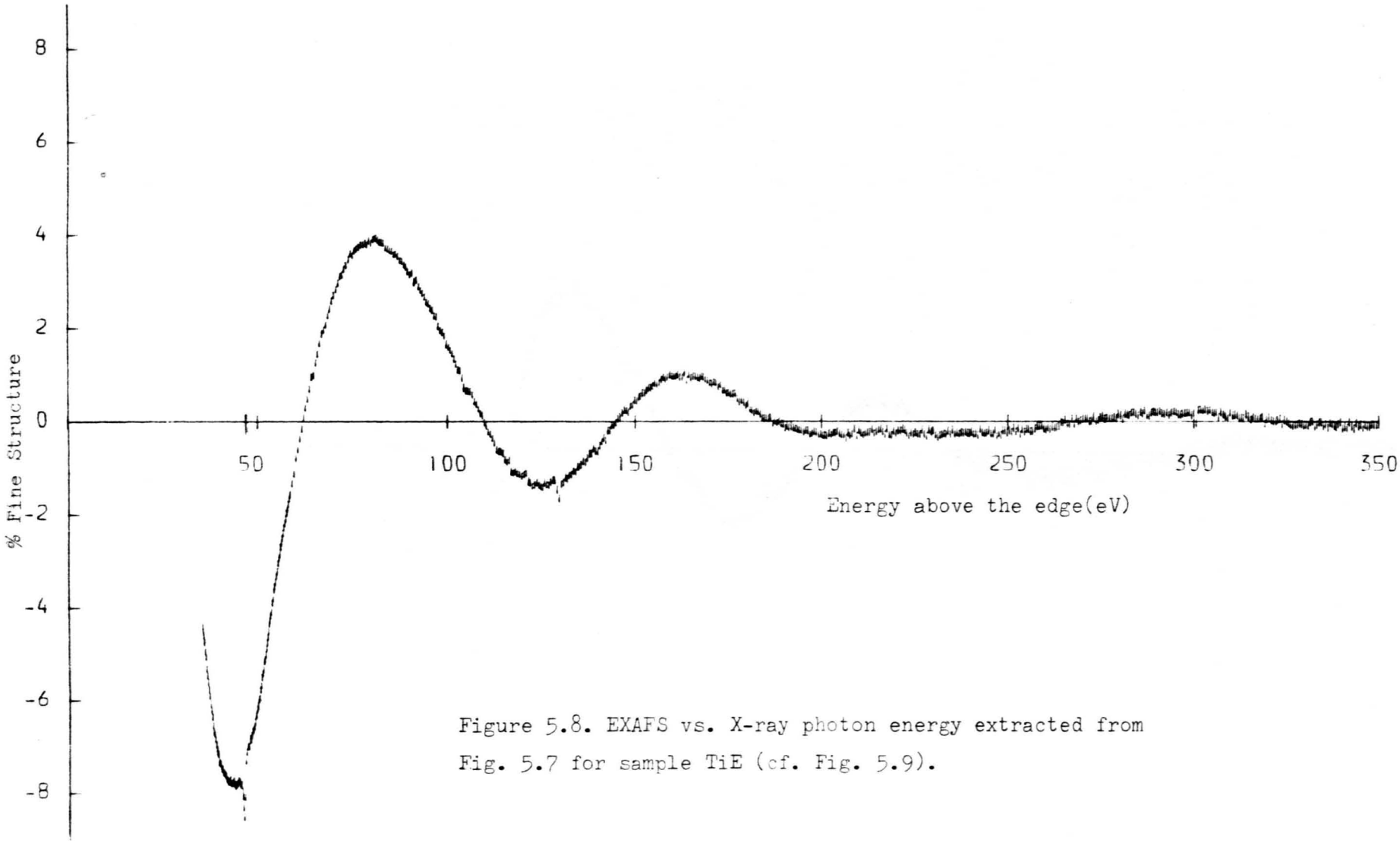

Figure 5.8. EXAFS vs. X-ray photon energy extracted from Fig. 5.7 for sample TiE (cf. Fig. 5.9).

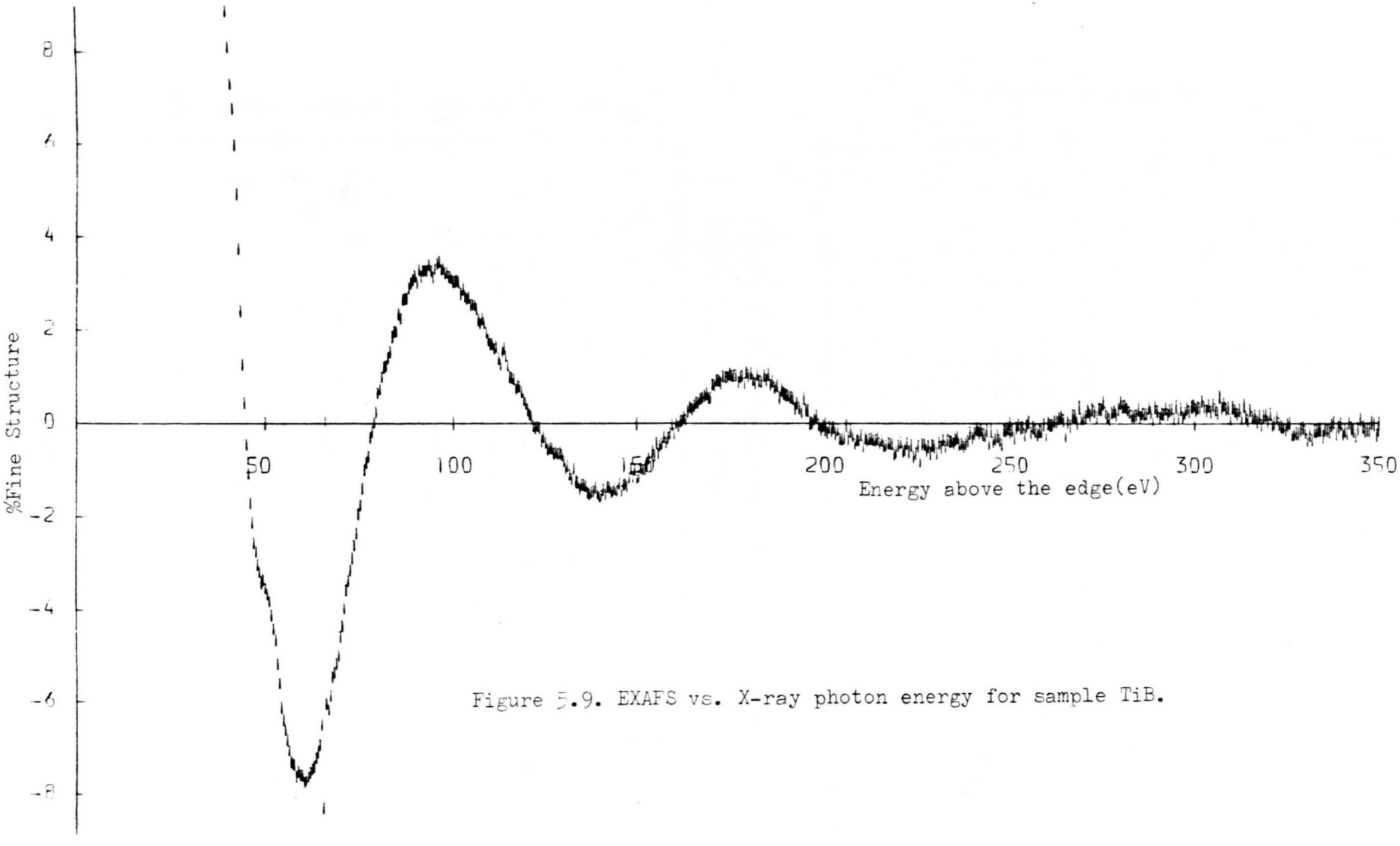

Figure 5.9. EXAFS vs. X-ray photon energy for sample TiB.

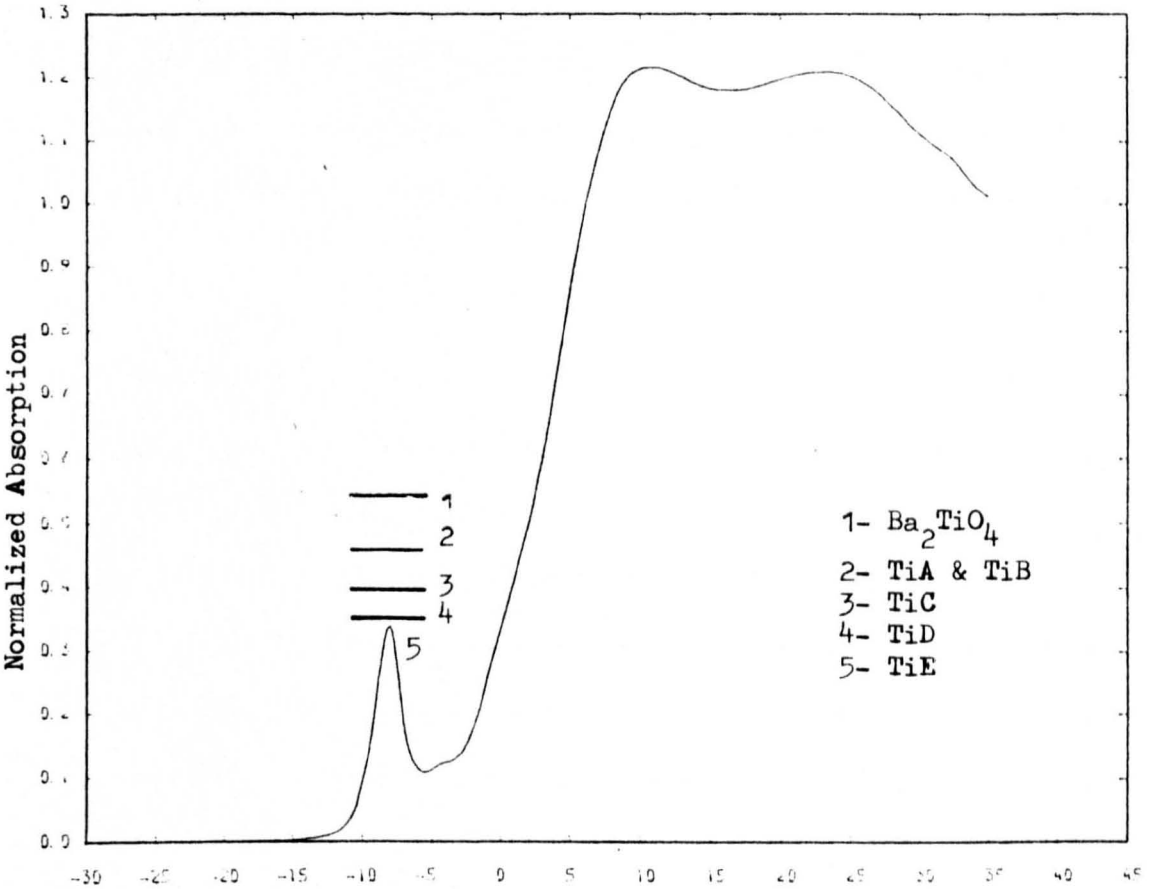

Figure 5.10. Pre-edge peak heights for glasses containing 25 mole % Na_2O.

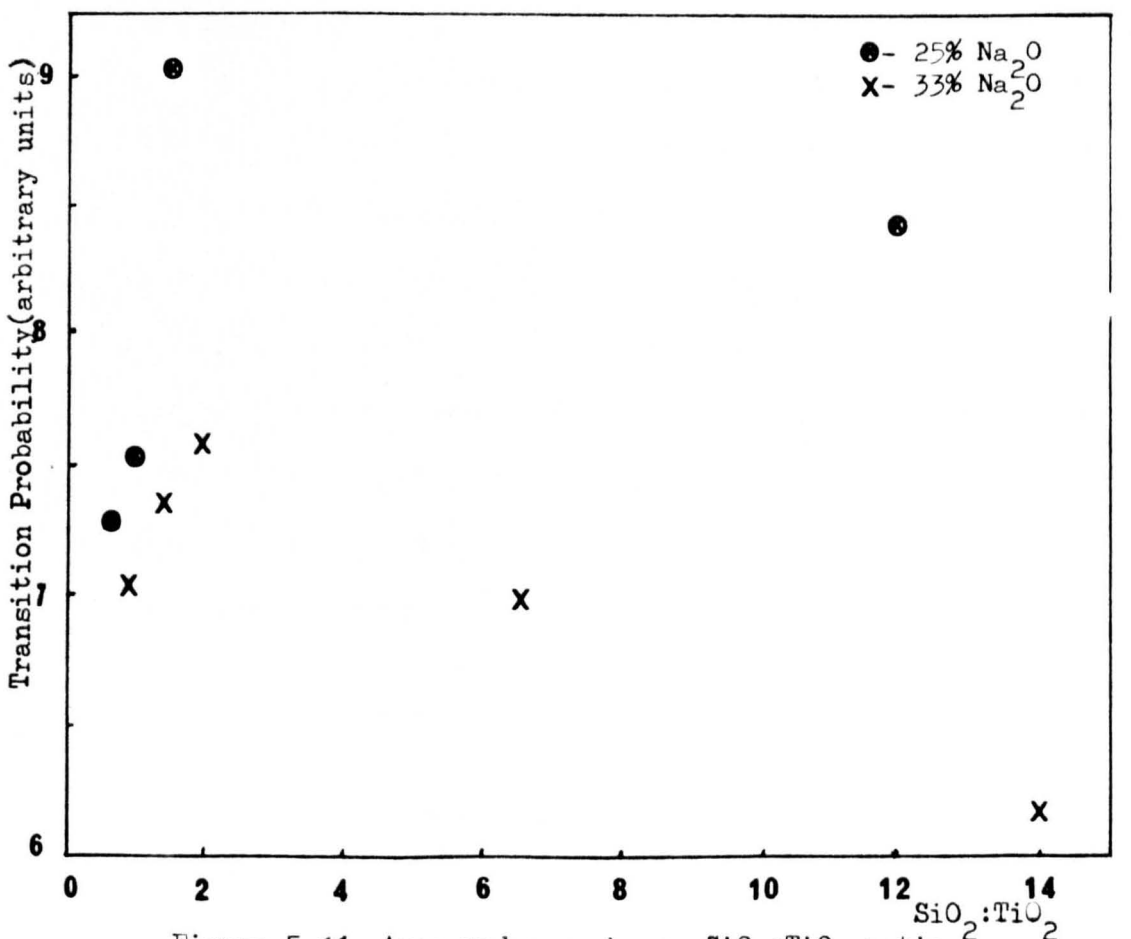

Figure 5.11. Area under peak vs. SiO_2:TiO_2 ratio.

TiO_2 content is observed in each glass system up to SiO_2:TiO_2 ratio of ~ 1-2. In this region, the transition probability exhibits a maximum. Overall the probability is larger in the system containing more alkali oxide.

5.3.4. Fourier Transform

The magnitude of the FT's for the EXAFS data discussed in Section 5.3.2. are shown in Figs. 5.13. and 5.14. The transforms were performed under the same conditions discussed previously for TiO_2. Due to the poor signal to noise ratio for low TiO_2 content, such a procedure could not be followed and only the data for TiO_2 contents greater than 10 mole % will be presented hereafter. As with the XANES data a general trend can be observed in the glasses for both 25 and 35 mole % Na_2O with increasing TiO_2.

For the glasses containing 25 % Na_2O the amplitude of the main oxygen peak decreases with increasing TiO_2 content and also becomes broader. There is no discernible shift in the peak position, which is found to be at 1.55 Å. Assuming the value obtained from TiO_2 (a/2 = 0.4 Å) this gives an average Ti-O distance of 1.95 ± .10 Å.

For glasses containing 33 mole % Na_2O this same reduction in amplitude is observable. Moreover for TiO_2 contents of ~ 30-40 mole %, the peak is severely distorted. Sample TiH displays a definite two shell oxygen environment. This behaviour at large TiO_2 concentrations is indicative of major changes in the Ti environment and verifies the same changes observed in the XANES data.

5.3.5. Curve Fitting

From the previous discussion it is apparent that within these glasses there exists the possibility of two Ti sites. For this reason, in the

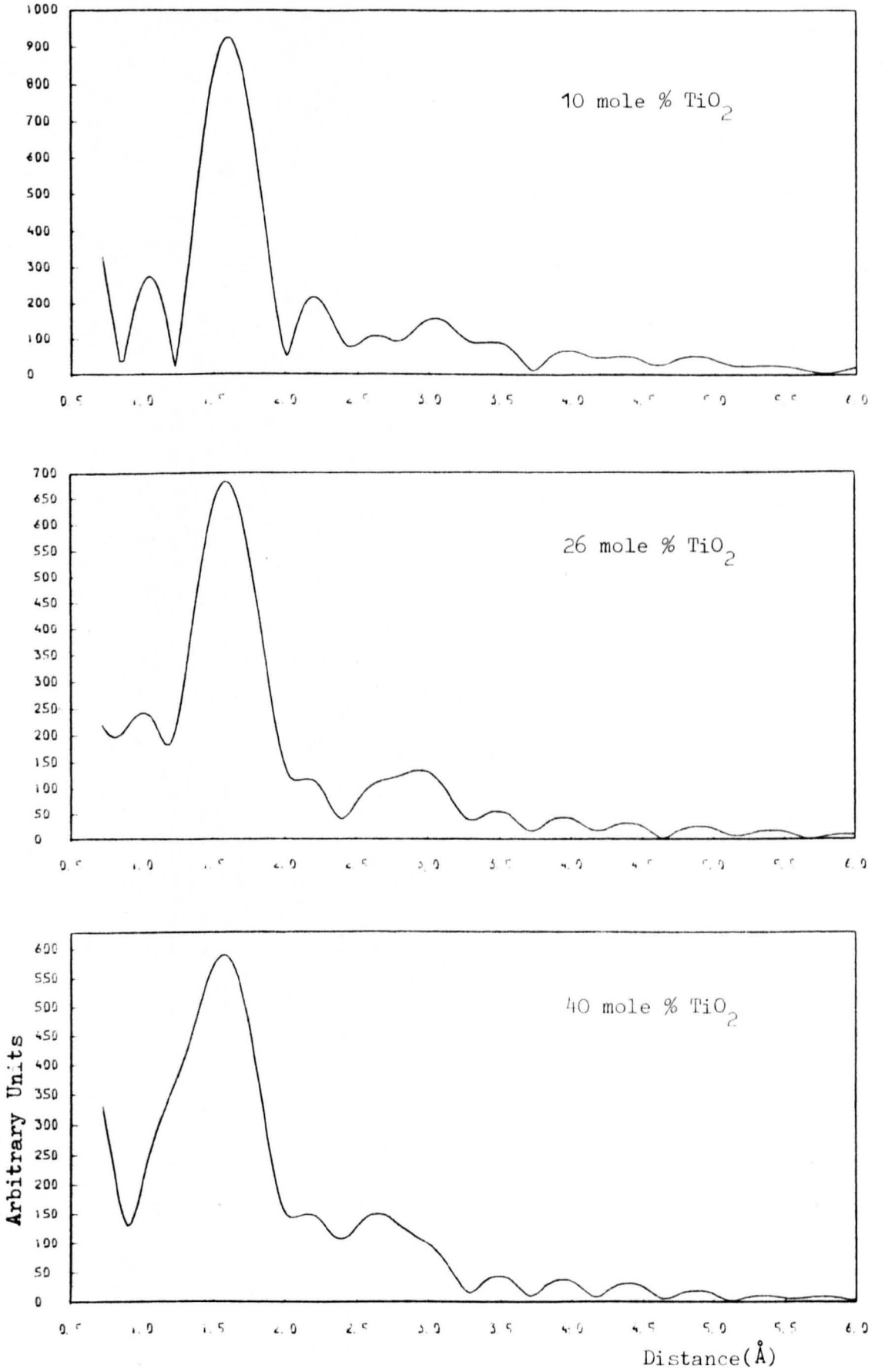

Figure 5.13. Magnitude of Fourier transforms for three TiO_2-containing glasses with 25 mole % Na_2O.

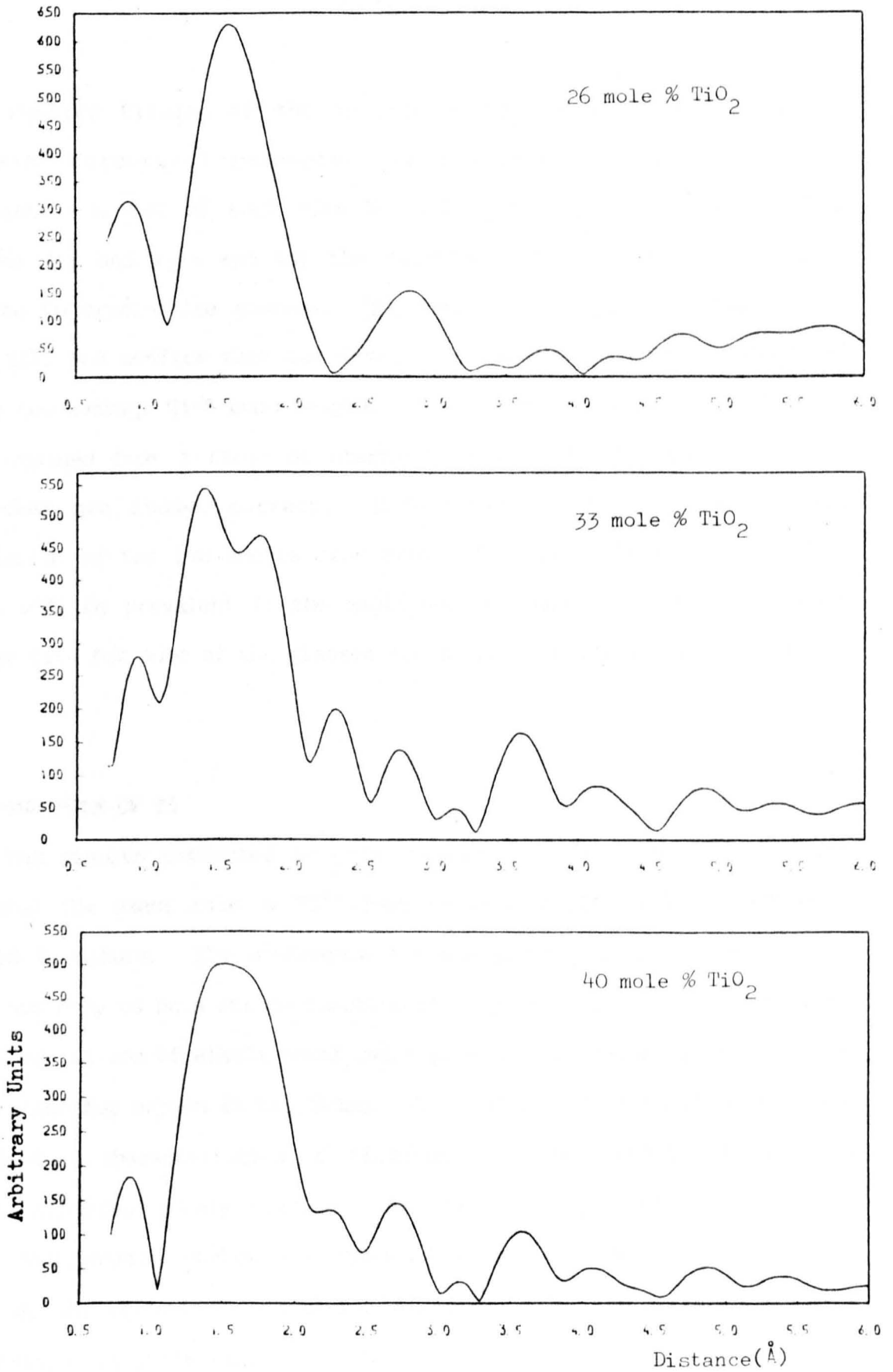

Figure 5.14. Magnitude of Fourier transforms for three TiO_2-containing glasses with 33 mole % Na_2O.

least squares fitting of the inverse Fourier transformed data, the following structural parameters were allowed to vary: (1) the coordination number of each site N_1 and N_2); (2) the average radial distance (r_1 and r_2); and (3) the relative disorder parameter $\Delta\sigma^2_{j=1,2}$ compared to crystalline anatase. The results of this are summarized in Table XIII and confirm that two distinct sites are resolvable, indicated by the two average Ti-O bond lengths. The parameters shown in Table XIII were obtained from a range of starting values strengthening the belief that they are indeed correct. Unfortunately, due to the negative correlation of the two shells true errors are difficult to judge. This effect will be prevalent in the amplitude parameters N and $\Delta\sigma^2_j$. Least squares fits for some of the glasses are shown in Figs. 5.15. and 5.16.

5.4. THE ROLE OF Ti

The results presented in this Chapter (and from previous studies) show that the exact role of Ti^{4+} ions is very complex and may indeed be twofold in nature. The preference for one particular site over another seems not only to be a strong function of TiO_2 content but also depends on the concentration of alkali metal oxide present, suggesting a considerable competition for oxygen in the glass. Previous results have shown that the coordination characteristics of titanium in these glasses are, at high silica contents, purely sixfold. As the amount of TiO_2 is increased, lower coordination states are observed (4 or 5) reaching a saturation point at the equimolar composition SiO_2:TiO_2 = 1, thereafter octahedral coordination is preferred.

At first sight the results seem to indicate that even at small TiO_2 concentration (~ 5 mole %) tetrahedral coordination is present because of the similarity between the pre-edge transitions in the glasses compared

SAMPLE	N_1 (± 0.4)	N_2 (± 0.5)	r_1 (Å) (± 0.05)	r_2 (Å) (± 0.05)	$\Delta\sigma_1^2$ (x 10^{-3} Å^2) (± 17)	$\Delta\sigma_2^2$ (x 10^{-3} Å^2) (± 20)
TiA*						
TiB	0.1	3.6	1.83	1.94	-19	15
TiC	1	4.6	1.82	1.92	-23	15
TiD	0.7	4.4	1.81	1.93	-18	20
TiE	0.2	4.0	1.86	1.97	-15	24
TiF*						
TiG	0.08	3.7	1.86	1.95	-20	14
TiH	0.16	2.62	1.83	2.0	-25	14
TiI	0.03	3.7	1.85	1.99	-28	15

* - No EXAFS data available.
1 - Tetrahedral.
2 - Octahedral

TABLE XIII

Structural parameters for TiO_2-containing glasses obtained from least squares fitting routine.

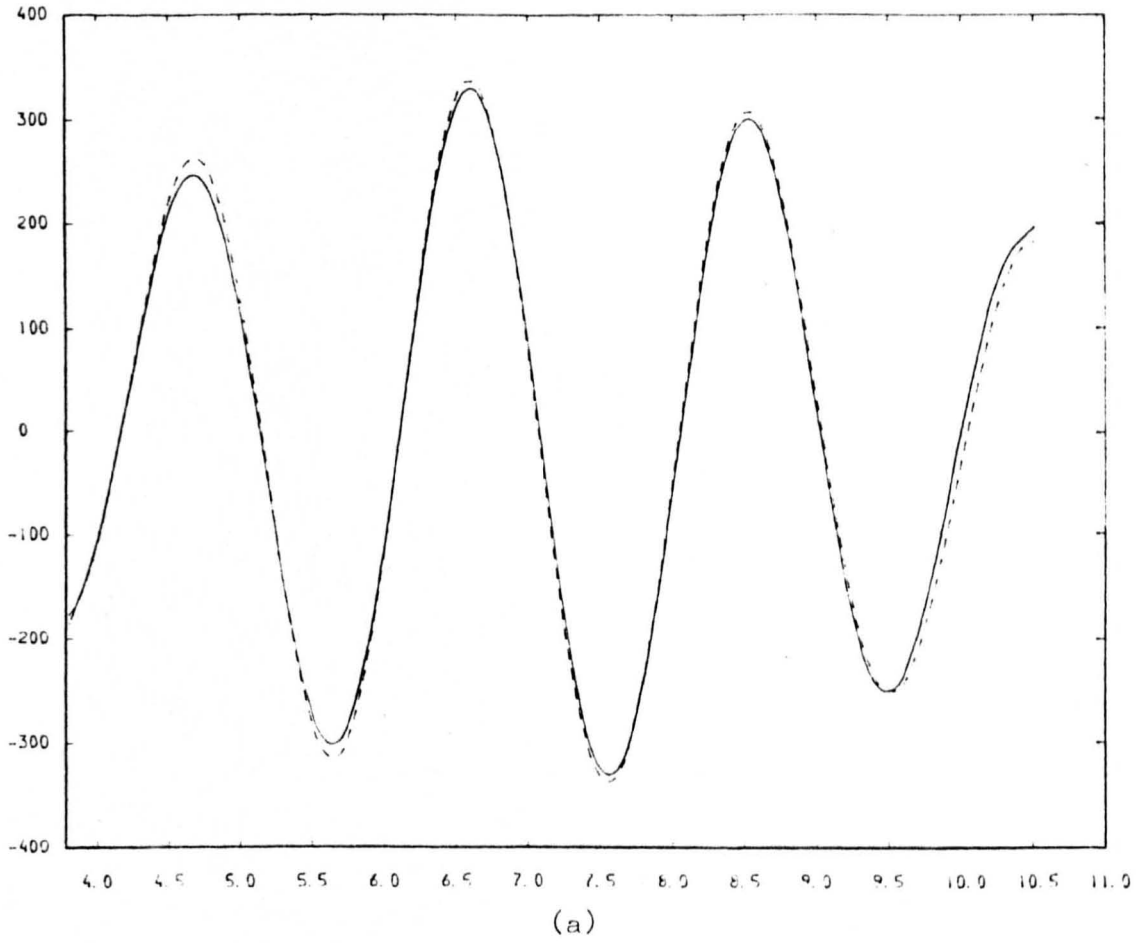

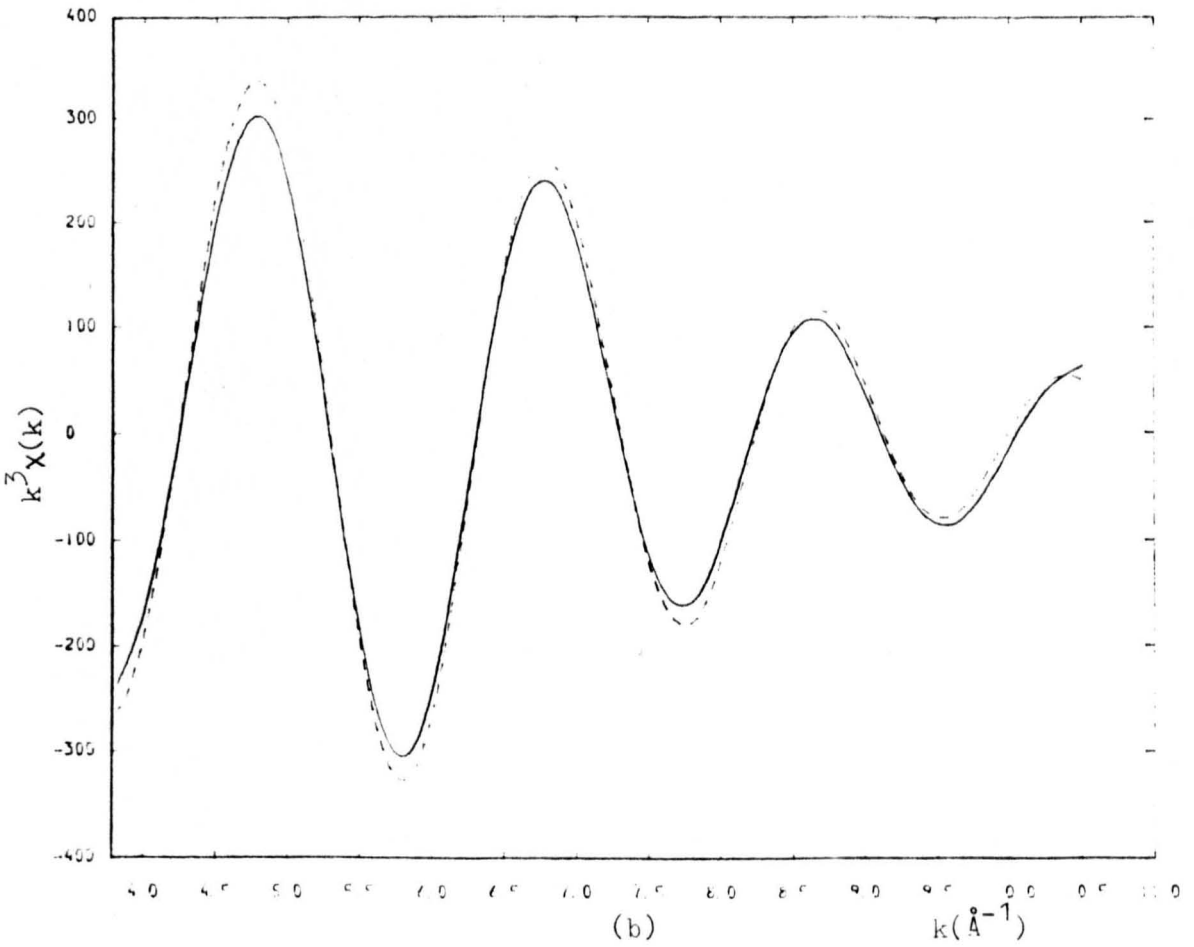

Figure 5.15. Least squares fit of oxygen EXAFS for (a) sample TiB and (b) sample TiE.

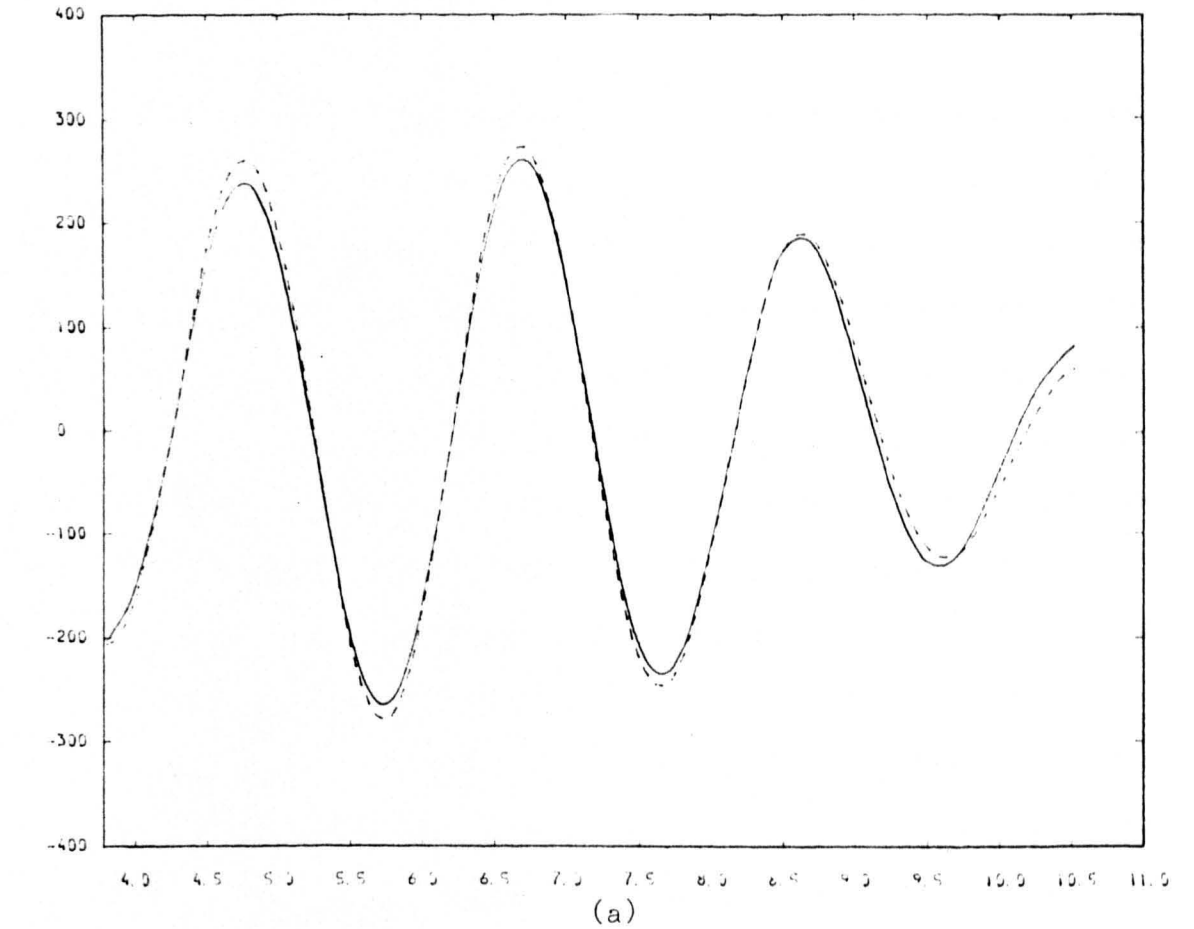

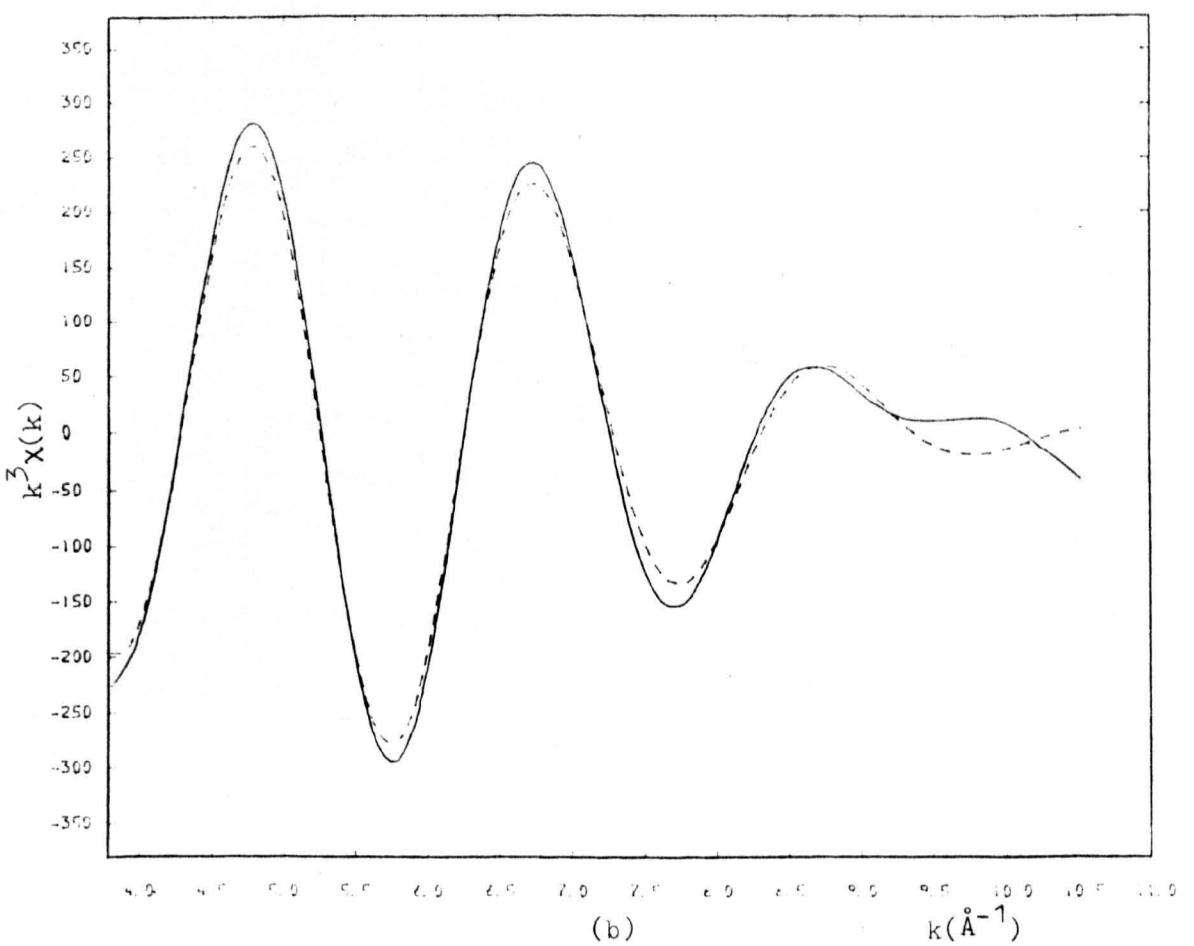

Figure 5.16. Least squares fit of oxygen EXAFS for (a) sample TiG and (b) sample TiH.

to that found in Ba_2TiO_4. Such a behaviour has been discounted before on the belief that $[TiO_6]^{2-}$ "clusters" persist in low TiO_2-silicate glasses, and it is these centres which may act as nucleation sites in the precipitation of crystalline phases on subsequent heat treatment. For example, in these glasses, Na_2TiO_5 has been shown to be the major phase after crystallization. Further evidence for the existence of low coordination states at relatively small TiO_2 contents is offered by the existence of the short Ti-O bond length ~ 1.8 A (vide infra). A similar bond distance is found in crystalline titanates possessing low coordination, e.g. Ba_2TiO_4 and K_2TiO_5 (Ti-O = 1.83 A) and is not observed in compounds having true octahedral symmetry. Such a model is quite contrary to previous results in the existence of these low coordination states at small TiO_2 concentrations. However, it must be remembered that any postulate on the structure of a glass should only be discussed within the context of its thermal history - a fact which is often overlooked. Weyl (1951) suggested that Ti^{4+} ions will assume a coordination of four at high temperatures. On the basis of this, McMillan (1964) conjectured that these states will be "frozen-in" on rapid cooling of the melt allowing Ti to occupy network forming sites by the isostructural replacement of Si. Furthermore, as this state will be metastable, subsequent heat treatment of the glass may, in some way, convert these low coordination states to the thermodynamically stable octahedral form resulting in a two-phase separation of the glass. Therefore, there seems no *a priori* reason why the existence of $[TiO_4]$ tetrahedra may inhibit crystallization: in fact, as was noted before, some ordering effects are observed prior to crystallization, and just such a phase separation may drive the mechanism of crystal growth!

The results from the previous Chapter show that ordering effects on annealing are observable using the EXAFS technique and, with hindsight,

such a study on the thermal history of TiO_2-containing glasses may elucidate this incipient phase separation, primarily from the difference in the strong pre-edge transition.

Further evidence for the existence of $[TiO_4]$ tetrahedra is obtained from the curve fitting analysis. Here N_1 and N_2 (see Table XIII) represent respectively, tetrahedral and octahedral coordination. As can be seen the major contribution comes from the N_2 site for which some structural change is observed for increasing TiO_2 concentration ($\geq$ 33 mole %), noticeably by the increase in the average Ti-O bond length. The second site with an average Ti-O distance of ~ 1.8 A is characteristic of an atomic arrangement, with Ti having less that six oxygen neighbours. The relative magnitude of the two sites varies with increasing TiO_2 content and with the concentration of alkali metal oxide. Within this approximation, the low coordinated tetrahedral sites will represent isostructural substitution of Si^{4+} ions in the glassy matrix. The negative value of the bond disorder parameter $\Delta\sigma_j^2$ may support previous results (Sandstrom et al.) and ties up with the earlier theory that the structural units comprising glasses are characterized by a higher degree of ligand ordering compared with their crystalline counterparts. However, as was mentioned before this parameter may suffer from considerable correlation effects.

For octahedral coordination the situation is more complex. $[TiO_6]$ units have been shown to exist either in modifying or forming roles. Unfortunately such a duality cannot be resolved in EXAFS measurements in view of the fact that only average coordination is measured.

Given the multiplicity of atomic arrangements that may be possible in TiO_2-containing glasses, to attempt to interpret structural changes as a function of composition will be exceedingly difficult. The major structural change that is observed with increasing TiO_2 is the increase

in $[TiO_4]$ tetrahedra. Sandstrom et al. found that once the initial solubility limit of TiO_2 in octahedral coordination had been reached Ti^{4+} ions entered the network substitutionally for Si. At a certain concentration of TiO_2, the network became saturated and phase separation ensued.

Such a trend is observable within these glasses too; although the degree of saturation is obviously affected by the amount of Na_2O. For larger Na_2O concentrations the degree of isostructural substitution is increased. This may be explained by considering the Na^+ ions acting in a secondary role whereby they release the strain imposed by the larger metal-ligand bond within the network, so lowering the free energy. Such a relaxation effect may involve the creation of non-bridging oxygens around Ti tetrahedra so producing areas within the glass that, in themselves, may act as nucleation sites. From this argument it follows that for the case of increased Na_2O content, the amount of $[TiO_4]$ units present will be consequently larger.

As the TiO_2 content is increased even further, there will occur a point at which this isostructural replacement saturates and thereafter phase separation will proceed, as observed in the increase in sixfold coordination. This effect is most readily observed by the FT's shown in Figs. 5.13. and 5.14. where the reduction in amplitude is due to interference between Ti sites resulting finally in a highly distorted oxygen first shell. This result is supported by XANES data shown in Fig. 5.11., where the maximum in fourfold coordination is evident at a SiO_2:TiO_2 ~ 1-2. Hanada and Soga have observed the structural change to occur at SiO_2:TiO_2 = 1.

The results presented here do suggest the existence of tetrahedrally coordinated Ti occupying substitutional sites within the glassy network. However, it must be noted that the obvious distortions of Ti in an

octahedral environment may be sufficient to produce an overall lack of inversion symmetry. Moreover, for the case of [TiO_5] polyhedra, asymmetries are again possible and it may be so that such effects will produce the fine structure present in these glasses. As yet very little information is available on this possibility, although for completeness it is mentioned here.

CONCLUSION

The main findings for the EXAFS and XANES results on quenched Na_2O-TiO_2-SiO_2 glasses are:-

1. At small concentrations (~ 5 mole %) Ti^{4+} ions, for the most part, attain a sixfold coordination, although the actual site is ill-defined. There also exists a small amount in a tetrahedral environment (network former).

2. The amount of [TiO_4] units present is a function of both TiO_2 and alkali concentration.

3. For SiO_2:TiO_2 ratios of the order of 1-2, the concentration of [TiO_4] units is a maximum and is a function of Na_2O content.

4. For increased TiO_2 content the glasses phase separate.

Chapter 6

GENERAL DISCUSSION AND CONCLUSIONS

6.1. INTRODUCTION

This Chapter is intended as a general discussion on the technique of EXAFS and its usefulness as a structural probe in the investigation of disordered systems. A summary of the relevant interpretational techniques is given. Their applicability in the light of the work undertaken herein is discussed, on the basis of which the possibilities for further studies in the field are suggested.

6.2. EXAFS AS A STRUCTURAL PROBE

In this thesis it has been shown that the EXAFS technique may be used to investigate the local atomic environment in very complex multi-component glass systems. In diffraction studies, the superposition of all the atomic pair-correlation functions severely complicates the analysis; a limitation which is overcome in EXAFS studies in view of the atomic-species sampling property, resulting in partial-RDF's.

Structural information about the type, number and position of scatterers around an excited atom rests in the amplitude and periodicity of oscillations above the absorption edge as expressed in eqn. 3.4. To calculate these highly desirable structural parameters, prior knowledge of the scattering amplitudes, $f_j(\pi)$, and phase shifts, $2\delta_{\ell,j}$ and ψ_j, is required and therefore, at a first level of approximation, the limitations in the analysis are imposed by the accuracy with which these functions may

be determined.

The simplified expression (eqn. 3.4.) is valid for photoelectron energies in excess of 100 eV above the edge. Below these energies, the curvature of the photoelectric wavefront and many-body effects become more important. This, together with the fact that at high energies the Debye-Waller factor, $(\exp -2\sigma_j^2 k^2)$, severely attenuates the EXAFS amplitude, means that structural information is limited in extent. Fortunately, for disordered systems, the dominant scattering is due to first-shell correlations, of principal interest, which occur, in general, at energies above the theoretical limit.

In view of the computationally difficult exercise of calculations of individual phase shifts and back-scattering amplitudes using the exact EXAFS equation, two tried and tested methods of analyzing the data were adopted. The first requires the Fourier transform of the EXAFS equation to obtain a partial quasi-RDF. This technique has proved to be beneficial in determining bond-length information by comparisons with known model compounds, under the assumption that the total phase shift is linear in k, the photoelectron wavevector. Although, this technique has been used in this work, the most beneficial aspect of the RDF is to give a real space picture of the material, on the basis of which, an initial guess is used in subsequent curve-fitting analysis.

Curve fitting techniques, other than by independent theoretical calculations, require the approximation of the phase and amplitude functions. This may be achieved by one of two, well-used routes: either the information is established from an analysis of a chemically similar, known compound and the parameters transferred to the unknown; or the tabulated values for the individual phase shifts and amplitudes given by Teo and Lee (1979) based on the theory of Lee and Beni (1977) are used. For the case of disordered systems, Eisenberger and Brown (1979) showed

that asymmetries in the pair correlation functions necessary restrict the chemical transferability of structural parameters.

As a first attempt in the curve fitting analysis, the data of Teo and Lee were approximated by suitable parameterized functions and used in a least squares fit to the EXAFS of a known compound. Assuming the crystalline data to be correct, no reasonable fit could be achieved at low energies, which may be due to inadequacies in the original theory. Furthermore, the split first shell character of the model compounds could not be properly described. For this reason, the curve-fitting analysis technique preferred required the calculation of an effective total phase shift, $\phi(k)$, and amplitude function $A(k)$, from the measurements of a model compound, for which possible inadequacies in the theory may be compensated for, as curved-wave effects will be similar in the unknown system (glass), i.e. the concept of chemical transferability is invoked: bearing in mind the reservations expressed by Eisenberger and Brown.

In the subsequent analyses, it was found to be advantageous to perform the minimization in k-space on a Fourier-filtered spectrum. This has the drawback of a further limited Fourier transform using a window function to isolate the contribution for one shell only and consequently care must be exercised in the choice of a suitable function. However, it does allow the shell-by-shell analysis of EXAFS to proceed.

6.3. CONCLUSIONS

6.3.1. ZrO_2-Containing Glasses

Using as a standard $ZrSiO_4$, the Fourier filtering of the first shell EXAFS enabled the split oxygen shell to be adequately matched, confirming the belief in the empirically determined phase shift parameters. These were then used to investigate the structure around the

Zr ion in a series of annealed R_2O-CaO-ZrO-SiO_2 glasses (R = Li, Na, K). Provisional real space interpretation confirmed the medium-range disordered nature of the glasses but suggested the possibility of a well ordered first shell. Subsequent curve-fitting analysis established that the Zr ion has, on average, 6 oxygen nearest neighbours at a distance of 2.09 ± 0.05 Å. The mean square relative displacement was found to be less in all the glasses compared to the crystalline value but varied as a function of composition, viz., the substitution of the alkali ion (K → Na → Li) produced an increase in the σ_j^2 value which can be related to the ionic field strength of each ion. A similar effect was observed on increasing Na_2O content which was attributed to the production of non-bridging oxygens. This net decrease in the mean square relative displacement may be envisaged as metal-ligand ordering in excess of that observed in crystalline compounds at the expense of medium to long-range periodicity, a pre-requisite in the latter. Thus, the limitations expressed by Eisenberger and Brown are not applicable to some disordered systems and the chemical transferability of phase and amplitude parameters is justified.

The above considerations of a well-defined octahedral site place the role of Zr as a network former. The substitution of Si^{4+} is not isostructural and necessarily requires the presence of modifying ions around the $[ZrO_6]^{2-}$ unit to conserve electrical neutrality. The high viscosity of these glasses and the small region of glass formation follow as a corollary of this theory as the addition of ZrO_2 will limit the production of non-bridging oxygens and dictate the low and high limits of alkali content.

For one particular glass composition, the possibility of structural change under varying thermal history was investigated. Here the structure of the annealed specimen was compared with that of its quenched

counterpart. Hitherto thought to be unobservable effects have been shown to be measurable by the EXAFS technique. The quenched specimen was found to possess a split-oxygen shell which may characterize the parent liquid as the structure is "frozen-in".

The above conclusions have led to important discoveries on the role of Zr in a soda-lime-silica base glass. These may be summarized as:-

(a) Zr ions occupy octahedral sites with a bond length of 2.09 ± 0.05 Å.

(b) The high degree of metal-ligand ordering, as expressed by a relatively small σ_j^2, is indicative of the Zr ion acting as a network former.

(c) The effects of alkali substitution and content are observable by the modification of the Zr environment.

(d) The effects of annealing have been shown to lead to discernible effects in the local structure.

(e) Physical and chemical properties may be explained in terms of this structure.

6.3.3. TiO_2-Containing Glasses

Previous investigations of TiO_2-containing glasses have concluded that the role and coordination of Ti is a strong function of the composition. In the investigation of a series of Na_2O-TiO_2-SiO_2 glasses it was anticipated that this propensity may cause complications as only average coordination in EXAFS analysis can be measured. However, the Ti K-edge is characterized by electronic transitions to bound states of

the excited atom which reflect the symmetry of the surrounding atoms. From the peak areas, the transition probabilities for the s-d transition (indicative of Ti in a tetrahedral environment) show that the isostructural substitution of Si^{4+} ions increases as a function of TiO_2 content up to a SiO_2:TiO_2 ratio ~ 1-2, whereupon phase separation ensues. This substitution is limited by the amount of modifying oxide present and is observed to be larger for increasng Na_2O. The existence of these $[TiO_4]$ units, even at low concentrations (~ 5 mole %) may be a direct result of the glass preparation process, as the samples were quenched in air. Previous work has held that at low concentration, the Ti has an octahedral coordination of $[TiO_6]^{2-}$ "clusters" which act as nucleation sites in the development of glass ceramics. However, there is no *a priori* reason why the existence of $[TiO_4]$ units should necessarily restrict nucleation as subsequent heat treatment of the glass below T_g may convert these units to the more thermodynamically stable octahedral phase and hence drive the mechanism of crystal growth.

Curve fitting routines on glasses containing more than 10 mole % TiO_2, although hampered by the high correlation of the two coordination shells, predict that although $[TiO_4]$ units exist, as shown by the two resolvable Ti-O bond-lengths, the predominant coordination is sixfold. Sandstrom et al. (1983) in an investigation of SiO_2-TiO_2 glasses showed that after the initial solubility limit of $[TiO_6]$ formation in the interstitial regions of a $[SiO_4]$ continuous network, Ti^{4+} ions substituted for Si^{4+} ions. Such an effect may take place in the ternary silicate, where it is envisaged that the presence of Na_2O allows the substitution of Si^{4+} ions to take place by breaking the longer Ti-O bond, so reducing the net increase in internal energy of the network by relieving the strain. This would impose a preferential site for the

Na^{2+} ion.

It is believed that the Ti tetrahedral site is a result of the substitution of Si^{4+} ions, and therefore Ti may be placed in a network forming role. For the case of octahedral symmetry this classification becomes vague as $[TiO_6]$ units have been shown to exist in an intermediate capacity. Such a duality cannot be resolved in EXAFS analysis.

The above conclusions may be summarized as follows:-

(a) Ti^{4+} ions possess both an octahedral and a tetrahedral coordination in quenched Na_2O-TiO_2-SiO_2 glasses.

(b) The ratio of tetrahedral/octahedral coordination increases with increasing TiO_2 content.

(c) The amount of isostructural substitution of Si^{4+} ions is a function of Na_2O content.

(d) A maximum in this ratio is reached at the molar compositional ratio of SiO_2:TiO_2 ~ 1-2. Thereafter, phase separation ensues with the appearance of a TiO_2 rich phase.

6.4. FUTURE WORK

Due to limited resources, many of the conclusions reached that may have been further investigated within the scope of this thesis could not be expanded on, but do however deserve merit. In particular, it was found that changes in the local atomic stucture due to heat treatments below the glass transition temperature are indeed observable by EXAFS. By the

monitoring of such changes important questions on the mechanism of crystal-growth may at last be answered. Both TiO_2 and ZrO_2 are known to act as nucleating agents in the phase development of glass ceramics and the author has already performed short studies on both ZrO_2 in a cordierite glass system (Appendix C) and the combined TiO_2-ZrO_2 sodium silicate system (Appendix B) and underlined the feasibility. For Ti K-edge studies, such effects may be directly observable by monitoring, the pre-edge peak intensity. Fluorescence EXAFS techniques could also be used to measure very low TiO_2 concentrations.

For the case of ZrO_2-containing glasses this work has proved its role within a soda-lime-silicate glass as being that of a network former. However, this role may change in other glass systems particularly in the presence of another known glass former, e.g. Na_2O-B_2O_3-SiO_2 and MgO-Al_2O_3-SiO_2 glasses (cf. RDF's for ZrO_2 in a soda-lime silica glass (Fig. 4.3.) and those for ZrO_2 in a cordierite system shown in Appendix C). Thus, this work may be extended to cover Zr in other glass systems.

From the previous two sections it was suggested that the particular site occupied by either Zr or Ti in their respective base glass systems, may require the presence of modifying ions in the vicinity of the network forming structural unit. As a result, one may expect that these ions may occupy two different sites within the glass. Such effects may be possible to detect by EXAFS with the availability of soft X-ray equipment, or by using "magic-angle" NMR Spectroscopy, for which the Na^+ resonance is readily measurable.

One interesting property of "Cem-Fil" type glasses is its increased chemical durability with the addition of small amounts of transition metal oxide. Such additions have been shown by Taylor (1984) to modify the atomic environment around the Zr^{4+} ion. In view of the very small

amounts of transition metal present (< 1 wt %) no EXAFS spectra is available on their K-edges although, as was explained above, by utilizing fluorescence techniques these edges may be measured.

Appendix A

LEAST-SQUARE FITTING ALGORITHM

For the purposes of this study, the non-linear least squares fitting algorithm used is due to Gill and Murray (1978). The function that is minimized corresponds to

$$F(\underline{x}_j) = \sum_{i=1}^{M} [f_i(\underline{x}_j)]^2 \qquad \text{(A.1.)}$$

where $\underline{x}_j = (x_1, x_2 \ldots x_N)$. $f_i(\underline{x}_j)$ is called the residuals and is defined as

$$f_i(\underline{x}) = \chi_{theor}(\underline{x}) - \chi_{exp}(\underline{x}) \qquad \text{(A.2.)}$$

The algorithm does not calculate a global minimum and therefore a reasonable (physical) guess is required for $\underline{x}$ in order to calculate a local minimum.

The minimization of $F(\underline{x})$ can be expressed in terms of the Hessian H, and Jacobian J, matrices, thus:

$$G(x) = 2[J^T(\underline{x})J(\underline{x}) + \sum_{i=1}^{M} f_i(\underline{x})G_i(\underline{x})] \qquad \text{(A.3.)}$$

where

$$G(\underline{x}) = \frac{\partial^2}{\partial x_i \partial x_j} F(\underline{x})$$

and

$$J(x) = \frac{\partial}{\partial x_i} f(\underline{x})$$

$G_i(x)$ is the Hessian matrix of $f_i(x)$, and the summations run from i = 1 ... M, where M is the number of data points and j = 1 ... N, N being defined in eqn. A.1.

At the final solution $G(\bar{x})$ may be approximated by $2J^TJ$. The variance of the parameter $\bar{x}_j$ is then

$$\text{var } \bar{x}_j = \frac{S}{M - N} (G_{jj})^{-1} \qquad \text{(A.4.)}$$

where S is the sum of the squares of the residuals.

Eqn. A.4. can also be derived from the fact that

$$\text{var } \bar{x}_j = \frac{S}{M - N} \varepsilon_{jj}$$

where ε_{jj} is the error matrix - see Bevington (1969).

The algorithm used outputs the Jacobian matrix and the final points $\bar{x}_j$. The Hessian or error matrix is then computed by inverting $2J^TJ$ by Crout's method of triangular decomposition.

Appendix B

TiO_2-ZrO_2 CONTAINING GLASSES

The inclusion of a combination of TiO_2 and ZrO_2 within some glass systems is known to increase the nucleation properties as compared to one of these constituents alone. For example, in the development of cordierite glass ceramics, near the stoichiometric composition, approximately 10 wt. % TiO_2 or ZrO_2 is needed to 'catalyze' the reaction. If both TiO_2 and zrO_2 are present, it is found that ~ 4 wt. % is sufficient. The phase development of these glass ceramics is characterized by a whole range of crystalline forms and quartz solid solutions that depend on heat temperature, the rate of heating and to a large extent on the composition. As yet no attempt has been made to profer a structural interpretation on this phenomenon.

It was noted in Chapter 5 that some ordering is evident in glasses containing TiO_2 prior to any observable phase separation. Such an incipient ordering may be observable at an even earlier stage in the glass itself. To this end, the compositions given in Table BI were chosen to have sufficient TiO_2 content so that EXAFS measurements were possible. This was found to be ~ 10 mole %. From the starting composition TZA, small amounts of ZrO_2 were added in place of SiO_2.

SAMPLE	TiO_2	ZrO_2	SiO_2	Na_2O
TZA	9	3	63	25
TZB	10	5	60	25
TZC	9	6	60	25

TABLE BI

Compositions of three TiO_2-ZrO_2-containing glasses.
Samples were quenched in air.

Unfortunately, only data on the Ti K-edge could be obtained. This was somewhat unfortunate as a dual study on both Ti and Zr would obviously have been beneficial to the interpretation.

From the EXAFS the magnitude of the FT's, for increasing ZrO_2, are shown in Fig. B.1. The first peak is attributed to oxygen scattering and given the concentrations of TiO_2 may be matched in shape to the ternary glass TiE (Chapter 5). The major difference between the glasses appears in the contribution from the second shell. From the physical properties of these glasses it has long been thought that the presence of the two cations may, in some way, influence the local atomic structure, although the exact nature of this interaction is unknown. Results show that there is indeed some discernible ordering taking place, not of the immediate oxygen environment but of the next nearest neighbour. This middle range ordering may explain the nucleation properties of these glasses.

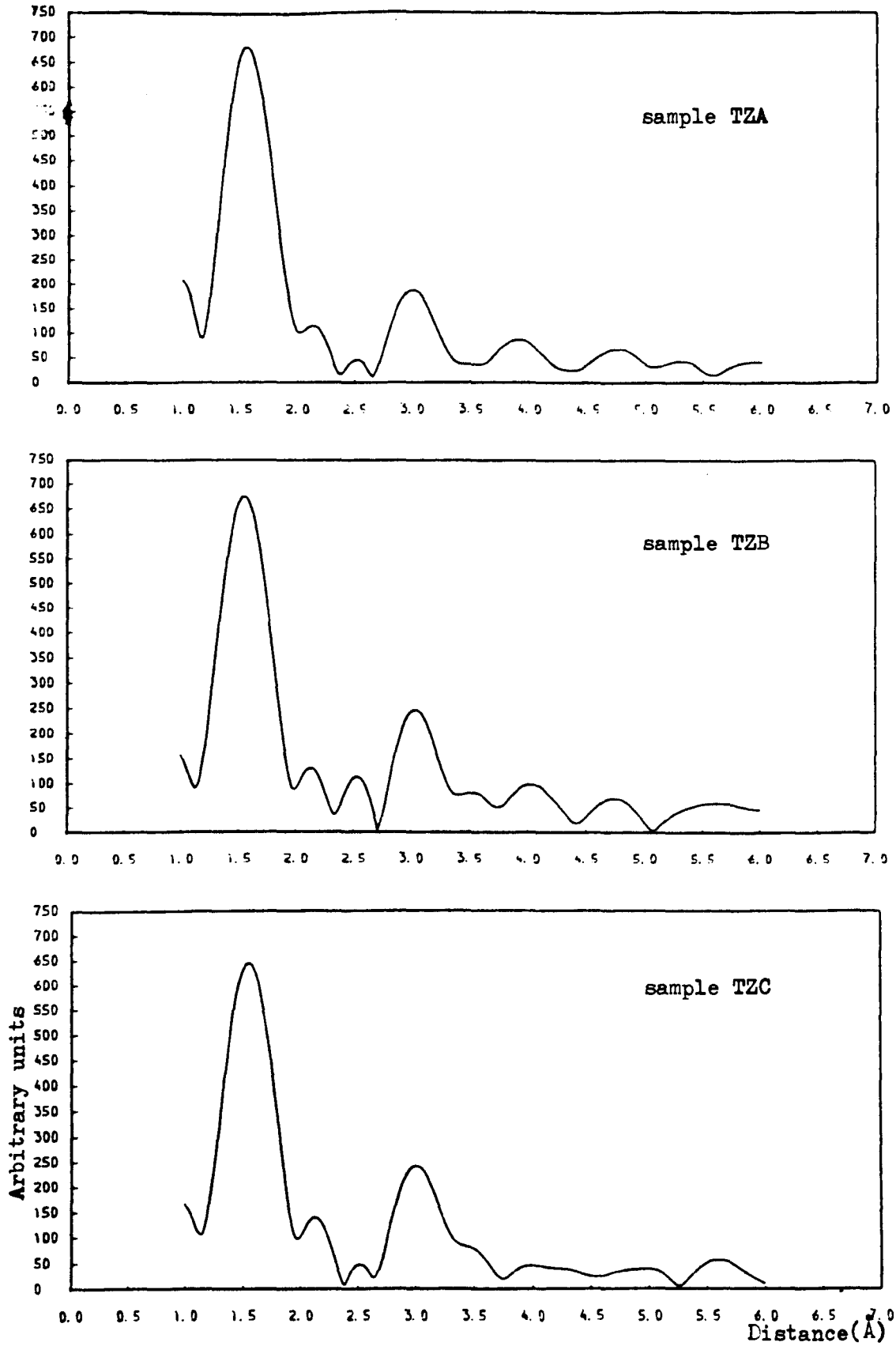

Figure B.1. Magnitude of Fourier transform for three TiO_2-ZrO_2-containing glasses.

APPENDIX C

EXAFS INVESTIGATION INTO THE ROLE OF ZrO_2 AS A NUCLEATING AGENT IN $MgO-Al_2O_3-SiO_2$ GLASS

J.M. Taylor and P.W. McMillan

Department of Physics, University of Warwick, Coventry CV4 7AL, UK

ABSTRACT

X-ray absorption measurements were undertaken on seven specimens of the magnesium aluminosilicate type containing 10 mole per cent ZrO_2 as a nucleating agent. For this system nucleation occurs at 780°C, with the onset of crystallization at about 900°C. The latter is characterized by an ordering of the near oxygen environment around the Zr ion and by a dramatic rise in the second-shell ordering, from the inherent static disorder of the glass to the well defined atomic co-ordination of tetragonal ZrO_2. Atomic ordering during nucleation is less pronounced and is characterized by a subtle ordering of the first oxygen shell.

1. INTRODUCTION

Zirconium dioxide as a constituent of certain oxide glasses is known to confer interesting physical characteristics. An important aspect is the use of this oxide as a nucleating agent in the formation of glass ceramics. In order to monitor such a transformation we have used a novel technique, that of EXAFS, with its ability to probe the immediate atomic environment around one particular constituent of the material, in this case Zr, to establish whether any structural re-arrangement occurs within the glass prior to crystal growth.

We have performed X-ray absorption measurements on several specimens which had received the thermal treatments summarized in Table 1.

Specimen Name	Heat treatment conditions		
	Time (h)	Temp (^{o}C)	Comments
Glass	-	-	)
2	2	750	)
3	2	800	) Cooled from melt to
4	2	850	) room temperature
5	2	900	)
6	0·5	1100	)
Crystal	2	1100	Cooled from melt to 1100^{o}C

TABLE 1. Thermal History of Glasses.

2. EXAFS ANALYSIS

2.1. Theory

The basic premises for the EXAFS scattering process are couched in terms of a single scattering model after Sayers *et al.* 1970. With further refinement (see for example Ashley & Doniach 1975) they lead to the now widely used expression for the EXAFS

$$\chi(k) = \frac{-1}{k} \Sigma \frac{N_j}{r_j^2} \exp(-\gamma r_j)\ t_j(2k)\ \exp(-\sigma_j^2 k^2)\ \sin(2kr_j + 2\delta_j(k)) \quad (1)$$

where the parameters have their familiar interpretation.

2.2. Analysis in Energy Space

Figure 1 presents the extracted EXAFS for all the samples shown in Table 1. By a simple comparison of these spectra it can be seen that the atomic environment has changed dramatically from the nucleated specimens, that is those specimens heat treated between 780^{o}C and 900^{o}C, to that of the crystallized samples (1100^{o}C), as the fine

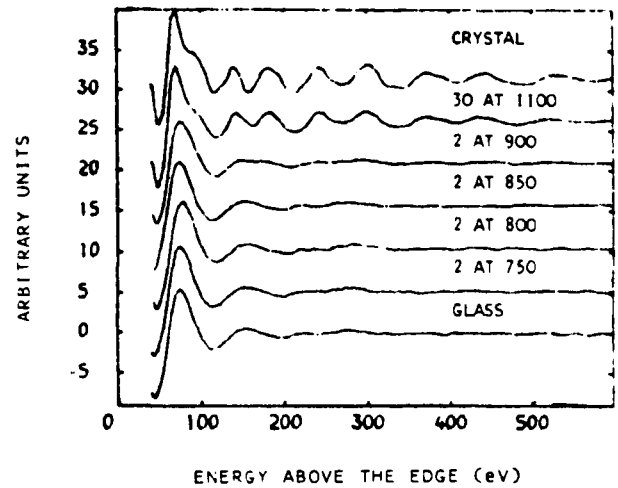

Figure 1. EXAFS oscillations of all the specimens plotted as a function of photoelectron energy.

structure in the latter extends to photon energies of about 600 eV, compared with about 200 eV for the non-crystalline case.

2.3. Analysis in real space

Although valuable information can be obtained from simple comparisons of spectra in energy space, the Fourier transform of the EXAFS function $\chi(k)$, equation (2), allows a thorough structural investigation to be undertaken.

$$\phi(r) = \int W(k)\chi(k)k^n dk$$

$$= \tfrac{1}{2} \Sigma \frac{N_j}{r_j^2 \sigma_j} \exp-(\gamma r_j) \exp[2(r - r_j)^2/\sigma_j^2] \qquad (2)$$

Owing to the limited range of data in k space, represented in equation (2) by $W(k)$ a cosine-tapered window function (Bourdillion *et al.* 1979), the Fourier transforms are restricted in their interpretation as termination ripples can sometimes be strong enough to produce ambiguous emitter-scatterer bond-distances.

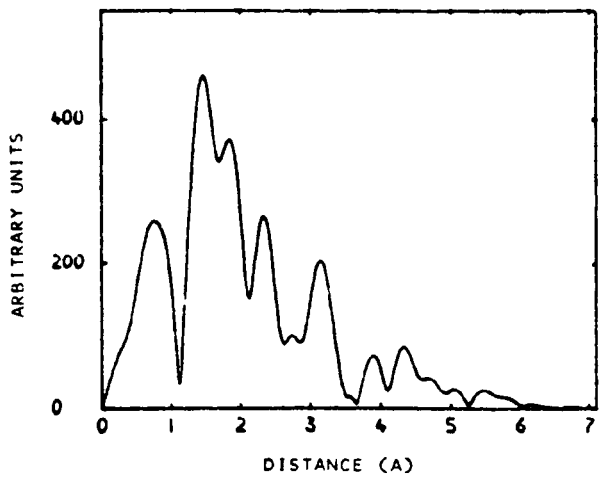

Figure 2. The Fourier transform $\phi(r)$ for the original glass (note, there is no correction for the central atom phase shift).

Figure 2 depicts just such a quasi-radial distribution function. The first peak is due to so-called atomic EXAFS and does not concern us here (see Holland *et al.* 1978). The second two peaks represent the 'oxygen cage' around the Zr ion. They occur at distances of 1·5 and 1·9 Å, shifted towards the origin by the central atom phase-shift that appears in equation (2). The height of these peaks is proportional to the structural parameters N_j, r_j and σ_j, number, distance and Debye-Waller factor for each shell. Their form in the glass and solely nucleated specimens, as compared with the crystallized samples, in which the major phase is tetragonal ZrO_2, is very disordered. This is illustrated in Figures 2, 3 and 4 by the growth of the first oxygen shell, labelled O, on an arbitrary unit scale.

In tetragonal ZrO_2, metal ions are eight-fold co-ordinated: $Zr\text{-}O_I(4) = 2{\cdot}065$ Å; $Zr\text{-}O_{II}(4) = 2{\cdot}463$ Å. This co-ordination is well

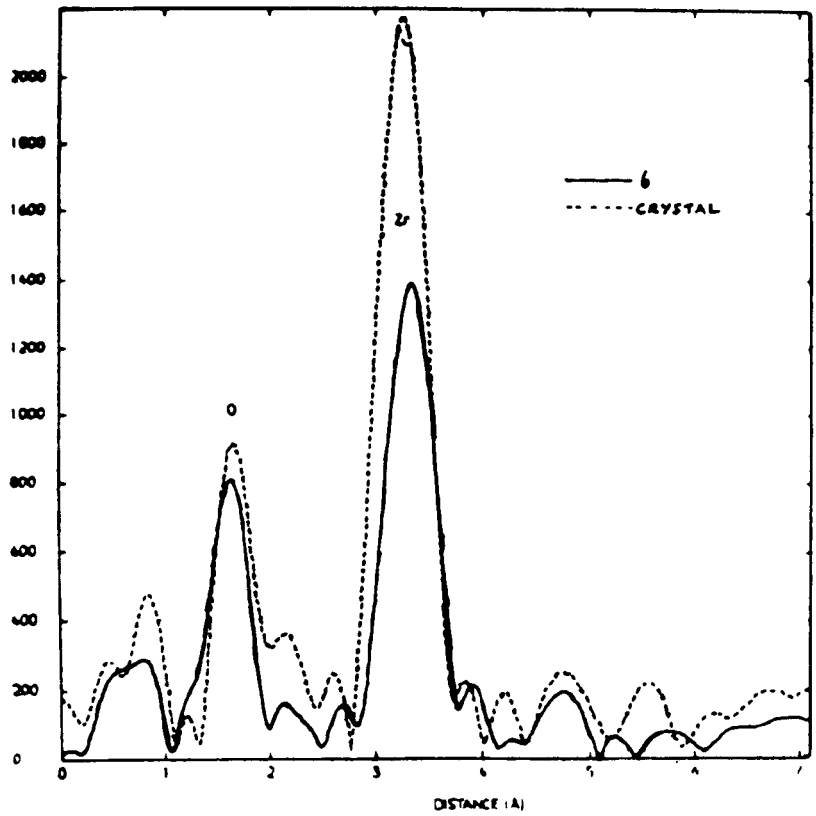

Figure 3. The Fourier transform $\phi(r)$ for two specimens 6 and 7 (called crystal) (note, there is no correction for the central atom phase shift).

defined, as we would expect, in the crystallized samples. Moreover, just such a split-shell co-ordination, although highly disordered, is evident in the glass and nucleated specimens, showing that there is some similarity between the near oxygen disposition about the Zr ion in the glass and in the crystal, albeit that its nature in the former is somewhat incipient.

One explanation for such a high degree of disorder in the first shell is the presence of a large Debye-Waller factor, σ_j^2. The latter appears in equation (1) as an overall damping term, and represents the mean square relative displacement of emitter and scatterer, i.e., thermal disorder. In a crystalline material, this 'thermal breathing' is the only contribution. However, in amorphous materials there is a second contribution due to an inherent static disorder. As

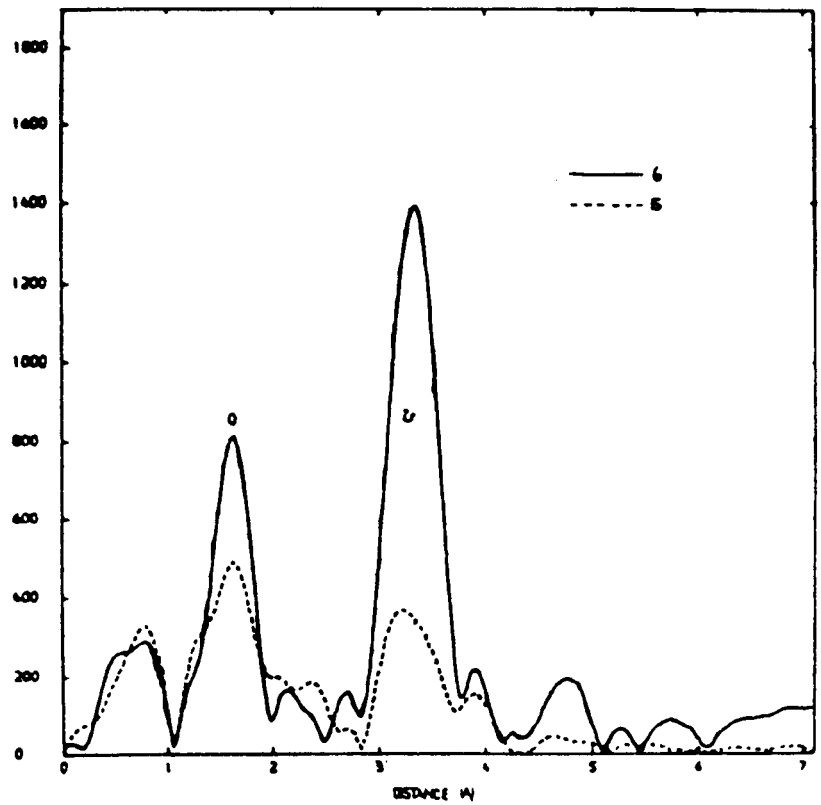

Figure 4. The Fourier transform $\phi(r)$ for two specimens 5 and 6 (note, there is no correction for the central atom phase shift).

such the Debye-Waller factor may be re-expressed as:

$$\sigma_j^2 = \sigma_{j,T}^2 + \sigma_{j,S}^2 \qquad (3)$$

where T and S refer to the contribution due to thermal and static disorder, respectively.

This disorder effect is evident in all the nucleated specimens together with a positive shift in bond-distance towards the crystalline value as a function of heat treatment temperature from (1·477 + a) Å for the original glass to (1·630 + a) Å for that of the crystal, a is a constant assuming that the phase shifts $\delta_j(k)$ are equivalent for both specimens. This assumption is valid if the concept of chemical transferability can be invoked and if so gives a value for the constant a of 0·41 Å. Eisenberger & Brown (1979) have

shown that asymmetries in the pair distribution function can lead to ambiguities in bond distance. That is, the pair distribution function is not a pure delta function but exhibits, at large distances, a gradual tailing off in the distribution producing an extra shift in bond distance, together with that of the central atom phase shift, which is proportional to the degree of asymmetry i.e., disorder. As such, the transfer of structural parameters from a model compound to that of an unknown material should be restricted to such compounds that possess similar pair distribution functions. The need for a more general theory for which these symmetries may be incorporated is fundamental in order to determine accurately co-ordination number and bond distances in disordered materials.

As was hinted at previously in Section 2.2., second-shell effects are observed with the onset of crystallization (about 900°C). The radial distribution functions for nucleated specimens show that contributions to the EXAFS from the second 'co-ordination' shell (about 3 Å) are indeed of little importance. However, for crystallized specimens (cf. Figures 2, 3 and 4; about 3 Å), coupled with the increase in order of the first shell, there is a dramatic rise in second-shell ordering. Moreover, a detailed examination of the type of second-shell scatterer has led to the conclusion that its origin is due to Zr-Zr scattering as opposed to what is reasonably thought to be Zr-Si scattering prior to crystallization. Zr-Zr distances (about 3·6 Å) are in agreement with what we would expect for the case of tetragonal ZrO_2 in which metal-metal distances are $Zr\text{-}Zr_I(4) = 3{\cdot}640$ and $Zr\text{-}Zr_{II}(4) = 3{\cdot}684$.

3. CONCLUSION

It has been shown that EXAFS measurements have a distinct advantage over other structural techniques, such as X-ray diffraction or electron microscopy, as structural rearrangement is observed in the process of nucleation long before the appearance of any micro-crystalline characteristics.

ACKNOWLEDGMENTS

Our thanks go to Dr. A.D. Cox for performing the EXAFS measurements and to the staff at EMBL, DESY for their assistance.

One of us (J.M.T.) thanks the SERC for the award of a CASE Studentship, in collaboration with Pilkington Brothers Ltd., which allowed the research to be undertaken.

REFERENCES

ASHLEY, C.A. & DONIACH, S., 1975, *Physical Review,* B11, 1279-1288.

BOURDILLION, A.J., PETTIFER, R.F. & MARSEGLIA, E.A., 1979, *Journal of Physics C,* 12, 3889-3897.

EISENBERGER, P. & BROWN, G.S., 1979, *Solid State Communications,* 29, 481-484.

HOLLAND, B.W., PENDRY, J.B., PETTIFER, R.F. & BORDAS, J., 1978, *Journal of Physics C,* 11, 633-642.

SAYERS, D.E., LYTLE, F.W. & STERN, E.A., 1970, *Advances in X-ray Analysis,* 13, 248-271.

REFERENCES

Abdrashitova, E. I., (1980): J. Non.-Cryst. Sol., **38** & **39**, 75.

Andersson, S. and Wadsley, A. D., (1961), Acta Cryst., **14**, 1245.

Ashley, C. A. and Doniach, S., (1975), Phys. Rev., **B11**, 1279.

Barry, T. I., Clinton, D., Lay, L. A., Mercer, R. A. and Miller, R. P., (1969), J. Mat. Sci., **4**, 596.

Belov, V. N., (1963), Chemistry of Large Cation Silicates, Consultants Bur. N.Y.

Bevington, P. R., (1969), Data Reduction and Error Analysis for the Physical Sciences.

Bland, J. A., (1961), Acta. Cryst., **14**, 875.

Bobovich, S. Y., (1964), The Structure of Glass Vol. III, Consultants Bur. N.Y.

Bockris, J., Mackenzie, J. and Kitchener, J., (1955), Trans. Faraday Soc., **51**, 1754.

Bonse, U., Materlik, G. and Schroder, W., (1976), J. Appl. Crystl., **9**, 223.

Botvinkin, O. K., Krokuis, E. A., Demichev, S. A. and Vlasov, V. A. (1964), Steklo Byul Vses. Gos Naucha Stekla, 2, 22 (In Russian).

Bragg, W. L. and West, J., (1930), Phil. Mag., **10**, 823.

Brosset, C., (1958), Trans. Soc. Glass. Tech., **42**, 125.

Brown, G. and Eisenberger, P., (1979), Sol. Stat. Comm., **29**, 481.

Brown, I. D. and Kang Kun Wu, (1973), Acta Cryst., **B29**, 2009.

Chandrasekhar, H. R., Chandrasekhar, M. and Manghnani, M. H., (1979), Sol. Stat. Comm., **31**, 329.

Chernov, A. N., Iluhin, V. V., Maskimov, B. A. and Belov, N. V., (1971), Sov. Phys. Cryst.,**16**, 65.

Citrin, P. H., Eisenberger, P. and Kincaid, B. M., (1976), Phys. Rev. Lett. **36**, 1346.

Cox, A. D. and McMillan, P. W., (1981), J. Non-Cryst. Sol., **44**, 257.

Cramer, S. P. and Hodgson, K. O., (1977), SSRP Report 77/07, Stanford, CA.

Cromer, D. T. and Herrington, K., (1955), J. Amer. Ceram. Soc., **77**, 4708.

Dupree, R., Holland, D. H., McMillan, P. W. and Pettifer, R. F., (1984), submitted to J. Non-Cryst. Sol.

Endell, K. and Hellbruge, J., (1942), Naturwosien Schaf. Ten., **30**, 42.

Eisenberger, P. and Brown, G. S., (1977), Sol. Stat. Comm., **24**, 201.

Farmer, V. C., (1974), The Infrared Spectra of Minerals, ed. V. C. Farmer, Adlard & Sons.

Forty, A. J., (1979), in "Proc. R. Inst. GB.", **50**, 1.

Fox, R. and Gurman, S. J., (1980), J. Phys. C, **13**, L249.

Gaskell, P. H., (1983), in "The Structure of Non-Crystalline Materials", ed. P. H. Gaskell, J. M. Parker and E. A. Davis, Taylor and Francis.

Gill, P. E. and Murray, W., (1978), SIAM. J. on Num. Anal., **15**, 977.

Goldschmidt, V. M., (1926), Skrifter Norse Viden. Akad. I. Math-Naturwiss KL., **8**, 7.

Goodman, C., (1983), Structure of Non-Crystalline Materials, ed. P. H. Gaskell, J. M. Parker and E. A. Davis, Taylor and Francis.

Greaves, N., Fontaine, A., Lagarde, P., Radux, D., Gurman, S. J. and Parkes, S., (1980), in "Proc. 1st EPS Condensed Matter", Antwerp.

Greaves, N., Fontaine, A., Lagarde, P., Radux, D. and Gurman, S. J., (1981), Nature, **293**, 611.

Hanada, T. and Soga, N., (1980), J. Non-Cryst. Sol., **38 & 39**, 105.

Hannu, R. and Su, G. J., (1964), J. Amer. Ceram. Soc., **47**, 597.

Hart, M. and Rodriguez, A. R., (1978), J. Appl. Spec., **11**, 248.

Hayes, T. M., (1978), J. Non. Cryst. Sol., **31**, 57.

Henninger, E. H., Buschert, R. C. and Heaton, C., (1967), J. Phys. Chem. Sol., **28**, 422.

Herman, F. and Skillman, S., (1963), Atomic Structure Calculations, Prentice Hall.

Huggins, M. L., Sun, K. H. and Silverman, A. J., (1953), J. Amer. Ceram. Soc., **26**, 393.

Jellison, G. E. and Bray, P. S., (1978), J. Non-Cryst. Sol., **29**, 187.

Jones, G. O., (1956), Glass, Chapman & Hall.

Jose, V. R. and Urnes, S., (1972), Phys. Chem. Glasses., **13**, 122.

Kincaid, B., (1976), Ph.D. Thesis, Stanford University.

King, T. B., (1953), The Physical Chemistry of Melts, 35PP, London.

Kozlowski, R., Pettifer, R. F. and Thomas, J. M., (1983), J. Chem. Phys., in print.

Krogh-Moe, J., (1965), Phys. Chem. Glasses, **6**, 46.

Kronig, R. de. L., (1931), Z. Physik, **70**, 317.

Krstanovic, I. R., (1958), Acta Cryst., **11**, 896.

Kutzler, F. W., Natali, C. R., Misemer, D. R., Doniach, S. and Hodgson, K. O., (1980), J. Chem. Phys., **73**, 3274.

Leadbetter, A. J. and Wright, A. C., (1972), J. Non Cryst. Sol., **7**, 23.

Lee, P. A. and Pendry, J. B., (1975), Phys. Rev., **B11**, 2795.

Lee, P. A. and Beni, G., (1977), ibid, 2862.

Lienard, A., (1898), L'Eclairase Elec., **16**, 5.

Loshmanov, A. A., Sigaev, V. N., Khodakovskaya, R. Y., Pavlushkin, N. M. and Yamzin, I. I., (1974), "Proc. 10th Int. Congress on Glass", **12**, 9.

Lukesh, J. S., (1942), "Proc. Nat. Acad. Sci.", **28**, 277.

Mackenzie, J. D., (1956), Chem. Rev., **56**, 455.

Manghnani, M. H., Ferraro, J. R. and Basile, L., (1974), J. Appl. Spec., **28**, 256.

Martens, G., Rabe, P., Schwentner, N. and Werner, A., (1979), Phys. Rev. Lett., **39**, 1411.

McCullough, J. D. and Trueblood, K. N., (1959), Acta Cryst., **12**, 507.

McMillan, P. W., (1964), Glass Ceramics, Academic Press.

Megraw, H. D., (1947), in "Proc. Royal. Soc.", **189**, 261.

Morinaga, M., Adachi, H. and Tuskada, M., (1983), J. Phys. Chem. Sol., **44**, 301.

Mott, D. L., (1963), Ph.D. Thesis, New Mexico State Univ.

Pauling, L., (1960), The Nature of the Chemical Bond, 644PP, Correll University Press.

Pavlushkin, N. M. and Yamzin, I. I., (1974), in "Proc. 10th Int. Cong. on Glass", **12**, 9.

Pendry, J. B., (1973), Low Energy Electron Diffraction, Academic Press.

Pettifer, R. F., (1977), Ph.D. Thesis, University of Warwick.

Pettifer, R. F., (1979), in "Proc. of 4th EPS General Conf.", London.

Phillippi, C. M. and Mazdiyansi, K. S., (1971), J. Amer. Ceram. Soc., **54**, 254.

Porai-Koshits, E. A., (1953), "Conf. on Structure of Glass", Consultants Bur. N.Y.

Potts, J. C., Brookner, G. and Barch, J., (1944), J. Amer. Ceram. Soc., **27**, 225.
Randall, J. T., Rooksby, H. P. and Cooper, B. S., (1930), Z. Krist. **95**, 196.

Rawson, H., (1956), in "Proc. IVth Int. Conf. on Glass", Paris.

Rogonzin, Yu. V., (1973), Proizoid Issled Stekla Silikat Mater, **3**, 147 (In Russian).

Sandstrom, D. R. Lytle, F. W., Wei, P. S. P., Greegor, R. B., Wong, J. and Schultz, P., (1980), J. Non-Cryst. Sol., **41**, 201.

Sandstrom, D. R., Greegor, R. B., Lytle, F. W., Wong, J. and Schultz, P., (1983), ibid, **55**, 27.

Sayers, D. E., Lytle, F. W. and Stern, E. A., (1970), Adv. in X-ray Analysis, **13**, 248.

Sayers, D. E., Lytle, F. W. and Stern, E. A., (1972), J. Non-Cryst. Sol., **8-10**, 401.

Shmidt, V. V., (1963), Bull. Acad. Sci. USSR, **27**, 392.

Shwinger, J., (1949), Phys. Rev., **75**, 1912.

Silver, A. H . and Bray, P. S., (1958), J. Chem. Phys., **29**, 984.

Smyth, T., (1972), in "An Introduction to Glass Science", ed. L. D. Pye, H. J. Stephens and W. C. La Course, Plenum Press.

Stanworth, J. E., (1948), J. Soc. Glass. Tech., **32**, 154.

Sun, K. H., (1947), J. Amer. Ceram. Soc., **30**, 277.

Taylor, J. M. and McMillan, P. W., (1983), in "The Structure of Non-Crystalline Materials", ed. P. H. Gaskell, J. M. Parker and E. A. Davis, Taylor and Francis.

Taylor, J. M., (1983), unpublished data.

Teo, B. K. and Lee, P. A., (1979), J. Amer. Chem. Soc., **101**, 2815.

Teo, B. K., Lee, P. A., Simons, A. L., Eisenberger, P. and Kincaid, B. M., (1977), ibid., **99**, 3854.

Teufer, G., (1962), Acta Cryst., **15**, 1187.

Todhunter, R., (1984), Ph.D. Thesis, submitted to University of Warwick.

Tossell, J. A., Vaughn, D. J. and Johnson, K. H., (1974), Amer. Miner., **59**, 319.

Valenkov, N. and Porai-Koshits, E. A., (1936), Z. Krist., **95**, 195.

Victoreen, J. A., (1962), International Tables for X-ray Cryst., Vol. III, Kynoch Press.

Warren, R. E., (1969), X-ray Diffraction, Addison Wesley.

Warren, B. E., (1937), J. Appl. Phys., **8**, 645.

Warren, B. E. and Biscoe, J., (1938a), J. Amer. Ceram. Soc., **21**, 49.

Warren, B. E. and Biscoe, J., (1983b), ibid, **21**, 287.

Weyl, W. A., (1951), Coloured Glasses, Soc. of Glass Technology.

Wong, J. and Angell, C. A., (1976), Glass Structure by Spectroscopy, Marcell Dekker Inc.

Wong, J. and Lytle, F. W., (1980), J. Non-Cryst. Sol., **37**, 273.

Wyckoff, R. W. G., (1927), Crystal Structures Vol. 3, Wiley and Sons.

Zachariasen, W. H., (1932), J. Amer. Chem. Soc., **54**, 3841.

Zarzycki, J., (1971), J. Mater. Sci., **6**, 130.